Characterization of miR-574-5p decoy to CUGBP1 in human lung cancer cells using a mass spectrometry proteomics approach

Vom Fachbereich Biologie der Technischen Universität Darmstadt

Zur Erlangung des akademischen Grades

Doctor rerum naturalium

(Dr. rer. nat.)

Dissertation von

M. Sc. Anne Caterina Emmerich

Erstgutachterin: Dr. Meike Julia Saul

Zweitgutachterin: Prof. Dr. Beatrix Süß

Darmstadt 2020

Emmerich, Anne Caterina: Characterization of miR-574-5p decoy to CUGBP1 in human lung cancer cells using a mass spectrometry proteomics approach
Darmstadt, Technische Universität Darmstadt
Jahr der Veröffentlichung der Dissertation auf TUprints: 2020
URN: urn:nbn:de:tuda-tuprints-91406
Tag der mündlichen Prüfung: 28.02.2020

Veröffentlicht unter CC BY-SA 4.0 International
https://creativecommons.org/licenses/

In der Wissenschaft gleichen wir alle nur den Kindern, die am Rande des Wissens hie und da einen Kiesel aufheben, während sich der weite Ozean des Unbekannten vor unseren Augen erstreckt.

Sir Isaac Newton (1643 – 1727)

Table of Contents

List of Figures

List of Tables

Summary

The bioactive lipid mediator prostaglandin (PG) E_2 is generated by the enzyme microsomal prostaglandin E_2 synthase-1 (mPGES-1). Especially in lung tumors, mPGES-1 was shown to be significantly overexpressed which contributes to a pro-tumorigenic microenvironment. Current medication interfering with the negative effects of PGE_2 comprise only non-steroidal anti-inflammatory drugs (NSAIDs). While these have effective analgesic properties and are commonly used as pain killers, treatment of tumor growth is still inconclusive. Probably, only subgroups of cancer patients exhibit an abnormal prostanoid profile. Therefore, a reliable biomarker is necessary to identify patients who could benefit from said treatment. In a recent study, it was discovered that a specific microRNA (miR) can induce mPGES-1 gene expression. The miR-574-5p prevents binding of the inhibitory CUG-RNA binding protein 1 (CUGBP1) to the 3´ untranslated region (UTR) of mPGES-1. This non-canonical decoy function of miR-574-5p leads to an increased mPGES-1 protein level. Following, an induction of PGE_2 formation triggers the progression of lung tumor growth *in vivo*. Interestingly, the entire influence on tumor progression could be blocked with the addition of a specific mPGES-1 inhibitor, confirming the huge influence of miR-574-5p on (patho-) physiological mPGES-1 functions. In this study, a proteomics approach was conducted in order to further characterize this decoy mechanism in human lung cancer cells. The aim was to gather global insights into the proteome changes related to miR-574-5p and CUGBP1, especially in a compartment specific manner. Further, it was aimed to identify new CUGBP1 targets and find out if they are also affected by the decoy function of miR-574-5p. Two new CUGBP1 targets were validated herein: NADH-Ubiquinone Oxidoreductase Core Subunit S2 (NDUFS2) and Mothers against decapentaplegic homolog 2 (SMAD2). However, both NDUFS2 and SMAD2 are independent from miR-574-5p levels. In a bioinformatical 3'UTR analysis of potential CUGBP1 targets, it was shown that the specific splicing pattern of mPGES-1 is unique, comprising two long CUGBP1 binding motifs with a 3'UTR intron in between. Only 11 other transcripts harbor a similar but not identical pattern in their sequence. Hence, it is assumable that this novel decoy mechanism is specifically regulating mPGES-1 in A549 lung cancer cells. This might be caused by the unique splice pattern of mPGES-1. However, further experiments are needed to confirm this hypothesis. Nevertheless, specificity of the decoy mechanism would open up new opportunities for lung cancer patients. By using miR-574-5p as a biomarker, one could stratify those patients with high mPGES-1 levels who have a higher chance to benefit from the anti-tumorigenic potential of NSAID therapy.

Zusammenfassung

Der biologisch aktive Lipidmediator Prostaglandin (PG) E_2 wird enzymatisch von der mikrosomalen Prostaglandin E2 Synthase (mPGES-1) generiert. Es konnte gezeigt werden, dass mPGES-1 speziell in Tumoren der Lunge stark angereichert ist. Durch die damit verbundene vermehrte Bildung von PGE_2 kommt es zu einer kanzerogenen Tumorumgebung. Hier setzen sogenannte *non-steroidal anti-inflammatory drugs* (NSAIDs) an. Während diese effektive analgetische Eigenschaften aufweisen und häufig als Schmerzmittel genutzt werden, ist die Behandlung von Tumoren dennoch umstritten. Es wird vermutet, dass nur eine Subpopulation von Krebspatienten ein entartetes Prostanoidprofil aufweist. Daher wäre ein verlässlicher Biomarker vonnöten, mit dem man diese Patienten identifizieren kann, die dann von einer NSAID-Therapie profitieren könnten. Kürzlich wurde eine spezielle mikroRNA (miR) identifiziert, die die mPGES-1 Genexpression induzieren kann. Die miR-574-5p verhindert die Bindung des inhibitorischen CUG RNA Bindeprotein 1 (CUGBP1) an den 3‘ untranslatierten Bereich (UTR) von mPGES-1. Diese nicht-kanonische *Decoy* Funktion von miR-574-p führt zu einem erhöhten mPGES-1 Proteinlevel. Dadurch kommt es zur vermehrten PGE_2 Synthese, welche daraufhin das Tumorwachstum *in vivo* begünstigt. Durch die zeitgleiche Gabe eines spezifischen mPGES-1 Inhibitors konnte jedoch der gesamte Einfluss auf das Voranschreiten des Tumors verhindert werden. Dadurch konnte der immense Einfluss der miR-574-5p auf die (patho-) physiologischen Funktionen von mPGES-1 gezeigt werden. In dieser Studie wurde nun der *Decoy* Mechanismus mit Hilfe einer Proteomik-Studie in humanen Lungenkarzinomzellen weiter charakterisiert. Das Ziel war es globale Kompartment-spezifische Einsichten in die miR-574-5p- und CUGBP1-vermittelten Änderungen des Proteoms zu erhalten. Des Weiteren sollten neue CUGBP1-regulierte Transkripte identifiziert werden, um herauszufinden, ob diese ebenfalls durch den *Decoy* Mechanismus der miR-574-5p beeinflusst werden. Zwei neue CUGBP1-regulierte Transkripte konnten dabei validiert werden: die *NADH-Ubiquinone Oxidoreductase Core Subunit S2* (NDUFS2) sowie das Signalmolekül *Mothers against decapentaplegic homolog 2* (SMAD2). Die Regulation beider Zielgene war jedoch unabhängig von miR-574-5p. In einer bioinformatischen Analyse aller 3’UTRs von möglichen CUGBP1-regulierten Transkripten stellte sich heraus, dass das spezifische mPGES-1 Spleißmuster einzigartig ist. Es umfasst zwei lange CUGBP1 Bindesequenzen, getrennt durch ein 3’UTR Intron. Ein ähnliches, wenn auch nicht identisches Muster, konnte in nur 11 weiteren Transkripten gefunden werden. Daher ist es annehmbar, dass der *Decoy* Mechanismus spezifisch nur die mPGES-1 Expression in A549 Lungenkarzinomzellen reguliert. Dies könnte potenziell auf das spezifische Spleißmuster zurückzuführen sein, obwohl weitere Experimente nötig sind, um diese Hypothese zu bestätigen. Nichtsdestotrotz könnte die Spezifität des *Decoy* Mechanismus neue

Möglichkeiten für Lungenkrebspatienten darstellen. MiR-574-5p könnte als Biomarker genutzt werden, um jene Patienten mit hohen mPGES-1 Leveln zu identifizieren. Diese könnten dann von den inhibitorischen Effekten einer NSAID-Behandlung auf das Tumorwachstum profitieren.

1. Introduction

Transcription is one of the most fundamental processes in biological systems. It reliably produces the required amounts of RNA which are necessary for the maintenance of general cellular functions but also for the reaction to rapid changes of environmental circumstances. In multicellular organisms, every individual cell shares the same genome, however expressing a characteristic cell type specific protein profile. To orchestrate this kind of specificity, a tremendous amount of regulatory action is required. In fact, various post-transcriptional regulation mechanisms are responsible for fine-tuning of the intracellular protein repertoire [1].

1.1 Post-transcriptional mechanisms of gene regulation

Post-transcriptional regulation can occur at any step of mRNA processing, from transcription to translation, both within the nucleus as well as in the cytoplasm [2]. Shortly, mRNA processing starts as soon as transcription is initiated by Polymerase II [3]. Afterwards, pre-mRNAs are capped, spliced, edited and polyadenylated. Then, mature mRNAs are exported into the cytoplasm through the nuclear pore complex [4]. In the cytoplasm, mRNAs can be translated into proteins, stored in stress granules, processing bodies (P-bodies) or they can be marked for degradation (see Figure 1).

All these steps are mediated by a myriad of factors, most of them RNA-binding proteins (RBPs) with some of them binding the pre-mRNA even during transcription [5]. Regulatory mechanisms include among others interference with splicing, editing or polyadenylation as well as mRNA (de-) stabilization, localization and finally translational inhibition [2]. For instance, polyadenylation is a critical step as it stabilizes the mRNA molecule and prevents rapid degradation in the cytoplasm [6]. The longer the 3’ poly(A)-tail, the longer the mRNA can survive in the cytoplasm, where it gradually gets shorter by deadenylation [7]. Initiation of translation however, stops further deadenylation which indicates that poly(A)-shortening is a mechanism of regulation. The deadenylation is mediated by the poly(A) ribonuclease (PARN) [8]. Recruitment of PARN is thereby mediated by binding of RBPs or miRs [9] [10] [11] [12].

Another example for a regulatory mechanism is mRNA storage in intracellular particles called P-bodies. mRNAs get recruited there by interaction with RBPs or miRs [13]. P-bodies were described to play a role in all kinds of mRNA decay mechanisms, however it was also demonstrated that mRNAs were temporary stored there for later translation [13] [14] [15].

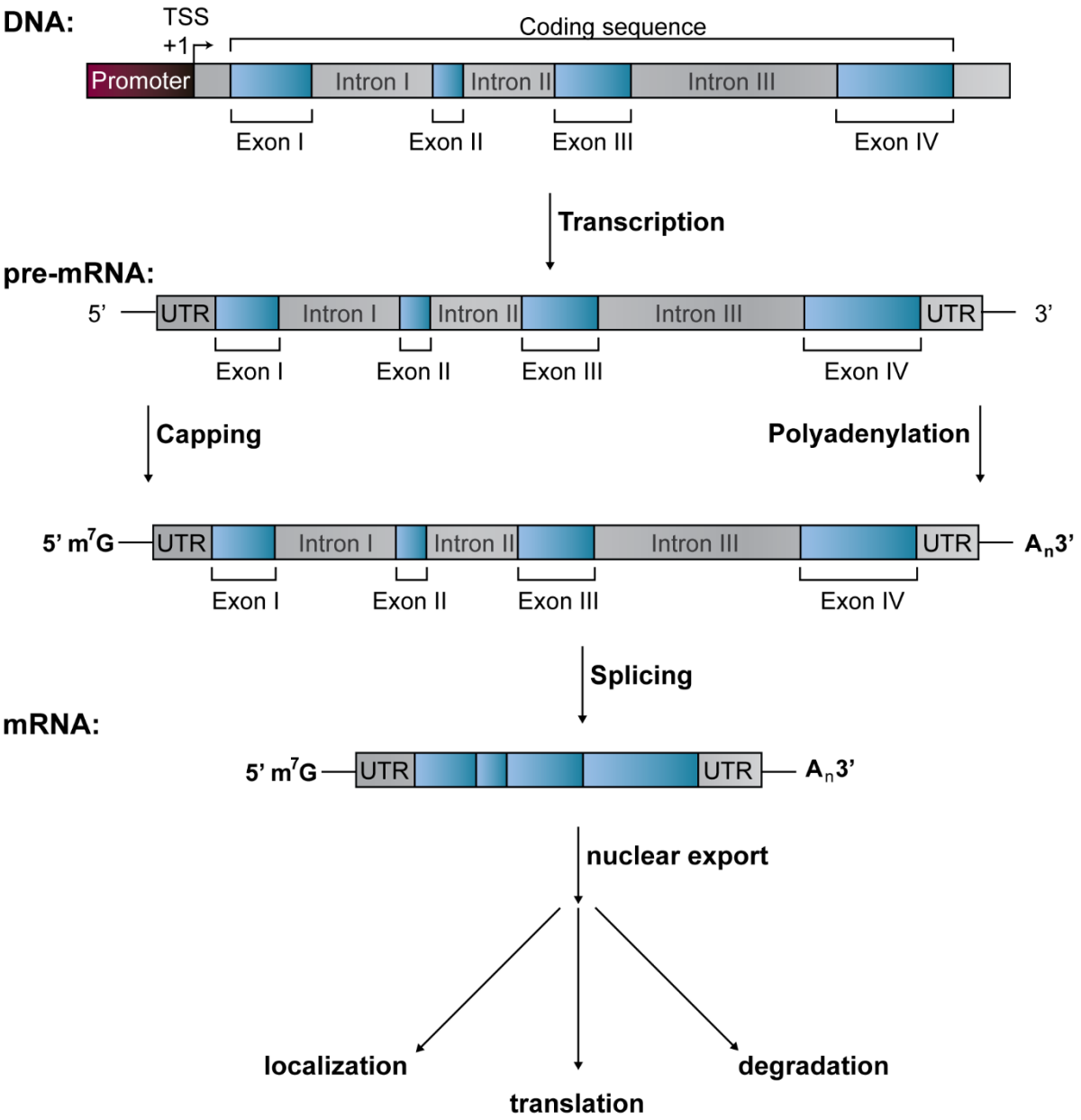

Figure 1: mRNA processing.
Genes consists of a promoter region directly upstream of the transcription start site (TSS), numerous exons and introns as well as untranslated regions at the 5' and 3' end. The DNA is transcribed by Polymerase II, generating the precursor mRNA (pre-mRNA). Processing includes addition of a 5' 7-methylguanylate (5' m^7G) cap, polyadenylation of the 3' end (A_n 3') as well as splicing to remove intronic sequences. All these processing steps can concurrently occur during transcription although a consecutive order is indicated in the figure for facilitation purpose. Mature mRNA is exported into the cytoplasm where its fate is influenced by localization, degradation or successful translation. Modified from [14] [15].

Post-transcriptional regulation is mainly based on cis-regulatory elements (CRE) [18]. In this context, CREs are defined as regions of non-coding DNA or RNA that provide binding sites for trans-acting factors such as RBPs or transcription factors. CREs can be upstream or downstream of coding sequences (CDS) or even within introns and are mostly termed

enhancers or silencers, depending on their regulatory function [19]. Of note, one CRE can be bound by numerous trans-acting factors and *vice versa*, which is called pleiotropy. Moreover, interactions, synergisms or competition of various trans-acting factors as well as the combination of activating or inhibitory CREs further elevates the complexity of gene expression regulation [18]. In the following chapters, three types of post-transcriptional regulation mechanisms are described in more detail as they stand in the focus of this thesis (see chapters *1.1.1 Alternative Splicing, 1.1.2 RNA-binding proteins (RBPs) and 1.1.3 microRNAs (miRs)).*

1.1.1 Alternative splicing

Alternative splicing (AS) is a fine tuning process of higher eukaryotes which enables a variation in the in- or exclusion of sequence parts of a pre-mRNA and thus provides greater biodiversity of proteins from an established number of genes [20]. There are several estimations towards how many of all transcripts are alternatively spliced which range up to 25% in *Caenorhabditis elegans (C. elegans)*, 60% in *Drosophila melanogaster* [21] and even 90% in humans [22] [23]. Investigations concerning different human tissues revealed that roughly 50% of alternatively spliced isoforms are differentially expressed among tissues indicating that AS also provides cell type specific isoforms [24]. However, there are recent publications questioning the impact of AS on protein diversity, as apparently many RNA isoforms could not be found on protein level in large scale proteomics studies [19] [20]. Nevertheless, this does not render the fact that AS is a pivotal process in regard of post-transcriptional regulation and physiological homeostasis. Defects in AS can even cause different diseases most of all cancer development and progression [27].

During the splicing process it is decided which parts of the sequence are included in the mature mRNA and which ones are removed [28]. Consequentially, several mature mRNAs can result from one pre-mRNA. There are distinct types of AS (see Figure 2). Constitutive splicing describes the canonical form including one exon after the other and removing all the intronic parts. One variant is exon skipping, which describes the case when one exon is cut out together with the adjacent introns. *Vice versa*, an intron can also be included in the mature mRNA. Further, there can be mutually exclusive exons, also called cassette exons. Finally, the 5’ and 3’ splice sites can vary. All these variations lead to different mRNAs and thereby also to different amino acid sequences during translation [29].

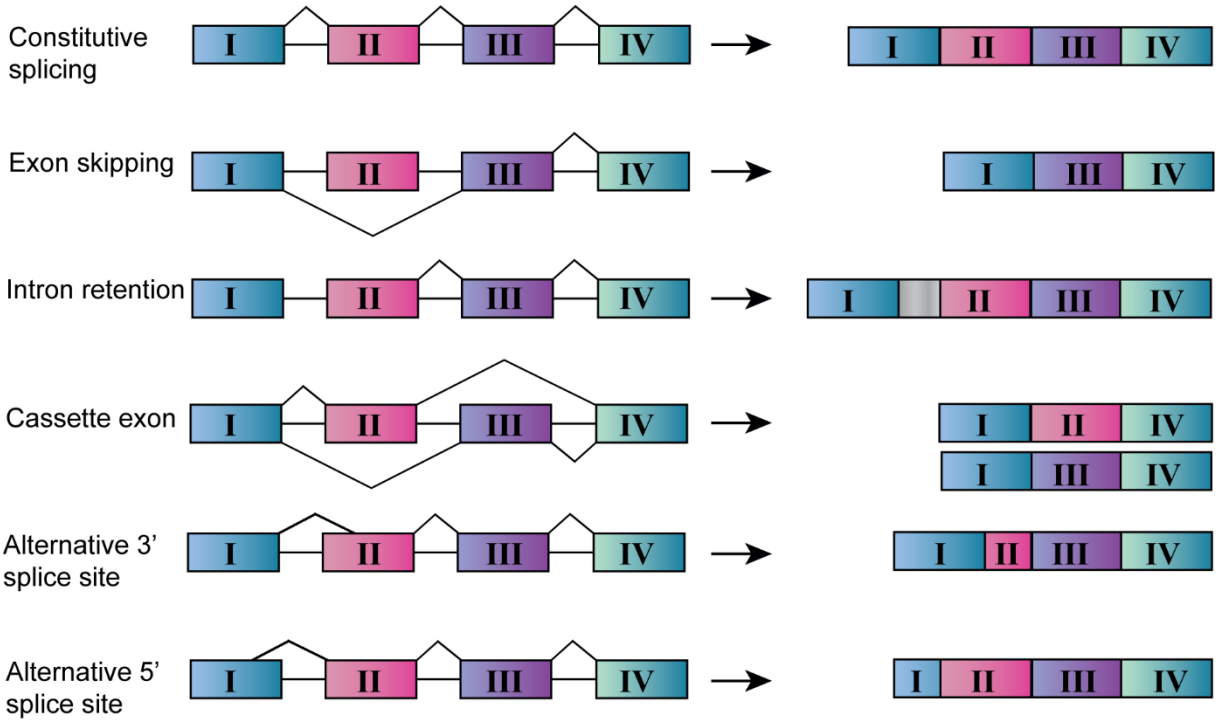

Figure 2: Different types of AS.
Colored boxes indicate exons; thin lines in between resemble introns. The different forms of AS can lead to distinct mature mRNAs which also influences the amino acid sequence of the proteins. Modified from [30].

The large complex which mediates the splicing process is called spliceosome. It comprises over 300 proteins and nucleic acids [31] [32], while the core is composed of five small nuclear ribonucleoproteins (snRNPs) U1-2, 4-6 [33]. Furthermore, additional trans-acting factors of the heterogeneous nuclear ribonucleoprotein (hnRNP) [34] or Serine/arginine (SR) protein family [35] act as repressors or activators by binding to silencer or enhancer regions to regulate splicing activity depending on the cell type, the developmental stage or the gene [36]. Generally, the spliceosome binds to splice sites and cuts out the intronic sequences. Thereby, assembly and dissociation of the spliceosome subunits appear periodically and recur for every intron [37]. Thus, the splicing process can be divided in three parts: assembly of the spliceosome, catalytic splicing (actual removal of the intron) and recycling of the snRNPs [29]. The decision which part of the pre-mRNA is an exon and which is intron depends on a number of cis-elements. Conserved cis-elements adjacent to splicing sites are called splicing acceptor sites. They are found on exon-intron-boundaries of pre-mRNAs and are often UG-rich such as UUCUG and UGUU [38] [39].

Generally, introns consist of a 5' donor site, a branch point and a 3' acceptor site. Apart from the few self-splicing introns [40], most introns need a spliceosome to be cut out. There are two types of introns: the most common type of intron is processed by the so-called major

spliceosome and has a 5’ GU and a 3’ AG, whereupon the GU is strictly conserved and surrounded by a less conserved sequence (see Figure 3). The much more uncommon AU-AC type intron is processed by the minor spliceosome [41].

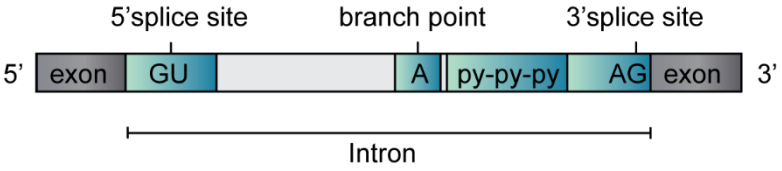

Figure 3: General structure of a GU-AG intron.
Framed by two exons, the intron starts with a 5’ splice site that contains a conserved GU within a less conserved sequence. The branch point containing a highly conserved A is followed by a pyrimidine rich region and finally the AG comprising 3’ splice site. Modified from [41] [42]. Py: Pyrimidine nucleobase (cytosine or uracil)

Interestingly, splicing not only occurs in the CDS of pre-mRNAs but also in UTRs. Removal of introns obviously has a tremendous impact on the length. Shorter 3'UTR isoforms have fewer binding sites for trans-acting factors such as miRs and are consequently more stable, resulting in higher protein level [43]. Higher expression rates in turn are linked to proliferating cells. Therefore, it is no surprise that shorter 3’UTRs can often be found in oncogenes and are associated with carcinogenic cells [44]. Nevertheless, it is often thought that 3’UTR splicing inevitable leads to nonfunctional transcripts due to nonsense-mediated decay (NMD). However, this is only the case when the intron is less than 55 nucleotides (nt) from a termination codon resulting in a pre-mature stop codon [45] [46]. Splicing within UTRs still does not gain much attention, although estimations on how many human UTRs contain introns range from 35% in 5’UTRs [47] to 6-16% in 3’UTRs [48] [49].
In general, AS has a crucial impact on all kinds of cellular functions. Dysregulation can even lead to variances in cell cycle control, proliferation or apoptosis [50]. Therefore, it is discussed in literature to announce AS an additional hallmark of cancer [51]. Especially genomic splice site point mutations seem to be affected. For instance, there are at least 29 different splice site mutations in the Tumor Protein P53 (TP53/p53) gene that are found in all kinds of tumor types including lung cancer, breast cancer and leukemia [52]. It is well described that during normal differentiation oncogenes are inactivated via AS, whereas in tumor cells AS is manipulated to inactivate tumor suppressors [53] [54] [55] [56]. This underlines the importance of AS and post-transcriptional regulation in general for physiological and cellular homeostasis.

1.1.2 RNA-binding proteins (RBPs)

RBPs fulfill a crucial role in post-transcriptional gene expression. Generally, it is proposed that unbalanced expression and function of RBPs occurs in the context of uncontrolled cell

proliferation and promotes tumor growth [57]. This reflects the relevance of protein-RNA interactions in cellular homeostasis. However, a definite causal connection has not yet been described [58] [59].

In fact, RBPs control stability, decay, translation as well as localization of mRNAs (see Figure 4A). They are able to shuttle mRNAs between the nucleus and the cytoplasm to actively translating ribosomes, stress granules or P-bodies [4] [60] [61] [62] [63] [64]. *Vice versa*, RBPs can also be the target of regulation by RNAs rather than being a regulating factor. The discovery of long non-coding RNAs (lncRNAs) and their association with the organization, scaffolding or inhibition of protein arrangement made it clear that RNA can also act on its bound protein, which contradicts the general view that it is normally the other way round. Thereby, RNAs can have an impact on localization, stability, interactions or functions of a protein (see Figure 4B) [65].

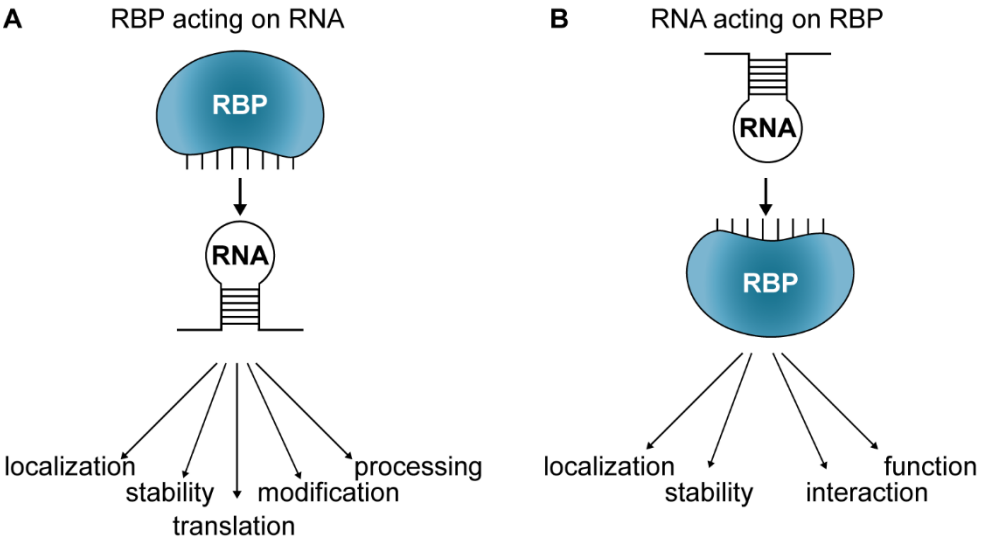

Figure 4: Interaction of RBPs with RNAs.
Functional crosstalk of RBP/RNA interaction can occur in both directions. (A) RBPs can bind to RNAs via RNA-binding domains, influencing various aspects of the RNAs functions and fate. (B) By displaying protein-binding activity, certain RNAs (e.g. lncRNA) can affect various protein functions. Modified from [65].

The formation of a RNA-Protein-complex, also called ribonucleoprotein (RNP) complex is mediated by specific RNA-binding domains (RBDs) [66] [67]. Thereby, different specificities and affinities are based on sequence and structure of the RNA target. RBDs can be classified as followed: RNA-recognition motifs (RRMs), double stranded RBDs or Zinc finger domains [4]. Those RBDs can then bind to CREs mostly in 3'UTRs of mRNAs.

One of the best described CREs are probably AU-rich elements (AREs). They are ubiquitously found in 3'UTRs of mRNAs [68] and interact with a variety of RBPs which can tag the RNA for

rapid degradation [69] but also stabilization [70]. In recent years, a similar sequence element called GU-rich element (GRE) was discovered. GREs are highly conserved throughout evolution and were primarily found in 3'UTRs of mRNAs with short half-lives [71]. Generally, GU-rich sequences appear in ca. 5% of RNAs in the human transcriptome [72]. They can regulate splicing, translation, deadenylation or mRNA decay, depending on the RBP they interact with during different intracellular settings [73] [74]. It was elucidated that GREs are specifically targeted by the CELF (CUG-Binding protein and embryonically lethal abnormal vision-type RNA binding protein like factors) family of RBPs [71].

1.1.2.1 CUGBP1 and the CELF family of RBPs

The CELF family influences a wide range of post-transcriptional processes, such as AS [75] [76] [77], deadenylation [9], C-U editing [78] [79], transport [80] [81] [82], translation [83] and most of all mRNA decay [84] .

The RBP family is evolutionary conserved and comprises 6 members: CELF1-6 [85] [86] [87]. All of them harbor three RRMs, two N-terminal RBDs and one in the C-terminal region [88] [89] (see Figure 5). The divergent domain is potentially important for functional regulation but this is still discussed throughout literature. While CELF1 (CUG-RNA binding protein 1; CUGBP1) and CELF2 (CUGBP2) are ubiquitously expressed among cell types and tissues and fulfill a role in embryonic development [90] [91] [92] [93], CELFs 3-6 are only expressed in fully developed cells and are exclusively found in nervous tissue [94] [95] [88]. Although, it was proposed several years ago that the family members have redundant functions in mRNA regulation [96], it was later demonstrated that all have specific RNA binding affinities and distinct functions [97]. Physiologically, CELFs are crucial regulators for all kinds of developmental processes. This is especially well described for xenopus [98]. Besides, there are also several mouse models describing CELF-mediated shifting from fetal to adult alternative splice variants of several skeletal muscle transcripts [75] [99] [100]. Whereas it is experimentally confirmed that CELFs bind to C/UG-rich splicing acceptor sites, a prediction if this inhibits or activates AS is impossible, as it strongly depends on the cellular context [101].

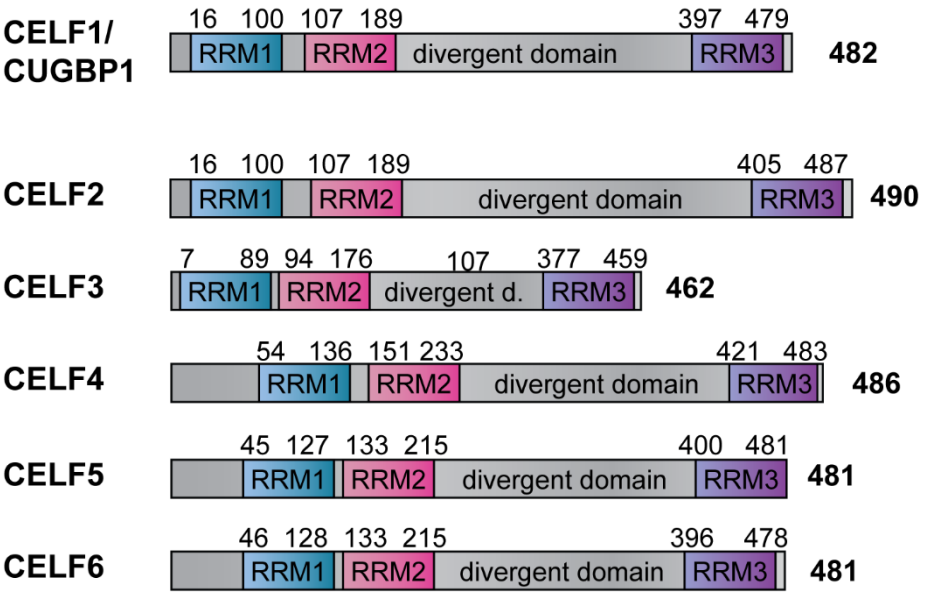

Figure 5: General structure of the CELF family members.
All CELF members consist of three RRMs: two N-terminal ones and one C-terminal RRM, with a divergent domain in-between that distinguishes them. Numbers indicate amino acids. Modified from [102].

CELFs preferentially bind to 15-22 nt long GU-rich sequences [103] [104] [105] whereas, most RBDs bind shorter (GU-rich) motifs like TAR DNA Binding Protein (TARDBP) [106]. GREs have defined consensus sequences based on the pentameric GUUUG (see Table 1) which was originally identified in human T-cells [71]. Today, it is known that GRE-containing transcripts appear in a variety of cells, including other immune cells, mouse brain cells or human cancer cells [84]. While the exact outcome mostly depends on cellular and environmental context, GREs also transfer instability when cloned in otherwise stable transcripts [71].

Table 1. Comparison of different GRE clusters.

Cluster	GRE sequences	Functional categories	Trans-acting factors
I	GUUUGUUUGUUUGUUUGUUUG	transcription factors, cell cycle, cell metabolism, cell–cell communication regulators	CELF1, CELF2, ELAVL4, RBM38, TARDBP, FUS
II	GUUUGUUUGUUUGUUUG		
III	GUKUGUUUGUKUG		
IV	KKGUUUGUUUGKK		
V	KKKU/GUKUG/UKKK		

GRE mRNAs were clustered (one mismatch allowed) into five subclasses based on the number of pentameric (GUUUG) repeats and surrounding sequences. K stands for G or U. Clusters I and II contain four or more overlapping GUUUG pentamers and are found in only a few hundred transcripts such as transcription factors, cell cycle regulators and intercellular communication genes. Clusters III, IV and V represent shorter sequences with less repetition and are found in several thousand transcripts. CELF: CUGBP Elav-Like Family Member; ELAVL4: Embryonic Lethal Abnormal Vision Like Neuron-Specific RNA Binding Protein 4; RBM38: RNA Binding Motif Protein 38; TARDBP: TAR DNA Binding Protein. Based on [107] and [72].

In the focus of this thesis is the CELF family member CUGBP1. It was first discovered in 1996 and described to regulate myotonic dystrophy type 1 (DM1) [108]. Initial SELEX experiments (systematic evolution of ligands by exponential enrichment) demonstrated that CUGBP1 preferably binds GU-repeat sequences (UGU) [104]. To date, it is also described to bind to GC-rich or even A-containing sequences [109]. CUGBP1 in general is known as an inhibitory post-transcriptional regulator. It is responsible for mRNA deadenylation [9], subsequent degradation [110] or AS [111] [112] and is conserved in a variety of species including humans, mice, drosophila and xenopus [113] [114]. It was found that knockdown of CUGBP1 led to a severe stabilization of GRE containing transcripts [115] [116] [117] which underlines its function as gene expression repressor. In contrast to its paralogue, CUGBP2 which rather stabilizes targets [118].

The activity of CUGBP1 is regulated via its phosphorylation status [119]. In total it has 9 described phosphorylation sites mostly on serines or threonines [120]. Through hyperphosphorylation by Protein Kinase C, CUGBP1 is stabilized and reveals elevated splicing activity in DM1 [121]. In mouse myoblasts, CUGBP1 is described to be phosphorylated at serine 28 by AKT Serine/Threonine Kinase 1, which influences its function as translational regulator during myocyte differentiation and murine heart development [122]. Finally, it was shown that phosphorylation by cyclin D3-CDK4/6 additionally interferes with CUGBP1's RNA binding capacity [123]. So overall, phosphorylation seems to be one key factor for CUGBP1 regulation on many levels.

As regulator of AS, CUGBP1-mediated exon skipping or inclusion depends on the developmental stage of the cell [112]. This function is best investigated in the context of DM1 [111]. The autosomal dominant neuromuscular disease is characterized by a trinucleotide repeat extension in the gene for myotonic dystrophy protein kinase (DMPK) resulting in an impaired gene expression [124]. In that regard, a balance between CUGBP1 and the splicing factor muscle blind like protein 1 (MBNL1) is essential. Gain of CUGBP1 function goes along with loss of function of MBNL1 which leads to AS of a variety of crucial transcripts [124]. The outcome can include heart conduction problems, impaired muscle strength, cataract development or insulin resistance [125]. Moreover, CUGBP1 influences ca. 50% of heart development-related transcripts by changing the splicing events between fetal and adult developmental stages [126].

Several promising studies with mouse models are investigating CUGBP1's effects on cardiac dysfunction and cardiomyopathy [126] [127]. However, CUGBP1 functions are too diverse to distinguish between effects based on AS, mRNA degradation or deadenylation. Interestingly, up to now it is not known how exactly CUGBP1 mediates deadenylation of human transcripts. Concerning mammalians, it is only known that CUGBP1 recruits PARN in the human hepatoma

cell line Huh7 [128] and cell-free assays [9]. Interaction with PARN surely does indicate involvement of deadenylation [84] but this is still under investigation. As deadenylation is a crucial step in degradation of mammalian transcripts [129] [130], it was consequential to investigate if CUGBP1 is involved in other mechanisms of mRNA decay. It is postulated that there exists some kind of CUGBP1-mediated decay process [71], but to date there are no studies elucidating the exact mechanism. It is well studied that CUGBP1 regulates whole networks of transcripts (regulons) involved in murine myoblast growth and differentiation, including crucial targets associated with cell cycle and survival [110]. In addition, CUGBP1 plays an important role in the rapid alteration of expression profiles during the activation of human T-cells through alternative polyadenylation [131]. In activated primary T-cells, hyperphosphorylation of CUGBP1 impairs its binding to target mRNAs. The results are increased protein levels of the targets which include a variety of proteins associated with an activated proliferative cell type [132].

Additionally, CUGBP1 also plays a role in the regulation of translation. It has activating properties, observed at many stages of cellular development [133] [134]. However, under stressful conditions CUGBP1 can also act as silencer and suppress translation in conjunction with several other proteins [135]. Additionally, the mode of action apparently depends on the context and cell type. It was recently described that in mesenchymal cells as well as MCF-10A breast cancer cells, CUGBP1 has a positive effect on translation of a variety of mRNAs involved in epithelial to mesenchymal transition (EMT) [136] [137]. Whereas in intestinal epithelial cells it represses translations of the insulin like growth factor 2 receptor mRNA. Overall, the mechanisms of how CUGBP1 is involved in translation, deadenylation and mRNA decay are not fully elucidated to date.

1.1.3 MicroRNAs (miRs)

MiRs are highly conserved non-coding RNAs and complete the complex network of post-transcriptional regulators covered within this thesis. MiRs are described as short single stranded RNAs of approximately 21 nt length. The first miR was discovered in 1993, when Lee et al. found lin-4 in the first larval stage of the nematode *C. elegans*. They discovered that this small RNA was able to repress the lin-14 gene expression by complementary binding to its 3'UTR [138]. The name "microRNA" was defined not before the year 2001, though [139].

There are several ways of miR biogenesis (see Figure 6). On the one hand, a subset of miRs is derived from introns (mirtrons) or even exons of protein-coding genes, meaning their expression is depending on the host gene [140] [141] [142]. On the other hand, miRs can also by transcribed from specific miR-genes by RNA polymerase II [143] [144]. Transcription of miR-genes creates so-called primary miRs (pri-miRs) which are further processed via splicing,

editing and polyadenylation [144] [145]. The double stranded pri-miRs are usually several hundred nucleotides long and form a hairpin structure [146] [147]. A large microprocessor complex comprising the RNA binding protein DiGeorge Syndrome Critical Region 8 (DGCR8) and the ribonuclease III Drosha further processes the pri-miR to generate the much shorter precursor-miR (pre-miR) [146] [148] [149]. In contrast, mirtron-derived pre-miRs are generated by the spliceosome and an additional processing step mediated by the debranching enzyme, to form a hairpin from a single stranded intron [150].

Nuclear export of all pre-miRs is then conducted by the shuttle protein exportin-5 which recognizes a two nt overhang at the 3' end of the hairpin [149]. During this energy consuming step, the Ras-related nuclear protein (RAN) provides the necessary guanosine triphosphate (GTP) [151]. Cytosolic pre-miRs need to be further processed. Therefore, the RNA Polymerase III Dicer is recruited [149] [152]. Enzymatically, the loop structure is removed from the hairpin by Dicer, resulting in an 18-22 nt long miR duplex [153]. Although either strand of the miR duplex is potentially functional, usually only one strand does fulfill physiological functions, while the other one is degraded [147] [154].

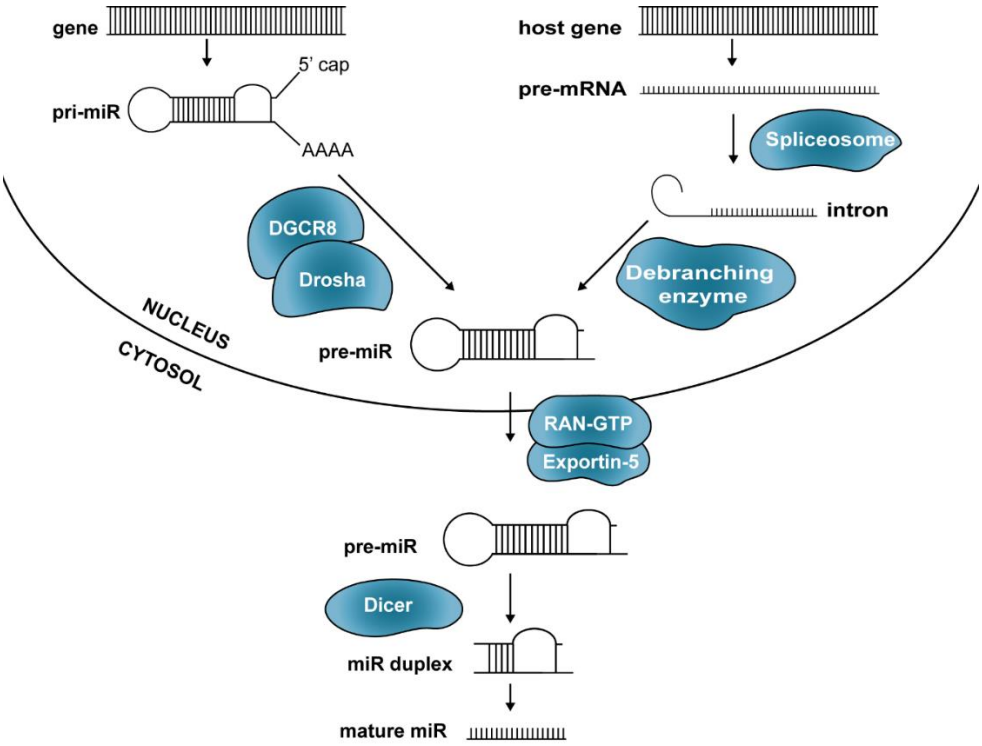

Figure 6: miR biogenesis.
miRs can either be transcribed from specific miR genes or spliced from intronic sequences of host genes. In the ladder case, the spliceosome and a debranching enzyme are necessary to generate the pre-miR. Specific miR genes produce an intermediate molecule called pri-miR which is capped and polyadenylated and further processed by Drosha to create the pre-miR. With the help of RAN-GTP and Exportin-5, the pre-miR is shuttled to the cytoplasm where it is processed by Dicer to generate a miR duplex, which finally leads to the mature miR of 18-22 nt length. Modified from [155].

MiRs fulfill an essential role in physiological homeostasis by regulating all kinds of cellular functions. Thus, it is no surprise that dysregulation of miRs can cause severe impairment of normal body functions and can lead to diseases including autoimmune conditions [156], heart [157] [158] [159] and kidney diseases [160], hereditary diseases such as non-symptomatic progressive hearing loss [161] and many different types of cancer [162].

Indeed, many miRs are associated with cancer development and progression and are intensively studied in that regard. In general, miRs that are associated with cancer are called oncomiRs [163]. This term applies to all miRs that show a differential expression level in tumor cells, if they act as oncogenes or tumor suppressors [164]. A prominent example is miR-21, which has been shown to be increased in most types of cancers including tumors of the colon, lung, breast, pancreas, as well as leukemia and lymphoma [165] [166] [167]. In contrast, in many tumors types, a global decrease in overall miR levels has been described [168] [169]. Additionally, a severe shortening of 3'UTRs was observed. Shorter 3'UTRs are beneficial because they provide a smaller number of miR binding sites, allowing for upregulation of oncogenes [170]. This is based on the canonical miR function as inhibitor of gene expression, which will be explained in the following chapter.

1.1.3.1 Canonical miR functions

Conventionally, miRs are known as global gene expression repressors. They bind to 3'UTRs of target mRNAs and impair proper translation or even lead to degradation of the mRNA. Either mechanism leads to a decreased protein level. This mode of action is called RNA interference (RNAi). Originally, it was described for small interfering RNAs (siRNAs) which act against viral infections [171].

Mainly in plants, miRs show a near perfect pairing, while target recognition in animals is mediated by a specific seed region within the miR sequence. It is located at position 2-8 on the 5' end of the miR [172]. In most cases, the seed region base pairs with responsive elements in the 3'UTR of the mRNA targets. Although, computational analysis reported that miR binding sites are also found all over 5'UTRs and coding-sequences [173] [174].

The key to canonical miR functionality is the formation of the RNA-induced silencing complex (RISC) [175]. This protein complex is formed minimally by Argonaute 2 (AGO2) [176] [177] and the respective miR, but usually it also comprises other proteins from the AGO family [178] as well as further RISC-associated proteins such as DEAD-box helicase 20 [179]. However, to date the exact composition of the RISC is not yet fully understood and seems to vary between studies.

The miR duplex is recruited to the RISC by Dicer. Within the complex, it is decided which strand of the duplex functions as guide strand and which one is degraded by RISC [180]. Usually, the

strand with higher 5' end stability is the functional one [181]. The bound miR is then used to target specific mRNAs via Watson-crick base pairing while the AGO proteins are responsible for the mode of action of gene regulation [180]. MiRISC can influence the gene expression of mRNA transcripts via two different mechanisms [182] [183]. Dependent on the level of complementarity, miR binding either leads to translational repression or RISC-mediated degradation of the mRNAs. These are the commonly known functions of miRs, however in the last few years diverse studies described a variety of further functions and modes of action that miRs are involved with.

1.1.3.2 Non-canonical miR functions

For a long time, miRs were only considered to bind to mRNAs and act as post-transcriptional repressors. Only a few years ago, it was discovered that miRs can also have a variety of totally different functions. For example, miRs which are secreted in exosomes are incorporated by donor cells and can interact with toll-like receptor 7/8 (TLR7/8) [184]. Fabbri et al. found that human miR-21 and miR-29a can both be secreted by tumor cells to act on human TLR8 or murine TLR7 in adjacent immune cells and induce a pro-inflammatory immune response [184]. In the following, several studies confirmed the interaction e.g. in the context of neuroblastoma [185], neuropathic pain [186] or murine myoblasts [187] or even in the context of Alzheimer's disease [188].

The discovery of this unusual miR function was accompanied by a variety of studies also describing novel modes of actions. For instance, miRs were found to act as activator or silencer of transcription. The first one was miR-327, which was described to induce Cadherin-1 (CDH1) and Cold Shock Domain Containing C2 (CSDC2) in human prostate cancer cells via a complementary promoter sequence [189]. Later, there was similar evidence for various other miRs, however the exact mechanism is still unclear.

Furthermore, miRs can also control miR maturation. For example, Let-7 forms a positive feedback loop by binding to its own pri-miR. In turn, further processing of the pri-miR is enhanced which elevates the mature let-7 levels in *C. elegans* [190]. On the other hand, miR-709 is able to block maturation of other miRs. It binds to a specific motif in the miR-15a/16-1 pri-miR structure in murine cells and inhibits further processing [191]. Moreover, miRs can also interact with other non-coding RNAs. It was found that 4% of all AGO-mRNA tags were associated with lncRNAs, indicating that miRs could recruit AGOs to lncRNAs to influence their stability or function [192].

This thesis focuses on the new non-canonical decoy function of miRs. Eiring et al. initially demonstrated that miR-328 can interact with the RBP hnRNP E2 [193]. In this context, miR-328 positively influences the gene expression of CCAAT/enhancer-binding protein alpha (CEBPA)

by acting as competitive inhibitor to hnRNP E2 in leukemic blasts. This new decoy function is independent of the miR's seed region and solely functions through interference with the RBP. In 2016, it was revealed that this novel mode of action does not only influence gene expression of CEBPA alone, but also S100A9 was validated as miR-328/hnRNP E2 decoy target in monocytes [194]. The list was recently extended to HMGB1 as well as 141 further proteins which were also predicted as decoy targets [195]. Hence, the miR-328 and hnRNP E2 decoy seems to have a global impact on a variety of targets and was even observed in different cell types.

Recently, this decoy mechanism was also described for miR-574-5p and CUGBP1 in A549 lung cancer cells [196] which will be discussed more closely in the following chapters.

1.1.3.3 MiR-574-5p

MiR-574-5p is a mirtron encoded in the first intron of the gene FAM114A1. This gene is coding for the nervous system overexpressed protein 20 (NOXP20), which is overexpressed in the brain [197] although NCBI GEO data [198] indicate that it might be expressed all over the body, especially in mesenchymal cells [199]. Nevertheless, there is still very little known about the function of NOXP20. Only the fact that it contains a caspase recruiting domain gives a hint that it might be involved in apoptosis [197]. It is implied that miR-574-5p expression is connected to NOXP20 expression. However, since there are no publications on the regulation of NOXP20 expression, no further conclusions can be drawn from that.

So far, only two publications describe how miR-574-5p expression is regulated. There is evidence that NFκB transcription factor p65 could regulate its transcription in mice in a context of neurological disorders [200]. Furthermore, it has been observed that the amyloid precursor protein APP influences the miR-574-5p level in the development of the cerebral cortex, although by an unknown mechanism [201].

Regulation of not the expression but rather the functionality of miR-574-5p is described more closely in literature. There are reports of three different lncRNAs to regulate miR-574-5p. While lncRNA-MFI2-AS1 (melanotransferrin) influences miR-574-5p in colon cancer cells [202], in breast cancer it is lnc-Zinc Finger Protein 469 (ZNF469)-3 which binds to miR-574-5p [203]. In papillary thyroid carcinoma cells, lnc-PTCSC3 (Papillary Thyroid Carcinoma Susceptibility Candidate 3) is described to have an impact by binding to miR-574-5p [204]. In this case, the interaction is further associated with Wingless-Type MMTV Integration Site Family Member 1 (Wnt) signaling. MiR-574-5p regulates β-catenin/Wnt-signaling via suppressor of cancer cell invasion (SCAI) and thereby influenced invasion and migration of the tumor cells [204].

Indeed, the relationship between miR-574-5p and Wnt signaling is described in several other studies. In colon and thyroid cancer, Wnt signaling was found to be activated by inhibition of

the RBP quaking (Qki) [205] [206]. In fact, miR-574-5p targets Qki-6/7 which results in a reduced protein level [205]. In turn, Qki no longer acts as suppressor of β-catenin and the Wnt signaling pathway is activated [207]. Both leads to further progression of tumor growth by facilitating proliferation and inhibiting apoptosis of the colon cancer cells. In contrast, miR-574-5p is also described to act anti-tumorigenic in two other colorectal cancer studies by targeting metastasis-associated in colon cancer protein 1 (MACC1) [208] or MYC Binding Protein (MYCBP) [202].

On the other hand, the influence of miR-574-5p on lung cancer development seems to be unambiguous. Several publications showed that miR-574-5p acts pro-metastatic and enhances tumor progression of (non-) small cell lung cancer ((N)SCLC) by targeting among others checkpoint suppressor 1 (CHES1) and protein tyrosine phosphatase receptor type U (PTPRU) [209] [210] [211]. Additionally, miR-574-5p also seems to promote cell growth in the context of coronary artery disease by binding to the mRNA of zinc finger DHHC-type containing 14 (ZDHHC14) [212]. Finally, miR-574-5p is described to repress the expression of ceramide synthase 1 (CerS1) together with HDAC1 [213], while it can also act in concert with miR-361-5p in white adipose tissue to regulate early B cell factor 1 (EBF1) [214].

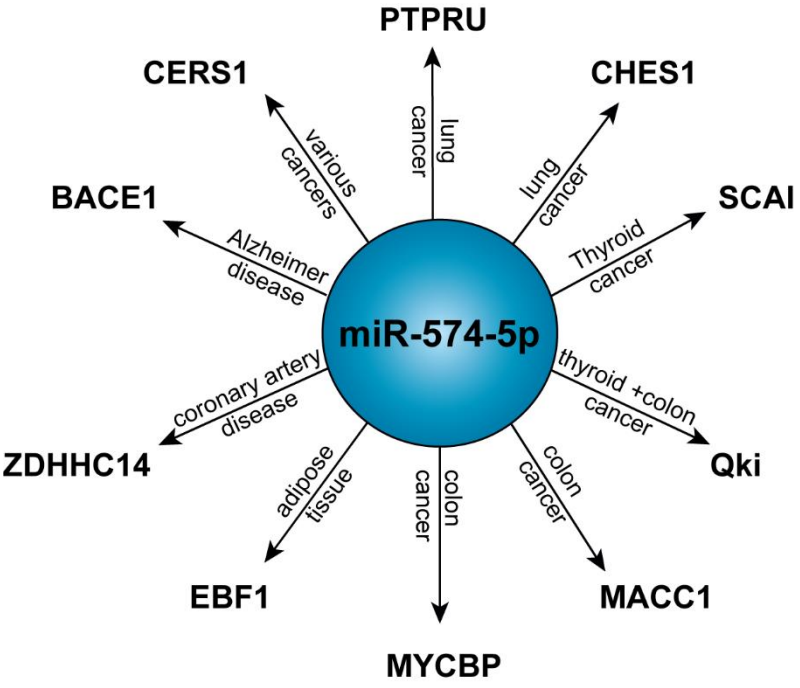

Figure 7: Canonical targets regulated by miR-574-5p.
miR-574-5p has been described to directly target a variety of mRNAs. Thereby, it influences various types of cancers, as well as cardiovascular and neurological conditions. miR-574-5p binds the mRNAs of the respective proteins, and downregulates the expression. Based on [200] [202] [204] [205] [206] [208] [209] [210] [211] [212] [213] [214].

It gets clear that miR-574-5p plays a role in a variety of diseases and cellular processes by direct interaction with various targets (see Figure 7). Besides the direct base pairing with a mRNA, miR-574-5p was recently described to interact with the RBP CUGBP1 [196]. By this mechanism, miR-574-5p has an impact on lipid metabolism and tumor progression which will be discussed in the next two chapters.

1.2 mPGES-1-derived PGE_2 in cancer development

In 2011, alteration in lipid metabolites was announced a hallmark of cancer [215]. Metabolic reprogramming of lipid mediators obviously also includes prostanoids such as prostaglandin E_2 (PGE_2). The metabolite PGE_2 is a bioactive lipid mediator which shows great importance in the regulation of a variety of physiological and pathophysiological processes, such as inflammation, pain and tumorigenesis [216] [217] [218] [219]. It is generated in a first step by the enzymes cyclooxygenase (COX)-1 or COX-2 by converting arachidonic acid to PGH_2.This instable intermediate is then further converted by microsomal prostaglandin E2 synthase 1 (mPGES-1) [220]. The generated PGE_2 is secreted by the cell and elicits a wide range of pro-tumorigenic functions by binding to the EP1-4 receptors. High levels of mPGES-1 could be observed in various types of cancers including colon [221], prostate [222] and lung cancer [223]. Increased levels of COX-2 as well as mPGES-1 are further associated with a poor overall survival rate [224]. MPGES-1 activity does not only have an impact on pain and inflammation in the tumor microenvironment but also enhances the progression of the tumor itself. Moreover, PGE_2 is responsible for the crosstalk of cancer and stromal cells within the tumor tissue. The result is a highly efficient immune evasion, which facilitates further tumor growth [219]. One example is cervical cancer-derived PGE_2 which was observed to induce monocyte differentiation into tumor-associated macrophages (TAMs) [225]. Furthermore, PGE_2 not only suppresses an anti-tumorigenic immune response but also facilitates tumor growth directly [226]. In the case of breast cancer, PGE_2 leads to lymph angiogenesis while the EP4 receptor seems to be the most important one in that context [227]. Also in lung cancer, EP4 is the crucial receptor, leading to enhanced tyrosine kinase c-Src activation and subsequently to an increased tumor growth as well as metastasis [228].

Overall, there are numerous publications describing the influence of PGE_2 on tumor progression (for reviews see [218] [229] [230] [231]). Therefore, it is no surprise that the pro-tumorigenic properties of PGE_2 attracted great attention to potential pharmacological inhibition of its synthesis. However, current approved medication to interfere with the negative effects of PGE_2 comprise only inhibitors of the COX enzymes. Especially in long time treatment, these therapeutic approaches show severe side effects like increased cardiovascular events or gastrointestinal bleeding [232] [233] [234] [235] [236]. With inhibition of the COXs, other

prostanoids like PGD_2, prostacyclin (PGI_2) and thromboxane (TXA) are also impaired (see Figure 08). For this reason, it would be much more reasonable to target mPGES-1 rather than COX-2 [237]. Inhibition of mPGES-1 would minimize side effects [238] and hypothetically also cause a shift towards PGI_2 and PGD_2, which would be beneficial for the cardiovascular system. [239] [240]. Several studies have shown that genetic deletion or pharmacological inhibition of mPGES-1 is indeed a promising tool against tumor growth [222].

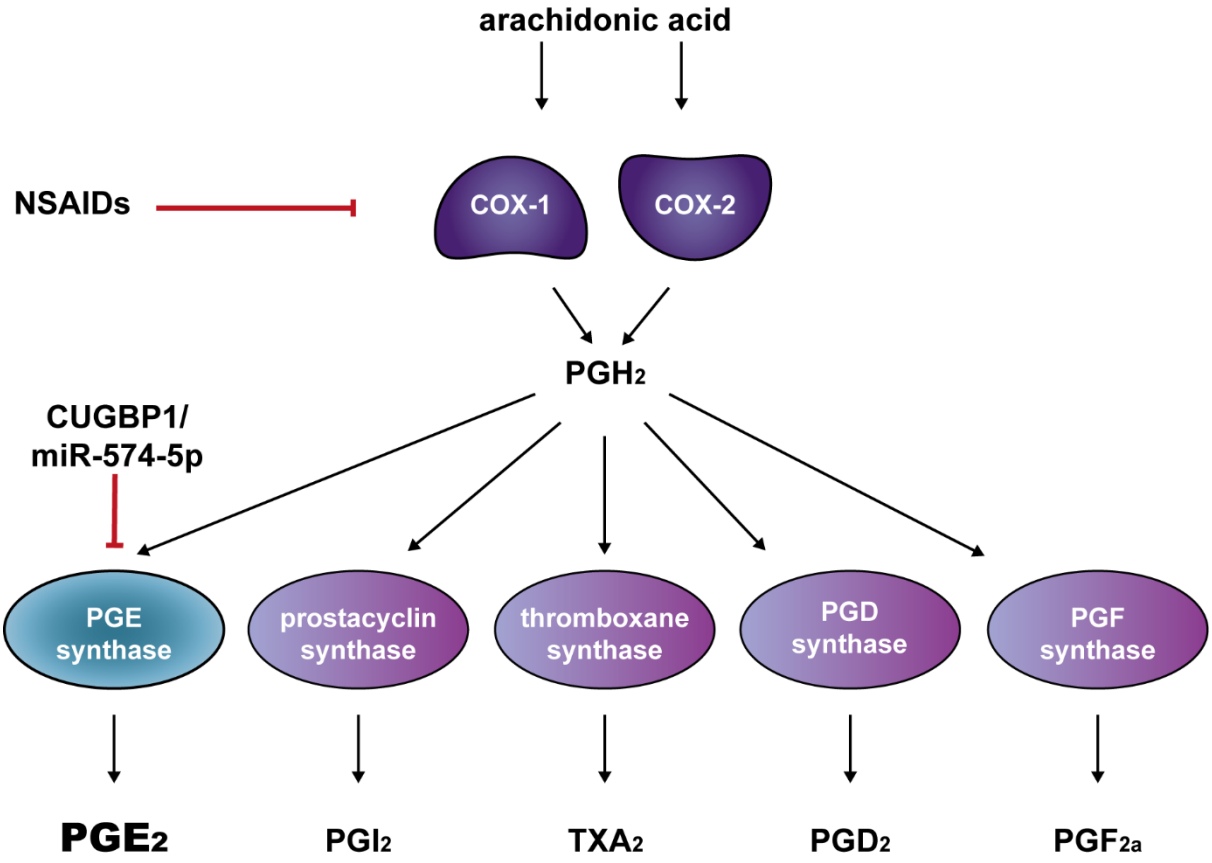

Figure 8: Prostanoid biosynthesis.
Arachidonic acid is converted by either COX-1 or COX-2. The resulting instable intermediate PGH_2 is then further processed by respective synthases to generate the prostanoids PGE_2, PGI_2, TXA_2, PGD_2 or PGF_{2a}. NSAIDs inhibit COX enzymes and therefore all prostanoids downstream of PGH_2. Therefore, inhibition of only PGE synthase (mPGES-1) by CUGBP1/miR-574 decoy would be more beneficial and should not affect other prostanoids. Modified from [241].

However, most of the developed mPGES-1 inhibitors have a problematic limitation: they do not work in mouse or rat models, since mPGES-1 is not conserved in rodents [242]. As murine and human mPGES-1 differ in three amino acids near the active site of the enzyme [243], the majority of human inhibitors does not repress the murine enzyme activity. Therefore, any kind of pre-clinical study is impossible, due to a lack of established animal models. An exception is Compound III which inhibits both human and murine mPGES-1 [244] [245] [246] [247] and was already shown in pre-clinical studies to be an efficient tool against neuroblastoma [246].

Besides pharmacological inhibition of mPGES-1, recently a post-transcriptional regulation mechanism was unravelled which will be described more closely in the next chapter.

1.2.1 Regulation of mPGES-1 by the miR-574-5p/CUGBP1 decoy mechanism in human lung cancer

Recently, the PGE_2-generating synthase mPGES-1 was found to be regulated in a non-canonical way [196]. Until then, it was not much known about post-transcriptional regulation of mPGES-1. In its 3'UTR there are two long GREs which represent binding sites for the RBP CUGBP1. A similar sequence can be found in miR-574-5p. In an inflammatory environment like stimulation with IL-1β, miR-574-5p is able to sequester CUGBP1 away from the mPGES-1 mRNA (see Figure 9). This eliminates the negative influence of the RBP and additionally results in an AS event. The mPGES-1 3'UTR is spliced which removes a conserved ALU element in between the two GREs. The shorter splice variant has a higher translational rate. Therefore, the decoy has an overall enhancing effect on mPGES-1 gene expression [196].

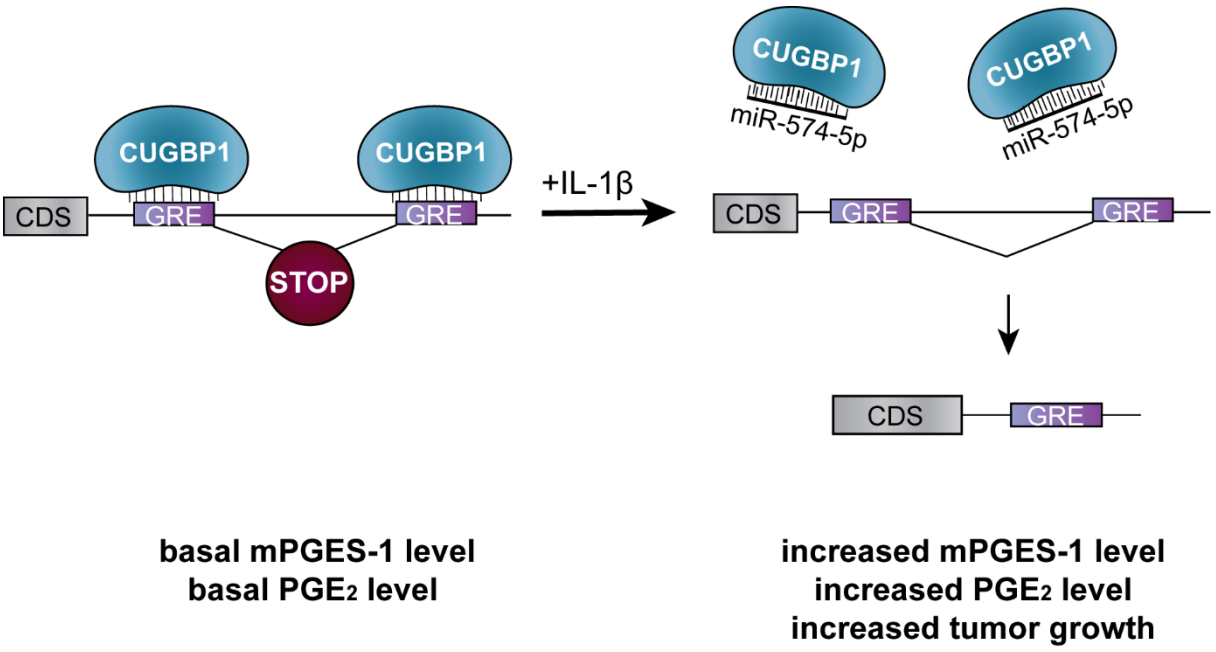

Figure 9: Regulation of mPGES-1 gene expression via the miR-574-5p/CUGBP1 decoy mechanism.
CUGBP1 binds to two GREs within the mPGES-1 3'UTR. Upon IL-1β simulation, miR-574-5p acts as decoy to CUGBP1, preventing it from binding to the GREs. This results in an AS event creating a shorter 3'UTR isoform with a higher translational rate. As a result, mPGES-1 levels and PGE_2 synthesis are increased as well as subsequent tumor growth *in vivo.* Modified from [196].

The increased mPGES-1 protein level then leads to a higher level of its enzymatic product PGE_2. As described above, PGE_2 has a crucial influence on the progression of cancer. In a xenograft mouse model, it could be demonstrated that this decoy mechanism has a tremendous impact on lung tumor growth. When miR-574-5p overexpressing lung cancer cells were injected into nude mice hind flanks, it was revealed that they displayed a strongly increased proliferation. The tumor weight and volume was significantly increased compared to control tumors. Moreover, urinary PGE-M levels linked this to enhance PGE_2 formation. Interestingly, progression of miR-574-5p overexpressing tumors was reduced back to control level with the simultaneous administration of the mPGES-1 inhibitor Compound III. This proved that the pro-tumorigenic effects of miR-574-5p were solely caused by the decoy-mediated mPGES-1 induction [196]. This conclusion is consequential because a delayed growth of murine xenograft tumors was already observed upon mPGES-1 knockdown in an earlier study [222]. Hence, this new non-canonical mPGES-1 regulation mechanism is an intriguing research topic in the context of future lung cancer research.

1.3 Aim of the study

With the discovery of the new decoy mechanism in human lung cancer, it would be possible for the first time to regulate mPGES-1 expression on mRNA level. In order to further characterize the miR-574-5p/CUGBP1 decoy in lung cancer, a TMT-based proteomics study was used to unravel the overall impact on cellular protein levels. It should be revealed if the miR-574-5p/CUGBP1 decoy has a global impact similar to the miR-328/hNRNP E2 decoy or if mPGES-1 could be the only target. In that case, this would open up new options for NSCLC patients. Not all patients benefit from a treatment with medication that aims to reduce PGE_2 levels [248] [249]. Potentially, because not all lung adenocarcinomas are comparably PGE_2-dependent. Therefore, levels of miR-574-5p could be used as stratification marker in order to identify those patients with higher mPGES-1 and PGE_2 levels. For this subgroup, a treatment with COX inhibitors could be highly beneficial in the fight against NSCLC.

2. Materials and Methods

2.1 Cell culture methods

2.1.1 Cell culture conditions

The human cell line A549 (ATCC Manassas, VA, USA) is derived from a 58-year old male with lung adenocarcinoma. Cells were cultured in Dulbecco's modified Eagle medium (DMEM, Life technologies) supplemented with 10% (v/v) fetal calf serum (FCS; Life technologies), 100 U/mL penicillin (PAA the Cell Culture Company) 100 µg/mL streptomycin (PAA the Cell Culture Company) and 1 mM sodium pyruvate (PAA the Cell Culture Company) (= fully complemented medium). Cells were grown in T75 cell culture flasks under standard growth conditions (humidified atmosphere of 5% CO_2 at 37°C). When the cells reached a confluence of ~ 70-90%, medium was aspirated and cells were washed with pre-warmed phosphate buffered saline (PBS). Then, they were detached using pre-warmed Trypsin-EDTA (Invitrogen) at 37°C for 5 min. Reaction was stopped adding pre-warmed full culture medium (1:1) to the cells and number of viable cells was examined by trypan blue staining and counted using Bio-Rad TC10 automated cell counter (both Bio-Rad Laboratories). Approximately 1 million cells were transferred into a new T75 culture flask. For all experiments, cells were seeded in 6-well plates à $5x10^5$ cells per well in 2 mL medium. Except for RIP assays, where 3×10^6 A549 cells were seeded in 10-cm dishes in 10 mL medium.

For preparation of liquid nitrogen stocks, A549 cells were detached as described above and resuspended in medium containing 10% (v/v) DMSO (Carl Roth). The suspension was transferred into cryo vials (VWR) and stored at -80°C for 2 days. Afterwards, cryo vials were transferred into a liquid nitrogen tank until further use. In order to thaw cells again, the cryo vials were carefully pre-warmed at room temperature until suspension began to thaw. Then, pre warmed medium was added and the cryo vial was rinsed until the whole suspension was thawed and transferred in a 50 mL reaction tube. Cells were precipitated in a centrifuge for 5 min at 1,200 rpm (Eppendorf Centrifuge 5702), to remove DMSO. Supernatant was discarded, the cell pellet was resuspended in fresh pre-warmed medium and transferred in a T75 cell culture flask.

2.1.2 Depletion of CUGBP1 using RNA interference

By using siRNA oligonucleotides, CUGBP1 was transiently knocked down. Therefore, a previously published siRNA (5´-GCUGUUUAUUGGUAUGAUU-3´) was used. 24 h prior to transfection, A549 cells were seeded in a 6-well plate as described above. For transfection, 20 pmol/µL siRNA oligonucleotides were transfected using Lipofectamin2000® (Invitrogen) according to manufacturer's instructions. A siRNA against GFP, naturally not expressed, was

designed (5´-UCUCUCACAACGGGCAUUU-3´) and used as negative control. After 24 h, cells were stimulated with 5 ng/mL interleukin (IL)-1β (Sigma-Aldrich). Further 24 h later, the samples were harvested using 500 µL pre-warmed Trypsin-EDTA (Invitrogen) as described above. Transfection efficiency was tested by Western blot analysis (see chapter *2.3.3 SDS-PAGE and Western Blot*).

2.1.3 Overexpression of miR-574-5p

For transient overexpression (oe) of miR-574-5p, the miRIDIAN hsa-miR-574-5p mimic (HMI0794, Sigma-Aldrich) and negative control (HMC0002, Sigma-Aldrich) were used. A549 cells were seeded 24 h prior to transfection in a 6-well plate. 20 pmol/µL per well of the mimics or control were transfected using Lipofectamin2000® (Invitrogen) according to the manufacturer´s instructions. After 24 h, cells were stimulated with 5 ng/mL IL-1β (Sigma-Aldrich). Further 24 h later, the samples were harvested using 500 µL pre-warmed Trypsin-EDTA (Invitrogen) as described above. The efficiency was assessed by qRT-PCR analysis (see chapter *2.2.2 mRNA or miR quantification by qRT-PCR*) as stated in [196].

For stable overexpression of miR-574-5p, the lentiviral particles Mission® lenti miR-574-5p (HLMIR0794, Sigma-Aldrich) or Mission® lenti control (NCLMIR001, Sigma-Aldrich) were used. A549 cells were seeded at a density of 5 x 10^5 per well in a 6-well plate 24 h prior to transduction. Lenti viral particles were rapidly thawn and added to the cells at a MOI of 0.83 for spinoculation (875 x g, at 32°C for 60 min). Transduced cells were incubated for 24 h in fully complemented DMEM before 10 µg/mL puromycin (Sigma-Aldrich) were added for four days to select the transduced clones. These stable A549 miR-574-5p overexpression and control cell lines were generously provided by Stefan Stein, Georg-Speyer Haus, Frankfurt [196]. The transduction efficiency was verified by qRT-PCR (see chapter *2.2.2 mRNA or miR quantification by qRT-PCR*).

2.1.4 Depletion of miR-574-5p by LNA™ inhibitors

Transient depletion of miR-574-5p was achieved using LNAs™ from Exiqon (miR-574-5p-LNA™ inhibitor and negative control MIMAT0004795). A549 were seeded 24 h prior to transfection at a density of 5 x 10^5 cells in a 6-well plate. 40 pmol/µL per well was transfected using Lipofectamin2000® (Invitrogen) according to manufacturer's instructions. After 24 h, cells were stimulated with 5 ng/mL IL-1β (Sigma-Aldrich). Further 24 h later, the samples were harvested using 500 µL pre-warmed Trypsin-EDTA (Invitrogen) as described above. Efficiency of the knockdown was measured by qRT-PCR analysis (see chapter *2.2.2 mRNA or miR quantification by qRT-PCR*) as stated in [196].

2.1.5 Wound healing assay

For determination of migratory behavior of A549 cells, wound healing assays were performed with stable A549 miR-574-5p overexpression and control cells. Therefore, cells were seeded in 6-well plates as described above. In order to minimize proliferation, cells were pre-starved for 24h in Opti-MEM (Life technologies). Each condition was assessed in duplicates. Scratching was performed in the middle of the well using a 10 µL pipette tip. Remaining cell debris was washed away with pre-warmed PBS, before reduced culture medium was applied (only containing 2% FCS). Images were taken immediately after scratching at time point t0 and after 24 h as described in chapter *2.6.2 Wound healing assay images*.

2.1.6 Trans-well migration assay

Trans-well assay, also called Boyden chamber assay, was performed with stable A549 miR-574-5p overexpression and control cells. Cultured cells were detached as described above and sedimented for 5 min at 1,200 rpm (Eppendorf Centrifuge 5702). The cell pellet was then resuspended in serum-free culture medium without any FCS. 5 x 10^4 cells were seeded in a volume of 100 µL in a 24-well cell culture insert (Corning, Cat. No. 353097). Those inserts have a membrane on the bottom with 8 µm pores to enable migration of A549 cells. The inserts were placed in a 24-well plate and cells were allowed to adhere for 20 min at room temperature. Subsequently, the bottom of the wells was filled with 700 µL of full complemented culture medium to encourage migratory behavior (see Figure 10). As negative control, one well was filled with serum-free medium which restrains migration.

Samples were cultured for 5 h at 37°C. Then, the inserts were washed in PBS. Non-migrated cells that were still on the inside of the insert were removed by swiping. Migrated cells on the bottom of the insert were fixed for 3 min at room temperature by placing the inserts in new wells filled with 700 µL of methanol (VWR). Afterwards, cells were stained with 0.5% crystal violet (Carl Roth) for 10 min at room temperature. Residual dye was remove by washing the inserts with autoclaved Millipore water (MQ) followed by an additional swiping step to remove cells from the inside of the insert. The membranes were then cut out using a scalpel and were mounted on cover slides with Pertex® (VWR). Number of violet migrated cells was counted under a light microscope using a manual cell counter. The protocol was kindly provided by Dr. Kati Turkowski and PD Dr. Rajkumar Savai, Max-Planck-Institute for Heart and Lung Research, Bad Nauheim.

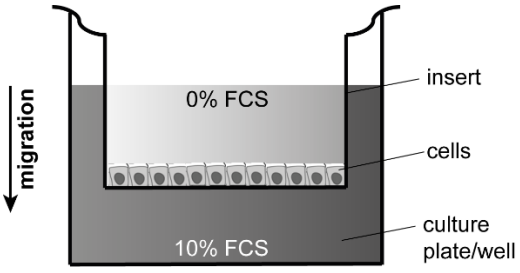

Figure 10: Boyden chamber set-up.
Cells are seeded in a cell culture insert with a membranous bottom (pore size 8 µm) and migrate towards an increased FCS concentration. After 5 h, migrated cells on the bottom of the membrane can be fixed, stained and counted under a light microscope.

2.2 RNA methods

2.2.1 RNA extraction

Total RNA was extracted using TRIzol Reagent (Invitrogen) performing a standard phenol chloroform protocol. In short, cell pellets were resuspended in an appropriate amount of TRIzol and incubated for 5 min. Then, 200 µL Chloroform (Carl Roth) were added and samples were thoroughly mixed before incubation on ice for 15 min. After centrifugation for 15 min at 4°C with 17,000 x g, the upper aqueous phase containing the RNA was transferred to a fresh tube and 500 µL isopropanol (VWR), 5 µL 3M sodium acetate (pH 6.5) (Carl Roth) and 1 µL GlycoBlue™ (Thermo Fisher Scientific) were added and mixed. Samples were incubated further 15 min on ice before another centrifugation step was performed. The precipitated RNA pellet was then dissolved in an appropriate amount of MQ. The RNA was then treated with Turbo DNase (Ambion) for 5 min according to the manufacturer's instructions to remove residual DNA. DNase digested RNA was incubated for 30 min at -80°C together with 100 µL ethanol (VWR), 2 µL 3 M sodium acetate (pH 6.5) and 1 µL Glyco blue™. RNA was then precipitated for 30 min at 17,000 x g at 4°C. The pellet was washed with 70% ice-cold ethanol by rinsing the pellet and a subsequent centrifugation for 5 min at 17,000 x g at 4°C. The RNA pellet was air dried for 5 min at room temperature and resuspended in an appropriate amount of MQ. RNA concentration and purity were then measured by UV spectroscopic measurement using the NanoDrop ND-1000 spectrophotometer (Thermo Fischer Scientific).

2.2.2 mRNA or miR quantification by qRT-PCR

For mRNA quantification, 1 µg of DNase-treated RNA was used for reverse transcription. Therefore, the High-Capacity RNA-to-cDNA Kit (Applied Biosystems) was used according to manufacturer's instructions. Generally, 10 µL 2x RT buffer and 1 µL RT enzyme were added to a RNA mix in 9 µL. Reverse transcription was conducted in a thermo cycler (Bio-Rad Laboratories) for 1 h at 37°C and 5 min at 95°C. Real-time PCR was then performed with the StepOne Plus™ Real-Time PCR System (Applied Biosystem) using Power Syber Green PCR Master Mix (Applied Biosystems). The PCR program can be found in Table 2. In general, one reaction contained 10 µL 10x Sybr Green Mastermix, 3.75 µL forward Primer (2 µM diluted in

MQ), 3.75 µL reverse Primer (2 µM diluted in MQ), 1.5 µL MQ and 1 µL cDNA (1:2 diluted in MQ). Each sample was set up in duplicates. To normalize variations in cDNA quantities throughout the samples, β-Actin was used as housekeeping gene. Fold inductions were calculated using the $2^{(-\Delta Ct)}$ method. A list of primers can be found in Table 3.

Table 2. PCR program for mRNA quantification

Step	Temperature	Time	Repeats
Initial denaturation	95°C	20 s	x
Denaturation	95°C	3 s	40 cycles
Annealing & Elongation	60°C	30 s	
	95°C	15 s	x
Melt curve	60°C	1 min	x
	95°C	15 s	x

Table 3. Primer used for qRT-PCR

Target	forward primer sequence	reverse primer sequence
β-Actin	CGGGACCTGACTGACTAC	CTTCTCCTTAATGTCACGCACG
cJun	TCG ACA TGG AGT CCC AGG A	GGC GAT TCT CTC CAG CTT CC
SMAD2	GGGATGCTTCAGGTAGGACA	TCTCTTTGCCAGGAATGCTT
SMAD3	CGCAGAACGTCAACACCAAG	GGCGGCAGTAGATGACATGA
COX-2	CCGGGTACAATCGCACTTAT	GGCGCTCAGCCATACAG
NDUFS2	GTTTTGCCCATCTGGCTGGT	CATGCCATGGCCTATGGTGAA
mPGES-1	GAAGAAGGCCTTTGCCAAC	CCAGGAAAAGGAAGGGGTAG
UBE2R2	ATGTGGCACCCCAACATT	TCCACCTTTCAGAAGGCAGT
CEP41	ACAGAACCCAAGATACCAGCATAT	GGGAGCTGGTAAGATACACACA
SLC39A6	GCACTTACTGCTGGCTTATTCA	CGGCTACATCCATGGTCACT
PAIP2	CCATTTGCAGAGTACATGTGGA	CCGTACTTCACCCCAGGAAC
GTF2E2	CCATGCAGGAATCTGGACCA	AATCCTTCAGCACTCCAGCC
LEO1	ACTGCCCAACTTTCTCAGTGT	AGATGATTGTGGTCGCCCTG

For miR quantification, the Qiagen miScript system was used according to manufacturer's instructions. One reverse transcription reaction comprised of 4 µL 5x miScript HiSpec Buffer, 2 µL 10x miScript Nucleic Acid Mix, 2 µL reverse transcriptase and 1 µg DNase digested RNA in MQ ad 20 µL. The reverse transcription was performed for 1 h at 37°C and 5 min at 95°C using the thermo cycler (Peqlab Biotechnologie GmbH, advanced primus 25). CDNA was diluted 1:2 in MQ afterwards. Following, real time PCR was performed using either the miR-574-5p specific primer (MS00043617, Qiagen) or miR-16-5p (MS0031493, Qiagen). Real-time PCR was performed according to the manufacturer's instructions (see Table 4). Generally, a mix for one reaction contained 12.5 µL QuantiTect Syber Green Mastermix, 2.5 µL 10x miScript Universal primer, 2.5 µL specific primer, 1 µL miScript cDNA and 6.5 µL MQ. Fold inductions were calculated as described above.

Table 4. PCR program for miR quantification

Step	Temperature	Time	Repeats
Initial denaturation	94°C	15 s	x
Denaturation	94°C	15 s	40 cycles
Annealing	55°C	30 s	
Elongation	70°C	30 s	
	94°C	15 s	x
Melt curve	60°C	1 min	x
	95°C	15 s	x

2.2.3 RNA immunoprecipitation (RIP)

The RIP protocol was kindly provided by Prof. Michaela Müller-McNicoll, Goethe University Frankfurt. In order to precipitate CUGBP1, the GammaBind Plus Sepharose beads (GE Healthcare) were used. In preparation, the beads were blocked with blocking buffer containing 0.2 mg/mL bovine serum albumine (BSA) in PBS (Sigma-Aldrich) and 0.1 mg/mL yeast tRNA for 90 min at 4°C. Then, beads were washed with PBS and stored at 4°C until further use.

A549 cells were seeded at a density of 3 x 10^6 in a 10-cm dish and incubated overnight. In case of stimulation, 5 ng/mL IL-1β were added for further 24 h. In order to harvest the cells, they were washed with 5 mL of ice-cold PBS and scraped in 5 mL PBS complemented with protease inhibitor EDTA-free (Roche). Cells were spinned down for 5 min and 400 x g at 4°C and resuspended in 1 mL lysis buffer (see Table 5). The suspension was incubated 10 min on ice and then sonicated 4 times for 10 seconds on 30% amplitude, with 20 sec pause (Branson Sonifier 250). Then, cell debris was spinned down for 10 min at 10,000 x g at 4°C. The supernatant was transferred into a fresh tube and 10% were taken as input sample.

Before usage, the blocked beads were washed 3 times with lysis buffer and were centrifuged at 300 x g for 5 min. Beads and antibodies were linked by mixing 50 µL bead suspension with 10 µg of CUGBP1 antibody (05-621 clone3B1, Merck) or normal mouse IgG antibody (12-371, Merck) followed by incubation for 30-60 min at 4°C. Afterwards, immunoprecipitation (IP) was conducted by dividing the lysate equally to the CUGBP1- /IgG-bead mixture and incubating for 2 h at 4°C. Then, samples were washed with each wash buffer B1-B3 (composition see Table 5) for 5 min in the cold room, with centrifugation steps of 5 min and 300 x g in between. After the last washing step, 10% of each precipitate was taken for Western blot analysis in order to validate the immunoprecipitation (see chapter 2.3.3 SDS-PAGE and Western Blot). The remaining precipitates were resuspended in 500 µL TRIzol reagent (Invitrogen) and RNA was isolated as described above (see chapter 2.2.1 RNA extraction). Thereby, it was important to take the exact same volume of aqueous phase from each sample, since the complete isolated RNA was then used for reverse transcription.

Since there was no housekeeping gene for analysis of the real time PCR, data analysis was conducted without building a difference to a Ct of a housekeeping gene. After calculating the $2^{(-Ct)}$, the Input value was multiplied by 10 to even out that it was 10% of the total cell lysate, while IgG-IP and CUGBP1-IP values were multiplied by 1.11 since 10% were taken for Western blot analysis and 90% were left. Then, a x-fold was calculated to obtain the RNA enrichment and the yield. The yield describes the amount of precipitated RNA in percent compared to the input, while the enrichment shows the specificity of CUGBP1-IP in comparison to IgG-IP. In this thesis, the graphs will depict the enrichment, as it gives the information if a certain RNA is indeed bound by CUGBP1.

$$yield = \frac{2^{-CT\ of\ IP} \times 1.11}{2^{-CT\ of\ 10\%Input} \times 10}$$

$$enrichment = \frac{2^{-Ct\ of\ CUGBP1} \times 1.11}{2^{-CT\ of\ IgG} \times 1.11}$$

Table 5. RIP buffer composition

Buffer	End concentration	Reagent
Hypotonic lysis buffer	10 mM	Tris-HCl pH 7.5 (Sigma-Aldrich)
	10 mM	KCl (Sigma-Aldrich)
	1.5 mM	$MgCl_2$ (Sigma-Aldrich)
	0.5 mM	Ll fac (Carl Roth)
	0.9%	NP-40 (Igepal) (Sigma-Aldrich)
	1x	Protease inhibitor cocktail (Roche)
	40 U/µL	Ribonuclease Inhibitor
	Ad 10 mL	MQ
Wash buffer B1	20 mM	Tris-HCl pH 7.5 (Sigma-Aldrich)
	150 mM	NaCl (Sigma-Aldrich)
	2 mM	EDTA (Roche)
	0.1%	SDS (Carl Roth)
	1%	Triton X-100 (Carl Roth)
	1x	Protease inhibitor cocktail (Roche)
	Ad 10 mL	MQ
Wash buffer B2	20 mM	Tris-HCl pH 7.5 (Sigma-Aldrich)
	500 mM	NaCl (Sigma-Aldrich)
	2 mM	EDTA (Roche)
	0.1%	SDS (Carl Roth)
	1%	Triton X-100 (Carl Roth)
	1x	Protease inhibitor cocktail (Roche)
	Ad 10 mL	MQ
Wash buffer B3	10 mM	Tris-HCl pH 7.5 (Sigma-Aldrich)
	250 mM	LiCl (Sigma-Aldrich)
	1 mM	EDTA (Roche)
	1%	Na Deoxycholate (Sigma-Aldrich)
	1%	NP-40 (Igepal) (Sigma-Aldrich)
	1x	Protease inhibitor cocktail (Roche)
	Ad 10 mL	MQ

2.3 Protein methods

2.3.1 Soluble and microsomal fraction preparation

As described in [250] [195], cell pellets of A549 cells were resuspended in 1 mL homogenization buffer (0.1 M potassium phosphate (Carl Roth) pH 7.4, 0.25 M sucrose (Scharlau), and EDTA-free protease inhibitor (Roche)). The suspension was then sonicated 4 x 10 seconds on ice with 20 seconds pause (Branson Sonifier 250). To remove all debris, samples were centrifuged with 5,000 x g at 4°C for 10 min and the supernatant was transferred in ultracentrifugation tubes. Then, samples were centrifuged at 100,000 x g at 4°C for 1 h (using Beckmann Optima XL-100K). The resulting supernatants contained the soluble fractions and were stored at -80°C while, the pellets were mixed with 500 µL 2.5 M NaBr (Sigma-Aldrich) and incubated for 45 min on ice with shaking. Another centrifugation step was performed at 4°C for 1 h at 100 000 x g. The supernatant containing membrane associated fraction was discarded, while the pellets resembled the microsomal protein fraction. They were resuspended in PBS supplemented with EDTA-free protease inhibitor (Roche) and sonicated on ice to improve dissolving of the proteins. All samples were stored at -80°C until further use. Concentration for Western blot analysis was measured using Bradford assay (Bio-Rad Laboratories) (see next chapter) while for proteomics samples the protein amount was determined by Pierce BCA Protein Assay (Thermo Fisher Scientific) following manufacturing instructions.

2.3.2 Determination of protein concentration

Concentration of the protein solution was determined by Bradford assay (Bio-Rad Laboratories) according to manufacturer's instructions. A standard curve with bovine serum albumin (BSA) concentrations of 50-500 µg/mL was used. 10 µL of the different BSA solutions or protein samples (diluted 1:20 in MQ) were mixed in a 96-well plate and 190 µL of Bradford reagent (diluted 1:5 in MQ) was added. Each sample and standards were measured in duplicates. The absorption at a wavelength of 595 nm was measured at a Tecan Infinte M 200 (Tecan Group). The protein concentration was calculated according to the standard curve.

2.3.3 SDS-PAGE and Western Blot

Proteins were separated by Sodium dodecyl sulfate polyacrylamide gel electrophoresis (SDS-PAGE). Depending on the approach, either 80 µg of soluble/microsomal proteins or for RIP samples 20 µL were mixed with 5 µL 4x protein loading buffer containing 50% glycerine, 1.5% bromphenol blue, 4% SDS, 15% β-Mercaptoethanol (all Carl Roth). Samples were then boiled for 5 min at 95°C in order to denature proteins and loaded on a 12% SDS-Gel (composition see Table 6). As a marker the Precision Plus Protein™ All Blue Standard (Bio-Rad

Laboratories) was also applied and the gel ran for ca. 1 h at 120 V. Afterwards, proteins were transferred to a HyBond ECL nitrocellulose membrane (Amersham) with 230 mA for 80 min. Subsequently, membranes were blocked with Odyssey blocking buffer (LI-COR® Bioscience) for 1 h at room temperature. Then, they were incubated over night at 4°C with primary antibodies (see Table 7). The next day, membranes were washed 3 times with PBS pH 7.4 complemented with Tween20 0.1% (v/v) (Carl Roth) (PBS-T) to remove residual unbound antibody. Then an infrared dye conjugated secondary antibody (IRDye®, *LI-COR*® Bioscience) directed against the certain host animal, was incubated on the membranes for 45 min at room temperature. Membranes were washed three times with PBS-T before visualization. Detection and quantification were performed using the Odyssey Infrared Imaging System (LI-COR® Biosciences) and the Image Studio Software.

Table 6. Gel composition for SDS-PAGE

Stacking gel (7.4 %)		**Separating gel (12%)**	
MQ	1.2 mL	MQ	1.6 mL
Acrylamide 30% (w/v)	266 µL	Acrylamide 30% (w/v)	2 mL
Tris-HCl, 0.5 M, pH 6.8	500 µL	Tris-HCl, 1.5 M, pH 8.8	1.3 mL
SDS 10% (w/v)	20 µL	SDS 10% (w/v)	50 µL
APS 10% (w/v)	12 µL	APS 10% (w/v)	50 µL
TEMED	3 µL	TEMED	4 µL

Table 7. Primary antibodies for Western blot analysis

Target	**Host**	**Supplier (order no.)**
β-Actin	goat	Santa cruz (sc-1616)
CUGBP1	mouse	Abcam (ab9549)
mPGES-1	rabbit	Cayman (cay160140)
NDUFS2	rabbit	Abcam (ab96160)
SMAD2	goat	Santa cruz (sc-6200)
SMAD3	rabbit	Abcam (ab28379)
SMAD4	mouse	Abcam (ab3219)
P38	goat	Santa cruz (sc-535-g)
CUGBP1 (RIP-Western blot)	rabbit	Abcam (ab129115)

2.3.4 TMT labelling and mass spectrometry

Soluble or microsomal proteins (see chapter 2.3.1 Soluble and microsomal fraction preparation) were solubilized in 50 µl buffer containing 0.05 M triethylammonium bicarbonate, 4 M Urea, 0.01 % SDS and 1 mg RapiGest SF Surfactant (Waters). From each sample 50 µg were taken for further preparation. Disulfide reduction was conducted for 30 min at 56°C by adding 5 µl 1 M DTT. Afterwards, sulfhydryl alkylation was performed by adding 4 µl 1 M iodoacetamide solution, while samples were incubated at room temperature for 1 h in the dark.

Trypsin (modified sequencing grade, Promega) was added in a ratio of 1:30 (trypsin: protein). Then, samples were incubated at 37°C overnight. By using tandem mass tags (TMT 6-plex) according to manufacturer's instructions (ThermoFisher Scientific), peptides were labelled. Using an SCX-cartridge (Phenomenex), excess reagents could be removed from the samples. Liquid chromatography tandem mass spectrometry (MS) of a TMT-labeled sample was performed on QExactive mass spectrometer (ThermoFisher Scientific).

Peptide pre-fractionation was conducted as previously described in [251]. TMT-labeled protein samples were separated over a 60-minute gradient (3-55 % B) on a 2.1 × 250 mm XBridge BEH300 C18 column (Waters) using a flow rate of 200 µL/min. Buffers A contained 20 mM ammonia in MQ, whereas buffer B contained 20 mM ammonia in 80 % acetonitrile. The specific fractions were collected every minute and the fractions covering the peptide elution range were concatenated to yield 12 final pooled fractions. These fractions were evaporated to dryness by vacuum drying and stored at -20°C until nano Liquid chromatography-mass spectrometry (LC-MS) data capture. A Q-Exactive mass spectrometer (Thermo Scientific) was used to performe online LC-MS measurements. Peptide samples were trapped on an Acclaim PepMap trap column (C18, 3 µm, 100Å, 75 µm x 20 mm). Separation took place on a 15-cm long C18 picofrit column with 100 µm internal diameter and 5 µm bead size (Nikkyo Technos) which was installed onto a nano-electrospray ionization source. Solvent A was 97% water, 3% acetonitrile, 0.1% formic acid; and solvent B was 5% water, 95% acetonitrile, 0.1% formic acid. At a constant flow of 0.25 µl/min, the curved gradient went from 3% solvent B up to 48% solvent B in 50 min. Fourier transform mass analyzers (FTMS) master scans with 70,000 resolutions (and mass range 400-1200 m/z) were followed by data-dependent MS/MS (17,500 resolution) on the top 10 ions using higher energy collision dissociation (HCD) at 31% normalized collision energy. Precursors were isolated with a 2 m/z window. Automatic gain control (AGC) targets were 3e6 for MS1 and 2e5 for MS2. Maximum injection times were 250 ms for MS1 and 200 ms for MS2. Dynamic exclusion was used with 20 s duration. Precursors were excluded when they showed unassigned charge state or charge state of 1. An underfill ratio of 1% was used.

2.4. Bioinformatical methods

2.4.1 3’UTR analysis

For the analysis of splice patterns, proteins that were upregulated at least 1.5-fold in response to ΔCUGBP1 in the mass spectrometry dataset were taken into account. This list of 399 proteins was then analyzed concerning their 3’UTRs. All described 3’UTR isoform sequences were downloaded from ensemble biomart (Human, GRCh38.p12 Ensembl variation resources [252]), resulting in a list of 1916 transcripts. Those sequences were then aligned with 42 known

binding motifs of CUGBP1 downloaded from the online tool *Splice Aid F* [109] [104]. Alignment was kindly conducted by Tobias Saul.

For the high stringency analysis, three criteria were applied: (I) the binding sites should be of 39 or 46 nt length, (II) there should at least be 2 binding sites and (III) those binding sites should span a potential intron of at least 1000 nt. For a second less stringent approach (referred to as low stringency analysis), the three criteria were mitigated: (I) the binding sites should at least be of 8 nt length, (II) there should be 2 or more binding sites and (III) those binding sites should span a potential intron of minimum 100 nt. Analysis was performed with Microsoft Excel 2016.

2.4.2 Mass Spectrometry data analysis

Acquired MS raw files were searched using Sequest-Percolator under the software platform Proteome Discoverer 1.4.1.14 (Thermo Fisher Scientific) against human Uniprot database (release 01.12.2015 [89]) and filtered to a 1% false discovery rate (FDR) cut off. A precursor ion mass tolerance of 10 ppm was used as well as product ion mass tolerances of 0.02 Da for HCD-FTMS and 0.8 Da for collision induced dissociation Ion Trap Mobility Spectroscopy (CID-ITMS). The algorithm considered tryptic peptides with maximum 2 missed cleavages; carbamidomethylation (C), TMT 6-plex (K, N-term) as fixed modifications and oxidation (M) as dynamic modifications. Quantification of reporter ions was done by Proteome Discoverer on HCD-FTMS tandem mass spectra using an integration window tolerance of 10 ppm. Only unique peptides in the data set were used for quantification. Fold values were calculated comparing proteins from ΔCUGBP1 to Scramble, ΔmiR-574-5p to negative control LNA and miR-574-5p oe to negative control mimic. Fold values of +1.5/-1.5 were considered up- or downregulated.

2.4.3 Ingenuity pathway analysis (IPA)

Most genes are regulated by a variety of upstream regulators or transcription factors with often opposing effects. As it is unknown which will dominate in this specific system, predictions become difficult. Therefore, a statistical approach was used. A quantity “z-score” was calculated that rates whether an upstream regulator has significantly more “activated” predictions than “inhibited” predictions ($z > 0$). The other way around, when there are more inhibited predictions than activating predictions, the z-score will be negative. All regulated proteins in soluble as well as microsomal fractions from all three conditions were analyzed using IPA (Ingenuity Systems, www.ingenuity.com). The 5 most affected canonical pathways were predicted. The canonical pathways with p-values ≤0.05 were defined as significant.

2.5 Fluorescent labeling techniques

To find if the two binding partners CUGBP1 and miR-574-5p co-localize within the cell, immunostaining as well as in situ hybridization techniques were performed by Julia Wellstein.

2.5.1 Immunostaining

Immunofluorescent stainings were performed to visualize CUGBP1. Therefore, A549 cells were seeded at a density of 2.5 x 10^5 per well in a 6-well plate on glass cover slips (12 mm, Neolab) and cultured overnight. Medium was removed and cells were washed with PBS, before fixation for 10 min with 4% formaldehyde (FA, Carl Roth). After 3 PBS washing steps for 3 min to remove residual FA, cells were permeabilized for 10 min with 0.5% Triton X-100 (Sigma-Aldrich) diluted in PBS. Subsequently, cells were blocked for 20 min with a 2% BSA solution (Sigma-Aldrich) in PBS. The CUGBP1 primary antibody (ab9549, Abcam) was diluted 1:500 in blocking solution applied on the cells and incubated for 1h at room temperature. Following, 3 washing steps à 5 min with 0.01% Tween20 (Carl Roth) in PBS were performed. Then, cells were incubated for 45 min at room temperature with the secondary antibody goat anti-mouse IgG (Alexa Fluor® 594, ab150116, Abcam) diluted 1:500in blocking solution. Finally, cells were washed with 0.01% Tween20 (Carl Roth) in PBS, counterstained for 5 min with 4′,6-diamidine-2′-phenylindole dihydrochloride (DAPI 1µg/ mL in PBS), Sigma-Aldrich) and mounted in Mowiol 4-88 mounting medium (Sigma-Aldrich).

2.5.2 Fluorescence in situ hybridization (FISH)

To visualize miR-574-5p within the cells, FISH was performed with A549. To that end, 2.5x10^5 A549 cells were seeded on glass cover slips (12 mm, Neolab) in 6-well plates and cultured for 24 h. Cells were washed with PBS and prefixed with 1% FA in PBS for 10 min. After 3 washing steps of 3 min with PBS, cells were permeabilized with 0.5% Triton X-100 in PBS for 20 min on ice. After additional 3 PBS washing steps of 3 min, cells were refixed for 10 min with 4% FA. Then, 3 further washing steps with PBS were followed by prehybridization for 30 min at 40 °C in microRNA ISH buffer (Qiagen). Then, hybridization took place at 54°C with 100 nM double digoxigenin (DIG) labeled miR-574-5p probe (Qiagen) diluted to final concentration of 100 nM in microRNA ISH buffer for 1 h. Afterwards, cells were washed twice for 5 min with 2x saline-sodium citrate buffer (Gibco) at 54°C and once at room temperature. Blocking was then performed with 2% BSA in PBS for 20 min. The rabbit anti-DIG antibody (9H27L19, Invitrogen, Thermo Fisher Scientific) was diluted 1:40 in blocking solution and cultured on the cells at room temperature for 1 h. Residual antibody was removed by washing with 0.01% Tween20 in PBS 3 times for 5 min. Secondary antibody goat anti-rabbit IgG (Alexa Fluor® 594, 111-585-144, Jackson ImmunoResearch) diluted 1:300 in blocking solution was incubated on the cells

for 45 min at room temperature. Finally, cells were washed with 0.01% Tween20 in PBS, counterstained with DAPI and mounted as described above.

2.6 Microscopy and image acquisition

2.6.1 Immunostaining and FISH images

In order to take confocal images of immunofluorescence and FISH samples, the Leica TCS SPE confocal point scanner mounted on a Leica DMi8 stand equipped with an oil immersion 63x Apochromat was used. In all cases, the 405 and 561 nm laser lines were used to perform excitation. Images were analyzed using the ImageJ software (http://imagej.nih.gov/ij/) and show one focal plane of the middle of the nucleus.

2.6.2 Wound healing assay images

Images were acquired with 10 x magnitude using Axiovert 200 (Zeiss) with the LSM 510 Meta (Zeiss) image-processing software. One image was taken per well at the exact same localization immediately after scratching (t0) and 24 h later. Analysis of the images was performed using ImageJ software (http://imagej.nih.gov/ij/). Therefore, the width of the scratch was measured at 3 random sites within each picture. Since there were two wells per condition, this resulted in 6 values per time point which were used to build a mean value.

2.7 Statistics

Results are given as mean +SEM of at least three independent experiments. Statistical analysis was carried out by Student's paired or unpaired t-test (two-tailed), respectively, using GraphPad Prism 5.0. Differences were considered as statistically significant for $p \leq 0.05$ (indicated as * for $p \leq 0.05$, ** for $p \leq 0.01$ and ***for $p \leq 0.001$).

3. Results

In the center of this thesis is the non-canonical decoy mechanism of CUGBP1 binding to miR-574-5p. This mechanism was recently described to regulate the expression of the CUGBP1 target mPGES-1 [196]. Therefore, the first steps were to proof the interaction of CUGBP1 with the mPGES-1 mRNA and with miR-574-5p.

3.1 Verification of CUGBP1 binding via RIP

In order to proof the interaction of CUGBP1 with mPGES-1 and especially miR-574-5p, RIP assays were conducted. Thereby, CUGBP1 was precipitated from a whole cell lysate of unstimulated or IL-1β-stimulated A549 cells with a specific antibody that was coupled to sepharose beads. As mock control, a normal mouse IgG antibody was used for precipitation. CUGBP1 protein as well as the RNAs bound by CUGBP1 could then be quantified via Western blot and qRT-PCR, respectively. Binding was assumed, if the specific mRNA showed an enrichment in CUGBP1-IP, compared to IgG-IP.

3.1.1 Establishment of CUGBP1 RIP protocol

In a first validation step, the precipitation of CUGBP1 had to be confirmed via Western blot analysis. Therefore, 10% of the input, as well as IgG- and CUGBP1-IP samples were applied on a SDS-Gel. The Western blot membrane was then incubated with a CUGBP1 antibody from another host animal than the RIP antibody. Otherwise the images were not evaluable, because the sepharose beads could not be removed from the samples and create a smear. The Western blot images demonstrated that a clear CUGBP1 band was detected in the CUGBP1-IP sample at 48 kDa but not in the IgG sample (see Figure 11A). Hence, precipitation was indeed successful. Naturally, the CUGBP1 band with the highest intensity was detected in the Input sample. The amount of precipitated CUGBP1 was calculated based on the input, revealing that 33.2% (±5.5 SEM) of total CUGBP1 were recovered.

Following, verification of RNA co-precipitation was necessary. Therefore, the first described CUGBP1 target cJUN was measured performing qRT-PCR [253]. Indeed, qRT-PCR results revealed a significant 2.4-fold enrichment compared to IgG-IP (see Figure 11B). Together with the Western blot analyses, this ensured the accuracy of the RIP experiments, allowing for quantification of other potential CUGBP1 targets in following experiments.

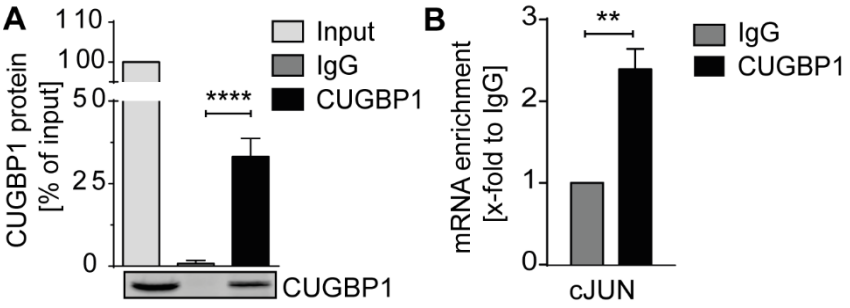

Figure 11: Validation of RIP protocol.
RIP of A549 cells with antibodies against CUGBP1 or normal mouse IgG. (A) Precipitated CUGBP1 protein was analyzed via Western blot analysis. Quantification was performed with Odyssey Infrared Imaging System (LI-COR® Biosciences). Input was set as 100%. Percentage of precipitated CUGBP1 is given as mean +SEM. One representative image of n=4 independent experiments is shown. (B) Co-precipitated cJUN mRNA was quantified using qRT-PCR. Relative enrichment normalized to IgG is given as mean +SEM of n=4 experiments., t-test, **p ≤ 0.01, ****p ≤ 0.0001

3.1.2 CUGBP1 binds to miR-574-5p and mPGES-1 mRNA

Previous work from our lab provided first evidence that the RBP CUGBP1 can bind miR-574-5p under inflammatory conditions, which prevents it from binding to its actual target, the mPGES-1 mRNA [196]. Within this thesis, the binding of CUGBP1 to both mPGES-1 and miR-574-5p needed to be confirmed. RIP of unstimulated A549 cells was conducted and in fact, mPGES-1 mRNA was significantly enriched in CUGBP1-IP in comparison to IgG-IP samples (see Figure 12A). As negative control, COX-2 was tested as it does not have any binding sites for CUGBP1 [196] and therefore was not enriched in the CUGBP1-IP samples. These findings further confirmed the interaction of CUGBP1 with mPGES-1 mRNA.

For miRs, IL-1β-stimulated A549 cells were used to initiate the decoy. MiR-16-5p served as negative control and was certainly not bound by CUGBP1. MiR-574-5p however, depicts a sequence homology to CUGBP1 binding motifs [196]. In fact, miR-574-5p was strongly enriched 22-fold in the CUGBP1-IP samples which proves the interaction (see Figure 12B).

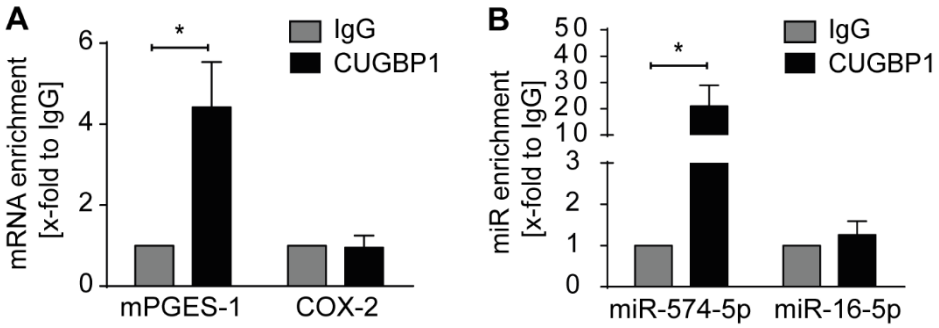

Figure 12: CUGBP1 binding to mPGES-1 mRNA and miR-574-5p in RIP assays.
RIP of A549 cells with antibodies against CUGBP1 or normal mouse IgG. Co-precipitated RNAs were quantified using qRT-PCR. (A) mRNA quantification of mPGES-1 and COX-2 in unstimulated A549 cell IP samples. (B) miR quantification of miR-574-5p and miR-16-5p in IP samples of A549 cells stimulated with IL-1β for 24 h. Relative enrichment normalized to IgG is given as mean +SEM of n=3 (A) or n=7 (B) experiments, t-test, *p ≤ 0.05.

These results further confirmed the existence of a decoy mechanism of miR-574-5p and CUGBP1. Thus, it was intriguing to further characterize this novel miR function and investigate if it influences the proteome of A549 cells in a broader way.

3.2. TMT-based proteomics study of IL-1β-stimulated A549 cells

A549 cells were cultured by Dr. Isabel Baumann, stimulated with 5 ng/mL IL-1β and transfected with siRNA, LNA or mimics, respectively. Cells with ΔCUGBP1, ΔmiR-574-5p or miR-574-5p oe were compared to their corresponding controls. Knockdown and overexpression of miR-574-5p were previously established by Dr. Isabell Baumann and revealed a significant ~ 80% decrease of miR-574-5p, while miR-574-5p was ~ 300-fold upregulated as quantified via qRT-PCR as stated in [196]. Knockdown of CUGBP1 was validated via Western blot analysis and showed a reduction of 67% in the soluble fraction and 83% in the microsomal fraction of A549 cells (see Figure 13).

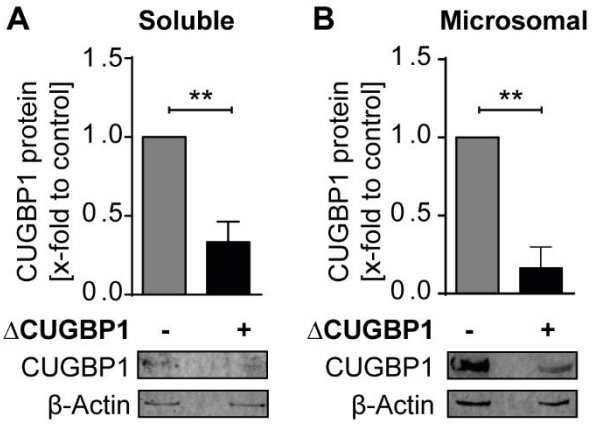

Figure 13: Quantification of CUGBP1 knockdown.
siRNA-mediated knockdown of CUGBP1 in A549 cells was followed by 24 h stimulation with IL-1β. Fractionation resulted in a soluble and a microsomal protein fraction which were analyzed via Western blot. One representative blot is shown from n=3 independent experiments. β-Actin was used as loading control. Quantification was performed with Odyssey Infrared Imaging System (LI-COR® Biosciences). Fold inductions compared to control are given as mean +SEM. t-test, **p ≤ 0.01.

In order to identify gene expression changes, A549 cells stimulated with IL-1β were used for a TMT-based LC/MS-MS study which was conducted by the group of Per-Johan Jakobsson, KI, Sweden (see Figure 14). Cell lysates were fractionated to separate soluble and microsomal proteins. All LC-MS/MS samples were then digested and labeled with TMT 6-plex to allow quantitative protein comparison. This technique facilitates a sensitive multiplex analysis and controls for technical variations [254]. TMT quantification is conducted by analyzing the intensities of fragment reporter ions released from the labels in the tandem MS mode (MS2) during peptide fragmentation. In the full scan mode (MS1) to be fragmented, precursor ions were selected.

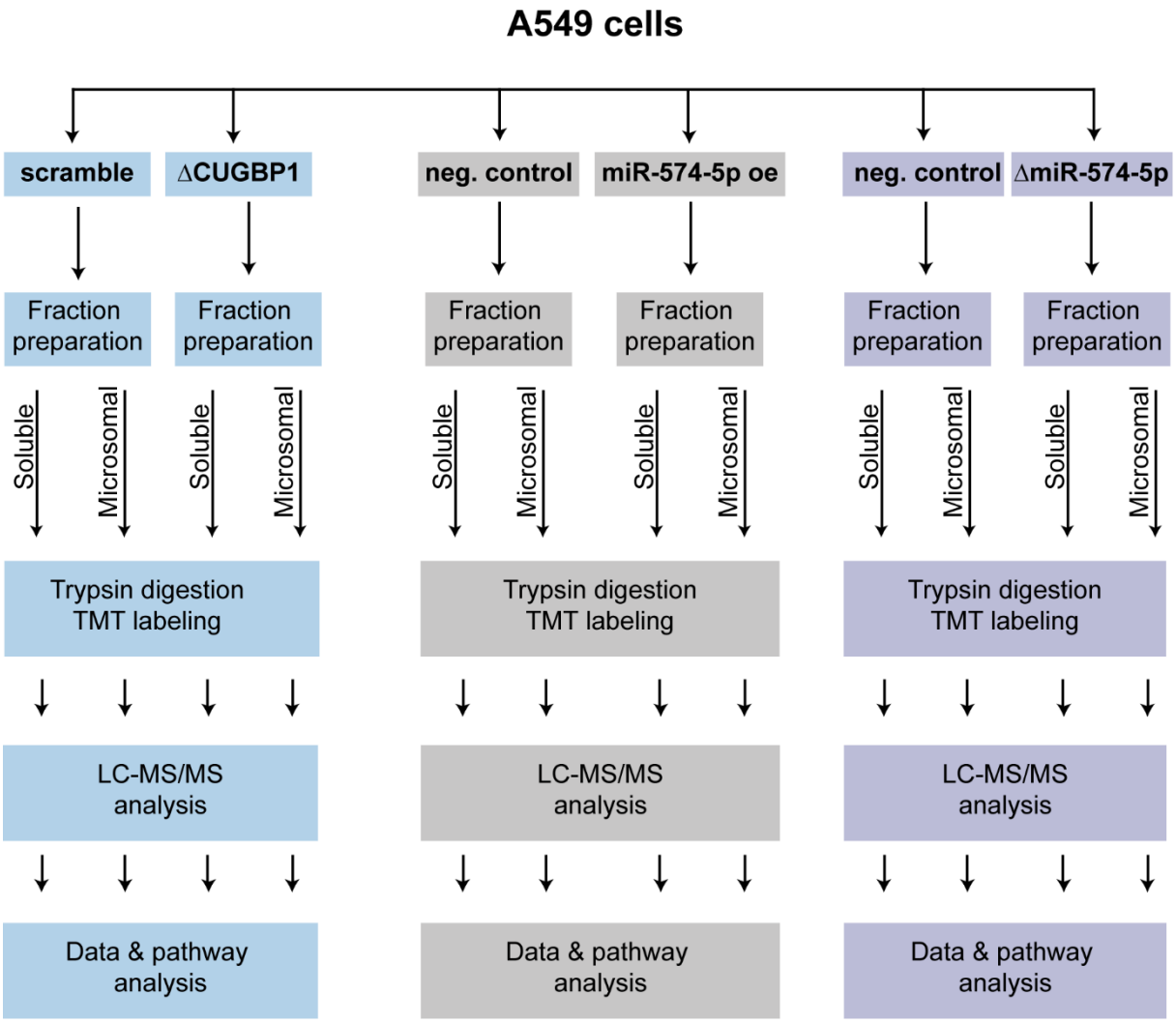

Figure 14: TMT based proteomics approach.
A549 cells were transfected creating ΔCUGBP1, ΔmiR-574-5p or miR-574-5p oe as well as respective controls and stimulated with IL-1β for 24 h. Fractionation of the cell lysates resulted in soluble and microsomal protein fractions which were separately analyzed. All samples were trypsin digested, labelled with Tandem mass tags (TMT) and analyzed by LC-MS/MS. Data were analyzed concerning fold-changes of protein levels compared to each control.

3.2.1 Proteome changes in A549 upon ΔCUGBP1, ΔmiR-574-5p and miR-574-5p oe

In the soluble fraction a total amount of 2441 proteins was detected in the ΔCUGBP1 samples, while in the ΔmiR-574-5p cells 2449 and in miR-574-5p oe samples a total number of 2450 proteins were measured. Whereas in the microsomal fraction a significantly higher number of proteins was detected: 3970 proteins in ΔCUGBP1 samples, 3967 proteins in ΔmiR-574-5p and 3968 proteins in miR-574-5p oe samples. Accordingly, roughly the same numbers of total proteins were identified throughout the three conditions. Besides the high numbers of total proteins, only small percentages of them exhibited up- or downregulation in comparison to the corresponding control samples (see Figure 16). In general, a protein was considered as

upregulated starting from a TMT ratio of ≥ 1.5 (fold change ≥ 1.5) and as downregulated with a TMT ratio of ≤ 0.5 (fold change ≤ -1.5).

Canonical CUGBP1 targets, as well as decoy targets, as a subpopulation of those, were supposed to show an upregulation in response to the knockdown (see Figure 15), while downregulation potentially indicated a secondary effect. In fact, 2% of the proteins detected in the soluble fraction were upregulated (61 proteins), while 8% (187 proteins) showed a decreased expression level (see Table 8). In the microsomal fraction, more proteins were up- than downregulated: 9% (338 proteins) exhibited an increased protein level, whereas only 4% (152 proteins) showed a reduced one. As described, decoy targets could not certainly be identified in the ΔCUGBP1 samples as they are thought to show the same regulation like canonical CUGBP1 targets. Thus, the two miR conditions were more relevant in that regard.

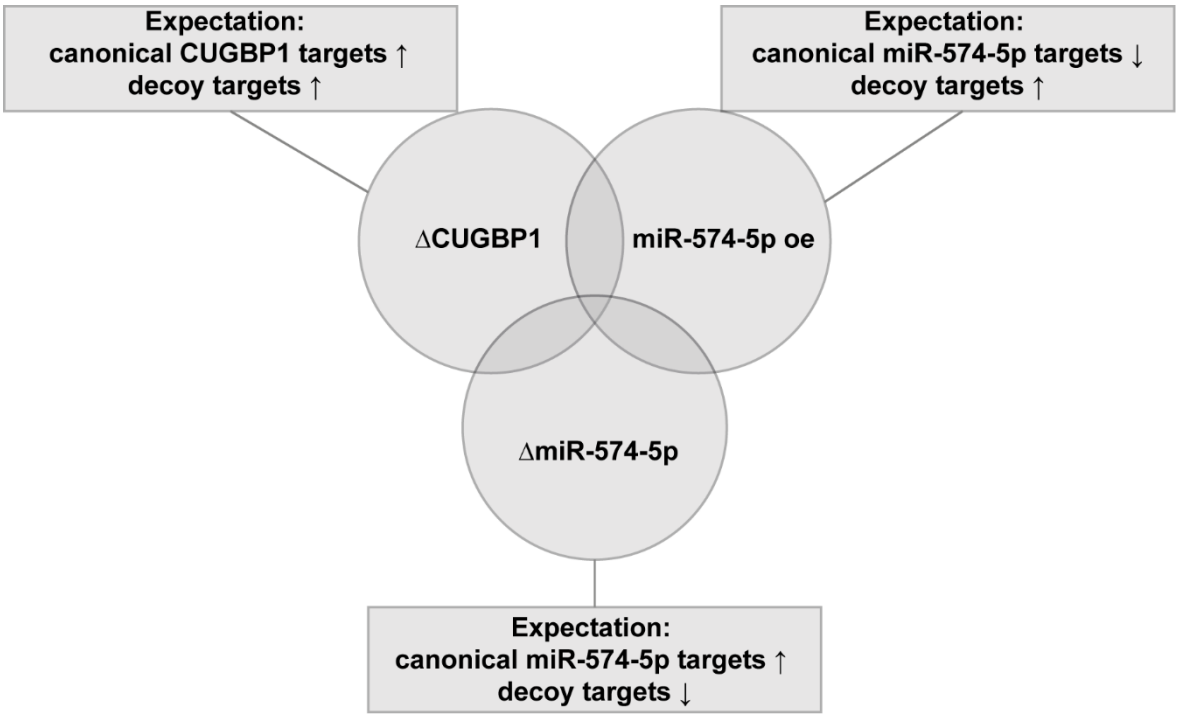

Figure 15: Expected regulations in the proteomics study.
Discrimination of canonical CUGBP1/ miR-574-5p and decoy targets via expected regulation on protein level. ↑ indicates increased protein level, ↓ indicates decreased protein level.

In miR-574-5p oe samples, decoy targets were expected to be increased in response to high miR-574-5p levels, whereas reduced protein levels would refer to canonical miR targets (see Figure 15). *Vice versa*, the opposite could be assumed for the ΔmiR-574-5p condition. In the soluble fraction of miR-574-5p oe samples, 2% (40 proteins) were up- and 3% (78 proteins) were downregulated. While 8% of microsomal proteins (303 proteins) were decreased upon the overexpression, only 3% of protein levels were elevated (124 proteins) (see Table 8).

In the soluble fraction, 1% (29 proteins) of the total protein amount was increased upon ΔmiR-574-5p, while 14 proteins showed a decrease. However, the microsomal proteins showed higher percentages, 9% were upregulated (345 proteins), while even 13% (504 proteins) showed a downregulation (see Table 8).

Table 8. Numbers of increased (↑) and decreased (↓) proteins in each fraction and each condition of the proteomics study compared to their respective controls.

		Soluble fraction	Microsomal fraction
ΔCUGBP1	↑	61	338
	↓	187	152
miR-574-5p oe	↑	40	124
	↓	78	303
ΔmiR-574-5p	↑	29	345
	↓	14	504

Proteins which showed increased levels upon ΔCUGBP1 were analyzed for CUGBP1 binding sites in their 3'UTRs. Sequences of the 3´UTRs of the specific proteins were downloaded from the database "UCSC Genome Browser" (Dec. 2013 GRCh38/hg38 https://genome.ucsc.edu/) [255]. Followed by identification of potential CUGBP1 binding motifs with the online tool "SpliceAid 2" (www.introni.it/spliceaid.html [256]). The algorithm recognizes GREs and other binding motives (e.g. CUGUCUG) in the provided 3'UTR sequences.

It was demonstrated that an excessive amount of the upregulated proteins does have a potential CUGBP1 binding site: in the soluble fraction 69% (42 proteins) and in the microsomal fraction 73% (246 proteins) of all detected proteins in the proteomics study (see Figure 16). This indicates that many primary effects were observed herein. Preliminary analysis of canonical miR-574-5p targets was accomplished by the microRNA.org. online tool [257]. Proteins that were upregulated upon ΔmiR-574-5p or downregulated upon miR-574-5p oe were analyzed for miR-574-5p seed regions in their 3'UTRs. On average, only 16% of them have a seed region, which strongly implies that there are many secondary effects observed in this study (see Figure 16).

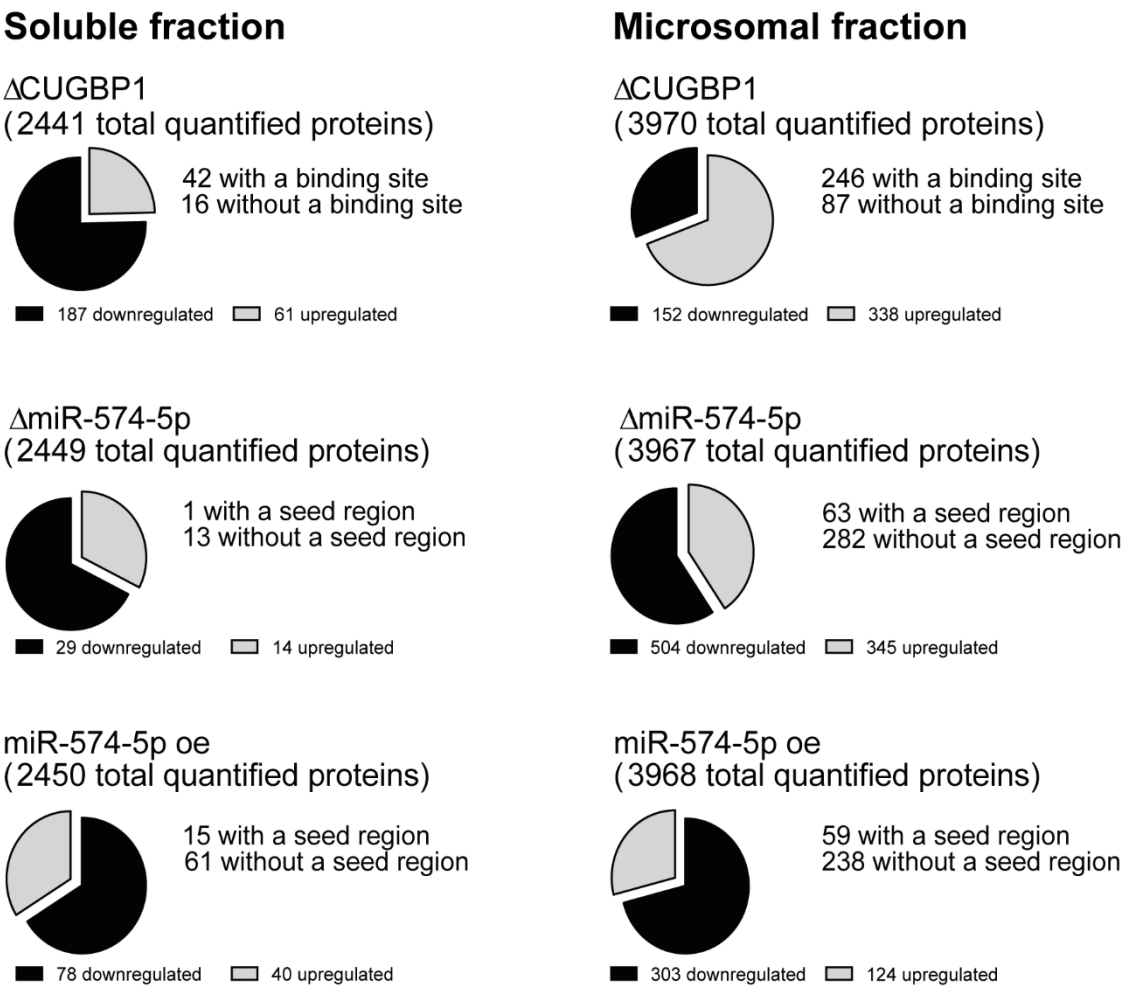

Figure 16: Numbers of proteins differentially expressed upon ΔCUGBP1, ΔmiR-574-5p or miR-574-5p oe in soluble and microsomal fraction of the proteomics study.
Cut-offs were set to 1.5-fold for upregulation (grey) and -1.5-fold for downregulation (black). CUGBP1 binding sites of upregulated proteins upon ΔCUGBP1 were predicted using splice aid [256]. MiR-574-5p seed regions were identified with the online tool microrna.org [257] of proteins revealing an upregulation upon ΔmiR-574-5p or a downregulation upon miR-574-5p oe.

Table 9 presents a list of the overlap of potential miR-574-5p targets from soluble and microsomal fraction as well as from the ΔmiR-574-5p and miR-574-5p oe samples. However, as the focus of this project was clearly on canonical CUGBP1 and decoy targets, this approach was not continued or further experimentally examined.

Table 9. Potential canonical miR-574-5p targets.

Fraction	Description	Gene name
Microsomal	Isoform 2 of Protein transport protein Sec24B	SEC24B
Microsomal	Mitochondrial inner membrane protein OXA1L	OXA1L
Microsomal	Isoform 2 of Methionine synthase	MTR
Microsomal	Isoform 2 of Phosphatidylinositol 5-phosphate 4-kinase type-2 gamma	PIP4K2C
Microsomal	Sterol O-acyltransferase 1	SOAT1
Microsomal	Transportin-3	TNPO3
Microsomal	Transmembrane protein 33	TMEM33

Overlap analysis of proteins from the proteomics study that were upregulated upon ΔmiR-574-5p (65 proteins) and downregulated upon miR-574-5p oe (59 proteins) and which have a seed region in their 3'UTR. From the microsomal fraction seven proteins were left, while no proteins in the soluble fraction fulfilled these criteria.

To summarize, these results demonstrate that on average 11% of all analyzed proteins could be somehow regulated by CUGBP1, whereas 9.7% of all detected proteins depict a regulation related to miR-574-5p. However, the distribution of the miR-574-5p regulated proteins varies considerably depending on the protein fraction.

3.2.2 Validation of TMT proteomics study using Western blot analysis

For validation, the mass spectrometry data needed to be confirmed via Western blot analysis. Distinct proteins were selected and it was examined whether they show the same regulation upon ΔCUGBP1, ΔmiR-574-5p and miR-574-5p oe in Western blot data than in the proteomics data. The proteomics study was a highly complex study with different conditions and fractions (see Figure 14), which is why validation is not necessarily based on physiologically connected proteins.

The first protein to be analyzed was NADH-Ubiquinone Oxidoreductase Core Subunit S2 (NDUFS2) which is a postulated CUGBP1 target in HeLa cells [84]. In the soluble fraction of the proteomics study, NDUFS2 showed a trend towards a slight upregulation in response to ΔCUGBP1 (1.3-fold) and miR-574-5p oe (1.4-fold). Western blot data proofed this regulation, revealing a fold change of 1.6-fold upon miR-574-5p oe and even 2.2-fold in response to ΔCUGBP1 (see Figure 17A, C). In ΔmiR-574-5p samples, NDUFS2 protein level seemed to be slightly decreased (0.8-fold) in the proteomics data. This could also be confirmed using Western blot analysis, where NDUFS2 was significantly reduced 0.8-fold in ΔmiR-574-5p samples as well (see Figure 17B). In the microsomal fraction, NDUFS2 revealed no strong changes in expression. For example, in response to ΔmiR-574-5p it showed a fold change of 1.1 in the proteomics data. This invariable protein level could also be demonstrated using Western blot analysis, revealing a fold change of 1.1 (see Figure 17D).

Apart from that, SMAD3 (Mothers against decapentaplegic homolog 3) was another protein which was investigated. It was clearly downregulated (0.5-fold) in response to ΔCUGBP1 in the soluble fraction of the proteomics study. This trend was successfully validated via Western blot, where SMAD3 was downregulation as well (0.6-fold) (see Figure 17F). In the microsomal fraction of the proteomics study, SMAD3 was only slightly regulated by 1.1-fold in response to ΔmiR-574-5p. Western blot data showed a stronger effect although it was not significant, revealing a tendency for an upregulation of 1.4-fold (see Figure 17G).

SMAD2, another member of the same protein family [89] [258], was also detected in the proteomics study. In the soluble fraction, SMAD2 levels were increased 1.2-fold upon miR-574-5p oe which was validated with a significant upregulation of 1.2-fold concerning Western blot data (see Figure 17E). In order to complete the protein family, it was logical to analyzed SMAD4, which was the only other SMAD detected in the proteomics study. However, neither in the proteomics study nor in the Western Blot images, it did depict any regulation upon ΔCUGBP1 (see Figure 17H) which validated the mass spectrometry data, but excluded SMAD4 as interesting potential target.

Finally, p38 (Mitogen-Activated Protein Kinase 14, MAPK14) was examined as it was one of the strongest downregulated proteins (0.3-fold) upon ΔCUGBP1 in the soluble fraction of the proteomics study. This strong decrease of p38 protein was confirmed using Western blot analysis which revealed a significant 0.5-fold reduction (see Figure 17I). Nevertheless, this seems to be a secondary effect, because CUGBP1 targets are supposed to be upregulated in response to the knockdown.

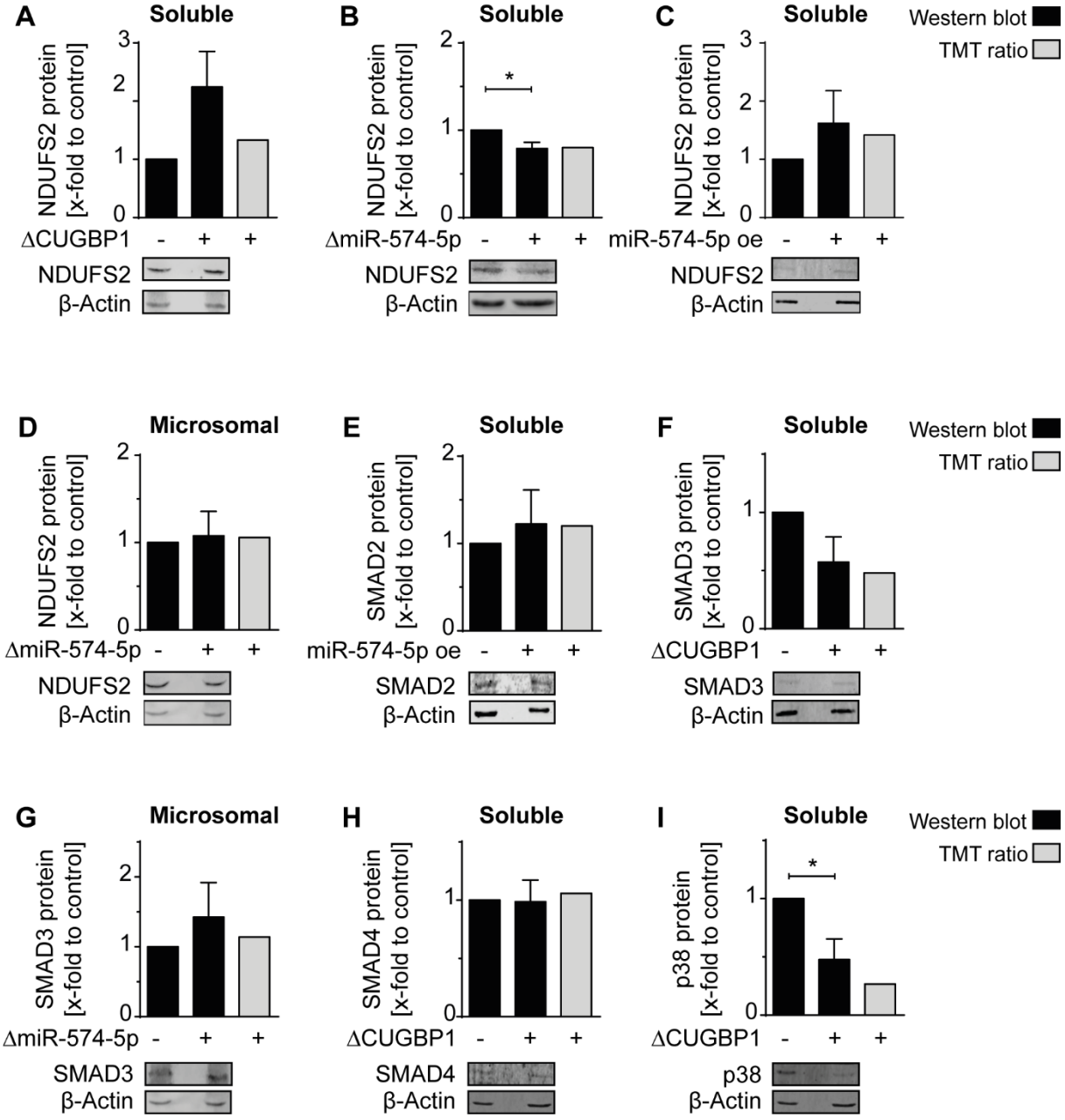

Figure 17: Proteomics validation using Western blot analysis.
Western blot analysis (black bars) of NDUFS2 (A-D), SMAD2 (E), SMAD3 (F, G), SMAD4 (H) and p38 (I) in microsomal or soluble protein fraction of IL-1β-stimulated A549 cells upon ΔCUGBP1, ΔmiR-574-5p or miR-574-5p oe as indicated. One representative blot is shown of n=3-6 independent experiments. β-Actin was used as loading control. Quantification was performed with Odyssey Infrared Imaging System (LI-COR® Biosciences). Fold inductions compared to control are given as mean +SEM. t-test, *p ≤ 0.05. TMT ratios of the respective proteins in the proteomics study are depicted in grey bars (n=1).

In summary, these Western blot results have clearly confirmed the proteomics study. Since the accuracy of the mass spectrometry data was assured, this allowed for further analyses of the data.

3.3 Physiological impact

3.3.1 Pathway analysis predicts canonical pathways, upstream regulators and biological functions

In a next step, all proteins in soluble as well as microsomal fraction were analyzed with the help of IPA (Ingenuity Systems, www.ingenuity.com). This tool uses the list of detected proteins and predicts canonical pathways and upstream regulators that could also be affected. Canonical pathways with p-values ≤ 0.05 were termed as significant. Analysis was conducted by the group of Per-Johan Jakobsson, KI Sweden. It was revealed that the five most affected canonical pathways in the soluble fraction were: Eukaryotic Initiation Factor 2 (eIF2) Signaling, Regulation of Eukaryotic Initiation Factor 4 (eIF4) and 70 kDa ribosomal S6 kinase (p70S6K) Signaling, tRNA Charging, Protein Ubiquitination Pathway and mechanistic Target of Rapamycin (mTOR) Signaling (see Table 14; appendix). Top regulated pathways in the microsomal fraction were: eIF2 Signaling, Protein Ubiquitination Pathway, Mitochondrial Dysfunction, Regulation of eIF4 and p70S6K Signaling as well as Oxidative Phosphorylation.
For the upstream regulators, IPA predicted: Hepatocyte Nuclear Factor 4 Alpha (HNF4A), Cystatin D (CST5), Rapamycin-Insensitive Companion of mTOR (RICTOR), MYC Proto-Oncogene, MYCN Proto-Oncogene, microtubule associated protein tau (MAPT) and p53 (see Table 15; appendix), which further underlines the influence of CUGBP1 and miR-574-5p on cancer development. Interestingly, in the IPA prediction of influenced biological functions in the soluble fraction, it was revealed that cancer metastasis could be highly affected by CUGBP1 and miR-574-5p.
As presented in Figure 18, migration-related processes were on position four, seven and eight under the top ten regulated bio functions. With help of an activation Z-score, likely regulated molecules could be predicted based on a pattern match of up- and downregulation [259]. Further, it gives a hint in which direction the respective process is regulated. Thus, it was predicted that migration is diminished upon ΔCUGBP1 and miR-574-5p oe, whereas ΔmiR-574-5p cells could possibly show a higher migration potential.

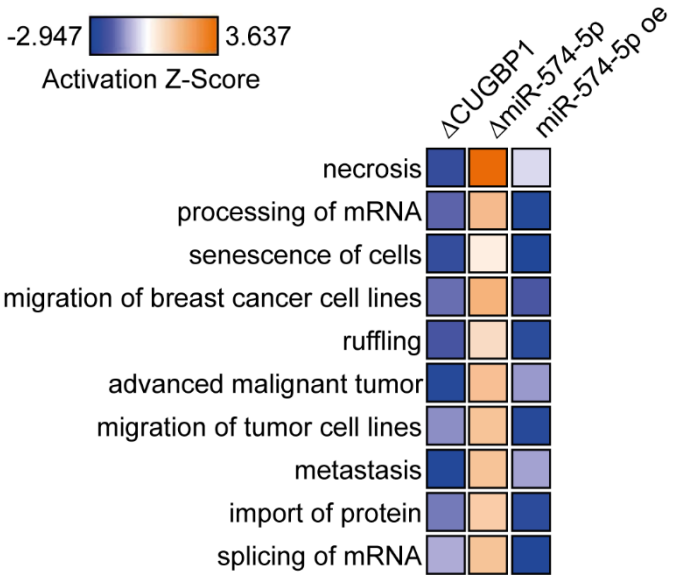

Figure 18: Top ten regulated biological processes predicted by IPA.
IPA analysis of soluble proteins from the proteomics study after ΔCUGBP1, ΔmiR-574-5p and miR-574-5p oe in IL-1β-stimulated A549 cells. Activation Z-Score indicates predicted direction of regulation.

3.3.2 Influence of miR-574-5p and mPGES-1 on migratory behavior of A549 cells

Following the IPA, migration of cancer cells became an intriguing topic to work on within this project. With two different techniques, the influence of miR-574-5p on lung cancer cell migration was investigated. Therefore, a stable miR-574-5p oe cell line was used [196]. In so-called wound healing or scratch assays, the ability of A549 cells to migrate into a previously scraped scratch within the cell monolayer was studied. Therefore, cells were starved to minimize proliferative effects. Microscope images were taken right after scratching and 24 h later. The width of the remaining scratch was measured with ImageJ software to calculate the migrated area. It turned out that there was no measurable difference between miR-574-5p oe and control cells concerning their migratory behavior (see Figure 19A). However, wound healing assays are controversially discussed in literature, as a proliferative effect can never be fully excluded. Indeed, miR-574-5p has a positive influence on proliferation of A549 cells as stated in [196]. Therefore, the system was switched to Boyden chamber assays. The same stable cell line was used and seeded in transwell inlays with a porous membrane on the bottom. Additionally, the influence of mPGES-1 was investigated. Therefore, cells were stimulated with IL-1β to induce mPGES-1 expression, whose activity was supposed to be repressed with the application of a selective inhibitor Compound III (CIII). Migrated cells were stained and counted under a light microscope. However, the numbers of migrated miR-574-5p oe and control cells were nearly the same, although high standard deviations were observed (see Figure 19B, black bars). Moreover, stimulation with CIII did not change migration of any of the cell lines (see Figure 19B, grey bars). Apparently, neither miR-574-5p nor mPGES-1 had any impact on migration of A549 cells.

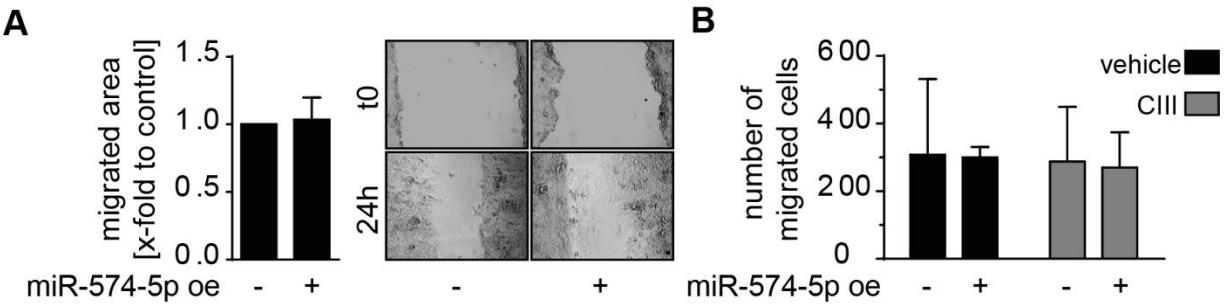

Figure 19: Migration assays.
A549 cells with stable miR-574-5p oe or control cells were analyzed concerning migratory behavior. (A) Wound healing assay showed no difference between migrated area of miR-574-5p oe or control cells after 24 h. (B) Boyden chamber assay of IL-1β-stimulated A549 miR-574-5p oe or control cells stimulated with 10 µM Compound III (CIII) or vehicle (DMSO) revealed equal numbers of migrated cells after 5 h. Results are given as mean +SEM of n=3 different experiments.

3.4 Identification of new CUGBP1 targets

3.4.1 Western blot analysis of microsomal proteins upon ΔCUGBP1

New canonical CUGBP1 targets were determined based on their expression levels in proteomics as well as Western blot data. It was assumed that CUGBP1 targets should exhibit increased protein level, when the inhibitory influence of CUGBP1 is missing after knockdown. As depicted in Figure 13, CUGBP1 protein was mainly found in the microsomal fraction. In consequence, the focus was set on that fraction for further analyses. The previously described CUGBP1 target and decoy target mPGES-1 served as positive control. Indeed, mPGES-1 did show a significant 1.4-fold increased protein level in response to ΔCUGBP1 (see Figure 20A). NDUFS2, another postulated CUGBP1 target was further analyzed via Western blot. Although it did not show strong changes in the microsomal fraction of the proteomics study, NDUFS2 revealed a clear induction of 1.4-fold upon ΔCUGBP1 via Western blot analysis (see Figure 20B). This confirmed it as a CUGBP1 target, despite the fact that further experiments were needed as final proof.

Since physiological experiments concerning cancer migration were conducted within this project, associated SMAD proteins came into the focus. Therefore, the SMAD protein family was analyzed more deeply. A variety of family members such as SMAD2, SMAD3 and SMAD4 were in fact found in the mass spectrometry data. SMAD4 did not exhibit any regulation upon ΔCUGBP1 though, neither in the proteomics study, nor in the Western blot images. For this reason, it was excluded as potential CUGBP1 target. The remaining SMADs however, were promising candidates. SMAD2 and SMAD3 both exhibit multiple binding motifs all over their 3'UTRs as determined with SpliceAid 2 [256]. Moreover, Western blot analysis revealed obvious changes in expression levels upon ΔCUGBP1. Compared to control samples, SMAD2

was significantly increased by 4-fold in response to the knockdown (see Figure 20C). Although this strong regulation was not measured in the mass spectrometry, the IPA also predicted that SMAD2 expression would be enhanced. Thus, the Western blot data validated this prediction successfully, making SMAD2 a promising CUGBP1 target. SMAD3 depicted slightly weaker regulation in response to ΔCUGBP1, as it was upregulated by 2.2-fold according to Western blot analysis (see Figure 20D). Again, this perfectly fitted IPA data that predicted SMAD3 levels to be increased 2.3-fold upon knockdown of CUGBP1.

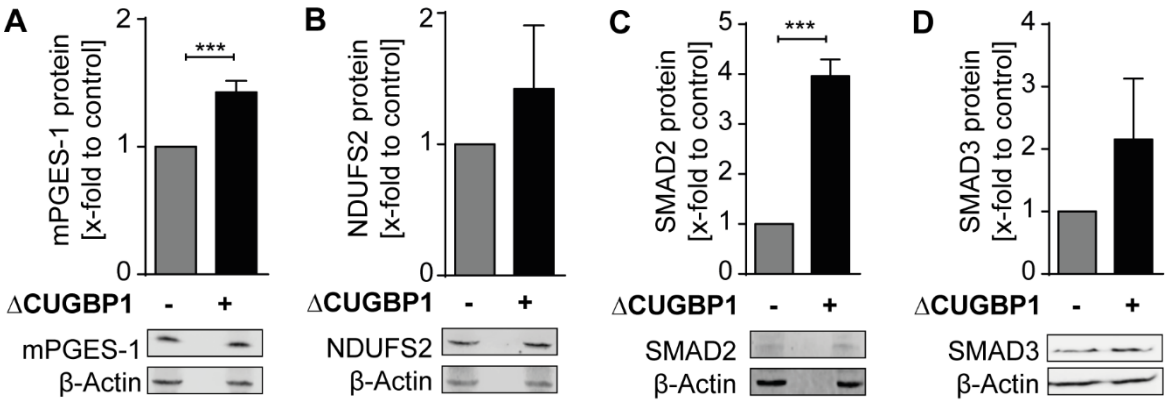

Figure 20: Protein levels of potential CUGBP1 targets in IL-1β-stimulated A549 cells with manipulated CUGBP1 levels.
A549 cells with or without ΔCUGBP1 were stimulated with IL-1β for 24 h. Microsomal fraction was analyzed via Western blot concerning (A) mPGES-1, (B) NDUFS2, (C) SMAD2 and (D) SMAD3 protein levels. One representative blot is shown of n=3-4 independent experiments. β-Actin was used as loading control. Quantification was performed with Odyssey Infrared Imaging System (LI-COR® Biosciences). Fold inductions compared to control are given as mean +SEM. t-test, ***p ≤ 0.001.

Taken together, these data provide first evidence that SMAD2, SMAD3 and NDUFS2 could be canonical CUGBP1 targets in A549 cells.

3.4.2 Binding of CUGBP1 to mRNAs of novel canonical targets

In order to further validate the newly postulated targets SMAD2, SMAD3, NDUFS2 as well as mPGES-1, binding of CUGBP1 to the respective mRNAs needed to be confirmed. Therefore, RIP assays were performed. After immunoprecipitation of CUGBP1, the bound mRNAs could be quantified via qRT-PCR. Binding of CUGBP1 was assumed, if the mRNA was enriched in CUGBP1-IP, compared to IgG-IP. Indeed, a significant enrichment could be observed for NDUFS2 and SMAD2 mRNAs (see Figure 21). While NDUFS2 was 2.2-fold enriched, SMAD2 showed a strong 6.4-fold enrichment compared to IgG. This confirms the interaction of CUGBP1 with the respective mRNAs. However, SMAD3 showed no enrichment in CUGBP1-

IP samples (see Figure 21) although it contains a binding site in the 3'UTR. This indicates that SMAD3 mRNA is not bound by CUGBP1 under the conditions examined herein.

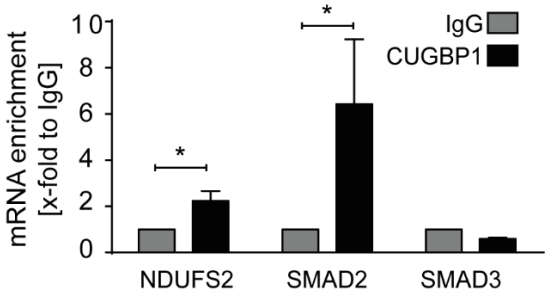

Figure 21: Binding of CUGBP1 to potential new target mRNAs.
RIP of A549 cells with antibodies against CUGBP1 or normal mouse IgG. Co-precipitated RNAs were quantified using qRT-PCR. mRNA quantification of NDUFS2, SMAD2 and SMAD3 in unstimulated A549 cell IP samples. Relative enrichment normalized to IgG is given as mean +SEM of n=3-4 experiments, t-test, *p ≤ 0.05.

Overall, CUGBP1 binding to two of the three postulated targets was confirmed: SMAD2 and NDUFS2. Since decoy targets were assumed to be a subpopulation of CUGBP1 targets, the next step was to investigate if these new candidates were also regulated by miR-574-5p.

3.5 Identification of novel miR-574-5p/CUGBP1 decoy targets

3.5.1 Investigating a "decoy regulation pattern" via Western blot analysis

In order to find new targets of the miR-574-5p/CUGBP1 decoy mechanism, the proteomics data were further analyzed in regard to a stringent "decoy regulation pattern" in the three conditions: (I) ΔCUGBP1, (II) ΔmiR-574-5p and (III) miR-574-5p oe:

(I) As subpopulation of canonical CUGBP1 targets, decoy targets are supposed to be increased in response to ΔCUGBP1 just as canonical CUGBP1 targets. With a reduced CUGBP1 level, the inhibitory influence on gene expression of the target is missing, leading to an upregulation on protein level (see Figure 22A). Without presence of CUGBP1, the level of miR-574-5p should not have an impact on the decoy targets. However, decoy targets cannot be distinguished from canonical CUGBP1 targets only by looking at the ΔCUGBP1 condition. To clearly identify targets of the decoy mechanism, the two miR conditions are more intriguing.

(II) Potentially, decoy targets are supposed to be downregulated upon ΔmiR-574-5p. In theory, lower intracellular levels of miR-574-5p allow higher binding capacity of CUGBP1. As CUGBP1 binding has mostly negative effects on the protein level, the respective decoy target should be downregulated (see Figure 22B).

(III) *Vice versa*, miR-574-5p oe should lead to an upregulation of potential decoy targets. Simply more miRs are accessible to prevent binding of CUGBP1 (see Figure 22C).

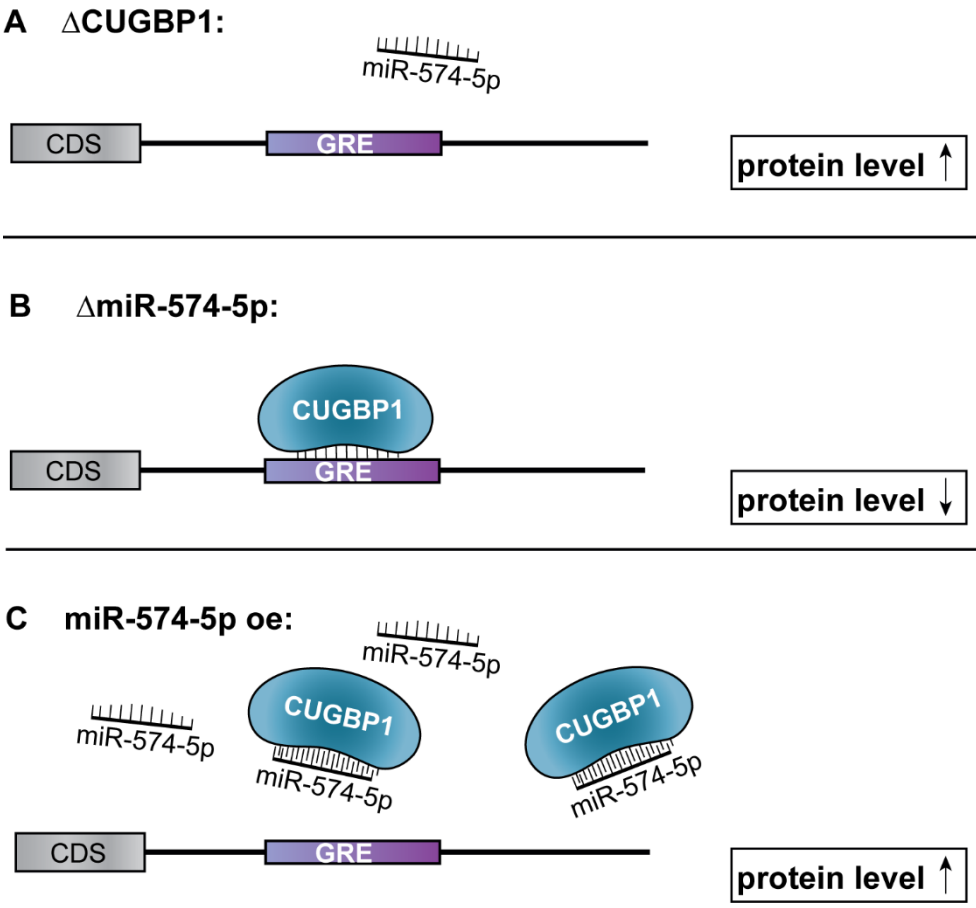

Figure 22: Schematic overview of the decoy mechanism.
Expected cellular processes in the three conditions: (A) ΔCUGBP1, (B) ΔmiR-574-5p and (C) miR-574-5p oe and their effects on potential decoy targets.

In a first analysis, proteins were included even if they only had a tendency for the "decoy regulation pattern" in the proteomics data. Such as only two conditions that met the criteria, with the third condition potentially not matching, but also not contradicting the "decoy regulation pattern". For instance, High-mobility group AT-hook 2 (HMGA2) protein was strongly upregulated upon ΔCUGBP1 (2.4-fold) and downregulated upon ΔmiR-574-5p (0.6-fold) but showed only a 1.1-fold TMT ratio in response to miR-574-5p oe. The newly postulated CUGBP1 target proteins and several other candidates were then analyzed via Western blot. As positive control, the previously described decoy target mPGES-1 was used.

The analysis demonstrated that mPGES-1 protein levels did indeed react as predicted: It was 1.4-fold upregulated upon ΔCUGBP1, significantly 0.6-fold downregulated upon ΔmiR-574-5p and 1.4-fold enriched in response to miR-574-5p oe (see Figure 23D). From the list of potential candidates, HMGA2, Glyoxalase Domain Containing 4 (GLOD4) or PABP-Interacting Protein 2 (PAIP2) were just a few examples that were only expressed on very basal level by A549 cells. Thus, many proteins could not be detected since the sensitivity of the Western blot system was too low compared to mass spectrometry. NDUFS2 however, was sufficiently

expressed, although it just showed a slight tendency for the “decoy regulation pattern” in the proteomics data. In the analyzed Western blot images, NDUFS2 levels did not change upon manipulated miR-574-5p levels (see Figure 23A). This indicated that it is just a canonical CUGBP1 target but not affected by the decoy with miR-574-5p.

SMAD3, although not bound by CUGBP1 in RIP assays, was still included here. As already described, SMAD3 levels were increased upon ΔCUGBP1. Surprisingly, in the two miR conditions SMAD3 depicted the opposite regulation than expected for a decoy target. It was slightly upregulated upon ΔmiR-574-5p and downregulated in response to miR-574-5p oe (see Figure 23B). The same regulation was observed for SMAD2 which showed significant reduction in response to miR-574-5p oe (see Figure 23C). This would have been an indication for canonical miR targets, however neither SMAD3 nor SMAD2 have a miR-574-5p seed region in their 3’UTRs. Nevertheless, both of them were excluded as potential decoy targets.

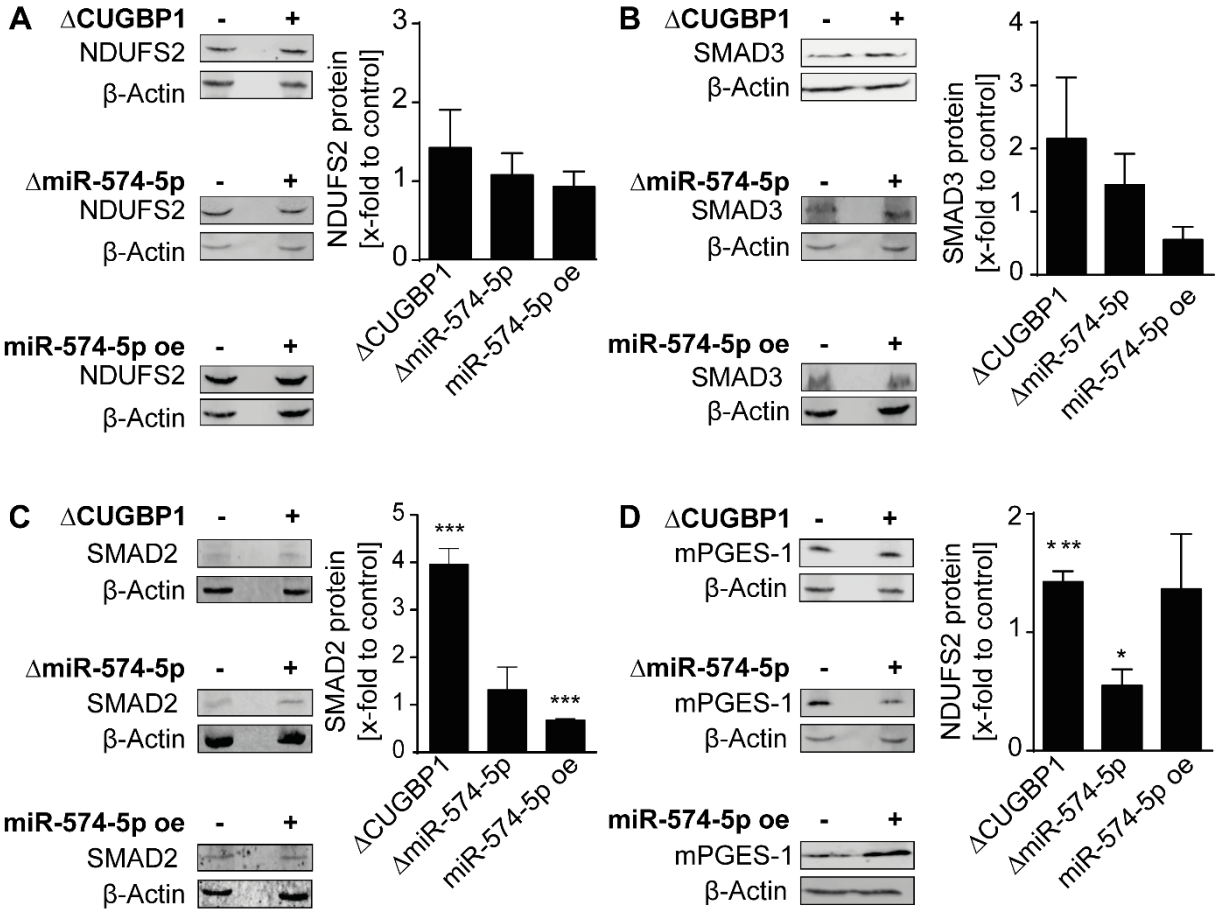

Figure 23: Investigating a “decoy regulation pattern” via Western blot analysis.
Western blot analysis of (A) NDUFS2, (B) SMAD3, (C) SMAD2, (D) mPGES-1 in microsomal fraction of IL-1β-stimulated A549 cells upon ΔCUGBP1, ΔmiR-574-5p or miR-574-5p oe. One representative blot is shown of n=3-6 independent experiments. β-Actin was used as loading control. Quantification was performed with Odyssey Infrared Imaging System (LI-COR® Biosciences). Fold inductions compared to control are given as mean +SEM. t-test, *p ≤ 0.05, ***p ≤ 0.001.

Taken together, for none of the detectable proteins the “decoy regulation pattern” could be elucidated via Western blot analysis. Neither SMAD2, SMAD3 or NDUFS2 showed the adequate pattern concerning the two miR conditions (see Figure 23). While other candidates, such as GLOD4 or HMGA2 which were found in the mass spectrometry data, were not detectable via Western blot. Thus, only mPGES-1 was left as CUGBP1/miR-574-5p decoy target.

3.5.2 Stringent “decoy regulation pattern” in the proteomics study

As the rather loose criteria in the first approach led to inconclusive results, the proteomics data were re-analyzed with more stringent criteria to find if the decoy mechanism is as global as expected. A closer look was taken on how many proteins exactly depicted the perfect “decoy regulation pattern” i.e. showed an upregulation of ≥1.5-fold in response to ΔCUGBP1, a downregulation of at least 0.5-fold after ΔmiR-574-5p and at least an upregulation of ≥1.5 fold in response to miR-574-5p oe.

It was revealed that, as expected, in the soluble fraction zero proteins matched all three criteria (see Figure 24A). This further underlines the hypothesis that the decoy mechanism mainly takes place in the microsomal fraction. Concentrating on the microsomal fraction, from originally 3970 proteins, only seven proteins (0.2%) matched this perfect “decoy regulation pattern” in all three conditions (see Figure 24B):

- Ubiquitin Conjugating Enzyme E2 R2 (UBE2R2)
- Centrosomal Protein of 41 kDa (CEP41)
- RNA polymerase-associated protein LEO1 (LEO1)
- General Transcription Factor IIE Subunit 2 (GTF2E2)
- Polyadenylate-Binding Protein-Interacting Protein 2 (PAIP2)
- Solute carrier family 39 member 6 (SLC39A6)
- GRIP1 Associated Protein 1 (GRIPAP1)

Of note, mPGES-1 was not under the seven proteins, since it did not depict the exact pattern in the proteomics data either. Although it displayed the “decoy regulation pattern” in Western blot images, it was not so prominent in the mass spectrometry data. This underlines that mass spectrometry data need to be validated, as artefacts can be detected and it therefore not necessarily reveals an accurate representation of the actual proteome within the cells.

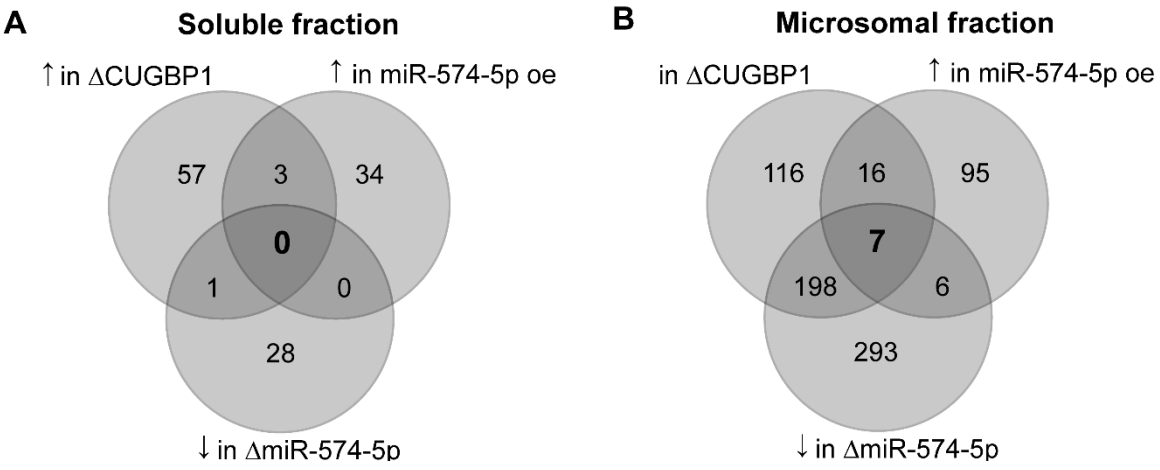

Figure 24: Proteins with a stringent "decoy regulation pattern" in the proteomics study. Venn diagram with numbers of proteins that exhibit a very stringent "decoy regulation pattern" in (A) soluble and (B) microsomal fraction of the proteomics study. ↑ indicates increased protein level, ↓ indicates decreased protein level.

This small number of proteins provided first evidence that the CUGBP1/miR-574-5p decoy seems to be a very specific mechanism and does not affect an extensive amount of proteins.

3.5.3 Binding analysis of potential decoy targets

The seven potential decoy targets were then further analyzed concerning binding behavior of CUGBP1. GRIPAP1 was the only exception, as it has no described 3'UTR according to ensemble database. The remaining six 3'UTRs were analyzed concerning CUGBP1 binding motifs [256]. It was found that all of them had at least one binding site in their 3'UTR. Subsequently, binding of CUGBP1 to the mRNAs was investigated by RIP assay. It turned out that none of the mRNAs was enriched in the CUGBP1-IP compared to mock control (see Figure 25).

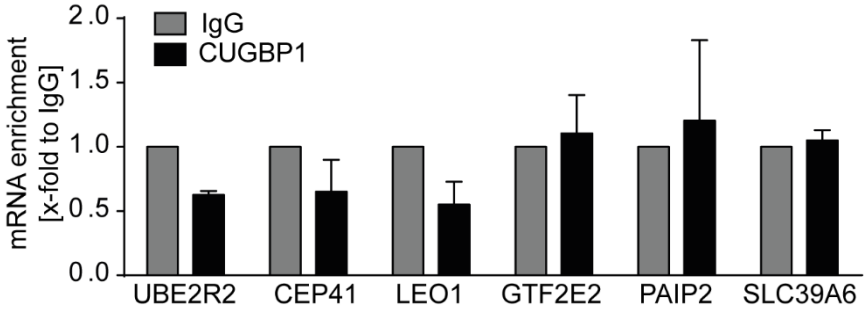

Figure 25: Binding of CUGBP1 to potential decoy targets.
RIP of A549 cells with antibodies against CUGBP1 or normal mouse IgG. Co-precipitated RNAs were quantified using qRT-PCR. mRNA quantification of UBE2R2, CEP41, LEO1, GTF2E2, PAIP2 and SLC39A6 in unstimulated A549 cell IP samples. Relative enrichment normalized to IgG is given as mean +SEM of n=3 experiments.

Although it cannot be excluded that one of the seven mRNAs is bound under different conditions or in a different cell type, they were excluded as interesting candidates.

3.6 Subcellular localization of CUGBP1 and miR-574-5p in A549 cells

Since the search for new decoy targets seemed to have an end at that point of the study, a different approach was needed to further characterize the decoy mechanism. As a next step, it was necessary to elucidate where exactly in the cell the interaction of CUGBP1 and miR-574-5p takes place. Therefore, subcellular localization of the two binding partners in A549 cells was visualized by performing immunofluorescence staining and FISH assay, respectively. Localization of miR-574-5p was determined by using a specific DIG-labeled LNA probe and a DIG binding antibody. Whereas immunofluorescence staining with a specific primary antibody was performed in order to localize CUGBP1. As control, the well-established nuclear marker DAPI was used. Interestingly, with these techniques it was demonstrated that both, CUGBP1 and miR-574-5p were mainly located in the nuclei of A549 cells (see Figure 26). Nearly no cytosolic signals were detected for miR-574-5p, which is quite unusual for a miR. CUGBP1 exhibited stronger cytoplasmic signals but was still predominantly located in the nucleus. IL-1β stimulation had no influence on subcellular localization of both CUGBP1 and miR-574-5p. All staining experiments were kindly performed by Julia Wellstein using established protocols.

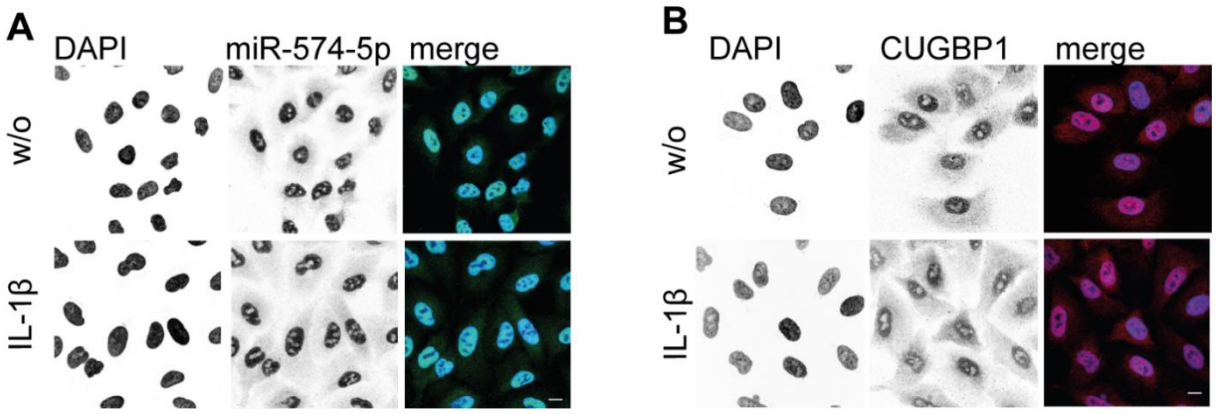

Figure 26: Subcellular localization of CUGBP1 and miR-574-5p in A549 cells.
(A) FISH assay and (B) immunofluorescence staining of A549 cells with or without IL-1β-stimulation for 24 h. miR-574-5p FISH was performed using DIG-labelled miRCURY LNA probes (green). Immunofluorescence staining with specific antibody visualized subcellular localization of CUGBP1 (red). Nuclei were counterstained with DAPI (blue). Scale bar = 10 µm. One representative image of n=3 independent experiments is shown.

Hence, it was concluded that the decoy mechanism mainly takes place in the nucleus, especially during the experiments performed herein. In case miR-574-5p interfered solely with CUGBP1's nuclear functions, this would shift the focus of this project from protein level regulation more to the direction of splicing regulation.

3.7 Bioinformatical analysis of 3’UTR splicing patterns

The main nuclear function of CUGBP1 is regulation of AS. Thus, it was consequential to continue with investigations concerning splicing. As the only known decoy target of CUGBP1 and miR-574-5p, mPGES-1 served as model, especially since it represents a very unique case. CUGBP1 binds to two binding sites in the mPGES-1 3’UTR and influences AS which creates a shorter 3’UTR isoform [196]. This was used as a paradigm, meaning other potential decoy candidates were analyzed in regard of this specific splicing pattern. For this comprehensive analysis, all 399 proteins which showed an upregulation in response to ΔCUGBP1 in soluble or microsomal fraction of the proteomics study were included. 3’UTR sequences from all described isoforms were downloaded, using ensemble biomart (GRCh38/.p12, version 91, [252]). This resulted in a list of 1916 3’UTR sequences which were then aligned with 42 described CUGBP1 binding motifs (see Table 10, using the online tool Splice Aid F [109]).

Table 10. List of potential binding motifs of CUGBP1

No.	Motif	Length (nt)
1	CUUGCUUGCUUGCUUGCUUGCUUGCUUGCUUGCUUGCUUGCUUGCUUGCUU GCUUGCUUGCUUGCUUGCUUGCUUGCUUGCUUGCUUGCUUGCUUGCUUGCU UGCUUGCUUGCUUGCUUGCUUGCUUGCUUGCUUGCUUGCUUGCUUGCUUG	151
2	CAGACAGACAGACAGACAGACAGACAGACAGACAGACAGACAGACAGACAGAC AGACAGACAGACAGACAGACAGACAGACAGACAGACAGACAGACAGACAGACA GACAGACAGACAGACAGACAGA	127
3	UCUGUCUGUCUGUCUGUCUGUCUGUCUGUCUGUCUGUCUGUCUGUCUGUCU GUCUGUCUGUCUGUCUGUCUGUCUGUCUGUCUGUCUGUCUGUCUGUCUGUC UGUCUGUCUGUCUGUCUGUCUGUCUG	127
4	CAGCAGCAGCAGCAGCAGCAGCAGCAGCAGCAGCAGCAGCAGCAGCAGCAGC AGCAGCAGCAGCAGCAGCAGCAGCAGCAGCAGCAGCAGCAGCAGCAGCAGCA GCAGCAGCAGCAGCAGCAG	122
5	CGGACGGACGGACGGACGGACGGACGGACGGACGGACGGACGGACGGACGG ACGGACGGACGGACGGACGGACGGACGGACGGACGGACGGACGGACGGACG GACGGACGGACGGACGGA	119
6	UCCGUCCGUCCGUCCGUCCGUCCGUCCGUCCGUCCGUCCGUCCGUCCGUCC GUCCGUCCGUCCGUCCGUCCGUCCGUCCGUCCGUCCGUCCGUCCGUCCGUC CGUCCG	107
7	CCGCCGCCGCCGCCGCCGCCGCCGCCGCCGCCGCCGCCGCCGCCGCCGCCG CCGCCGCCGCCGCCGCCGCCGCCGCCGCCGCCGCCGCCG	90
8	CGGCGGCGGCGGCGGCGGCGGCGGCGGCGGCGGCGGCGGCGGCGGCGGCG GCGGCGGCGGCGGCGGCGGCGGCGGCGGCGGCGGCGGCGG	90
9	CCCGCCCGCCCGCCCGCCCGCCCGCCCGCCCGCCCGCCCGCCCGCCCGCCC GCCCGCCCGCCCGCCCGCCCGCCCGCCCGCCCG	84
10	UGUGUGUGUGUGUGUGUGUGUGUGUGUGUGUGUGUGUGUGUGUGUGUG	48
11	CUGCUGCUGCUGCUGCUGCUGCUGCUGCUGCUG	33
12	UGUGUGUGUGUGUGUGUGUGUGUGUGUUUUU	31
13	CUCUCUCUCUCUCUCUCUCUCUCUCUCUCU	30
14	CUGCUGCUGCUGCUGCUGCUGCUGCUGCUG	30
15	GUUGGUUGGUUGGUUGGUUGGUUGGUUGGU	30
16	UAUGUAUGUAUGUAUGUAUGUAUGUAUGUA	30
17	UGGUGGUGGUGGUGGUGGUGGUGGUGGUGG	30
18	UGUGUGUGUGUGUAUGUGUGUGUGUGUGUG	30
19	UGUGUGUGUGUGUGUGUGUGUGUGUGUGUG	30
20	UUGUUGUUGUUGUUGUUGUUGUUGUUGUUG	30
21	UGUGUGUGUGUGUGUGUGUGUGUGUUUUU	29
22	CAUGCAUGCAUGCAUGCAUGCAUGCAUG	28
23	CCUGCCUGCCUGCCUGCCUGCCUGCCUG	28

24	UAUGUAUGUAUGUAUGUAUGUAUGUAUG	28
25	UGUGUGUGUGUGUGUGUGUGUGUUUUU	27
26	GUGUUUGUGUUUGUGUGUGUUUGUU	25
27	CUGCUGCUGCUGCUGCUGCUGCUG	24
28	CUGCUGCUGCUGCUGCUGCUGCUG	24
29	GUUUGUUUGUUUGUUUGUUUGUUU	24
30	UUUUUUUGUUGUGUUUUUUCCUU	23
31	UUUCUUGUUUGUUUGUUUGGGU	22
32	UGUUGUGUGUGUGUGU	16
33	UGUGUUGUGUGU	12
34	UGUGUGUGUGU	11
35	UGUGUGUGUG	10
36	UGUGUGUGU	9
37	UGUGUGUG	8
38	CUGUCUG	7
39	UGUGUGU	7
40	UGUUUGU	7
41	UGUGUG	6
42	UGUGU	5

According to Splice Aid F; used in the bioinformatical 3'UTR analysis [109].

In a first step, a high stringency analysis was performed, looking for the exact splicing pattern of mPGES-1 (see Figure 27A). However, it turned out that none of the transcripts exhibits this exact pattern with two very long binding sites and a 1000 nt intron in between. Therefore, it was considered that the splicing pattern might not be identical.

In a second low stringency analysis, criteria were loosened, screening for transcripts containing 2 or more binding sites of at least 8 nt length and with at least 100 nt in between (see Figure 27B).

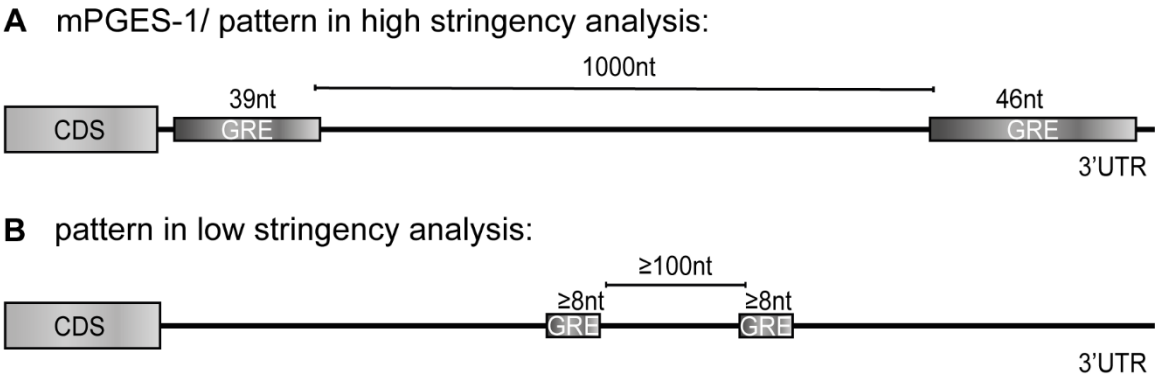

Figure 27: High stringency and low stringency approach in bioinformatical 3'UTR analysis.
All 3'UTRs of potential CUGBP1 targets were analyzed concerning a (A) high stringency/ mPGES-1 splice pattern or (B) low stringency pattern with two or more CUGBP1 binding sites (≥ 8 nucleotides), with potential intron (≥ 100 nucleotides).

As listed in Table 11, 575 transcripts resembling 30% of the originally 1914 3'UTRs, contained a CUGBP1 binding site. Restricting it to binding sites that were 8 nt or longer, only 118 transcripts (6%) were left, as a lot of them were shorter (see number 38-42 in Table 10). By applying the criterion that at least 2 distinct binding sites of at least 8 nt length should be in the

sequence, only 33 transcripts were left (1.7%). Eventually, by looking for an additional intron of at least 100 nt in between the binding sites, only 11 transcripts (0.6%) fulfilled all the criteria. Due to the binding motifs of CUGBP1 which often are repeats of only two nt (e.g. UG/TG) the last step also removed transcripts that had several UG-repeat binding motives but only 2 nt apart, meaning that these were actually the same binding sites. For instance, the 3'UTR of Lysosome-associated membrane protein 2 harbors a 40-nt UG-repeat, which is why it was predicted to have 17 CUGBP1 binding sites (of number 37, Table 10). However, when looking at the exact positions within the 3'UTR sequence, it becomes clear that these predicted distinct binding sites are at position 420, 422, 424 etc., belonging to the same 40-nt UG-repeat. Therefore, the last criterion was not only used to find potential introns but also to support the second criterion of two distinct binding sites.

Table 11. Number of transcripts fulfilling the low stringency analysis criteria.

Criterion I	Criterion II	Criterion III	
Binding site length	**Number of binding sites**	**Space between binding sites**	**Number of transcripts left**
All	All	All	575
binding site of ≥8 nt	All	All	118
binding site of ≥8 nt	≥2 binding sites	All	33
binding site of ≥8 nt	≥2 binding sites	≥ 100 nt intron	11

Those 11 transcripts that were finally left, belong to 9 different genes (see Figure 28, and Table 17; appendix)

- MAF BZIP Transcription Factor K (MAFK)
- UBX Domain Protein 2B (UBXN2B)
- Complexin 2 (CPLX2)
- UBE2R2
- Superoxide dismutase 2 (SOD2)
- CUB domain-containing protein 1 (CDCP1)
- CEP41
- RNA Binding Motif Protein 23 (RBM23)
- SET Domain Containing Lysine Methyltransferase 7 (SETD7)

In ten of the 3'UTRs, exactly two CUGBP1 binding sites were found, while the 3'UTR of CPLX2 harbors three distinct binding sites. However, the first and the second one at position 1233 and 1250 do not span a potential intron of ≥ 100 nt. Binding motifs were mostly 8 nt long (number 37 in Table 10), except for CEP41 which harbors a 9 nt binding motif (number 36 in Table 10) and SOD2 which harbors a 11 nt binding motif (number 34 in Table 10). The potential introns

in between the two binding sites range from rather small 199 nt for CEP41 up to 7537 nt for SOD2 (for more details see Table 17; appendix).

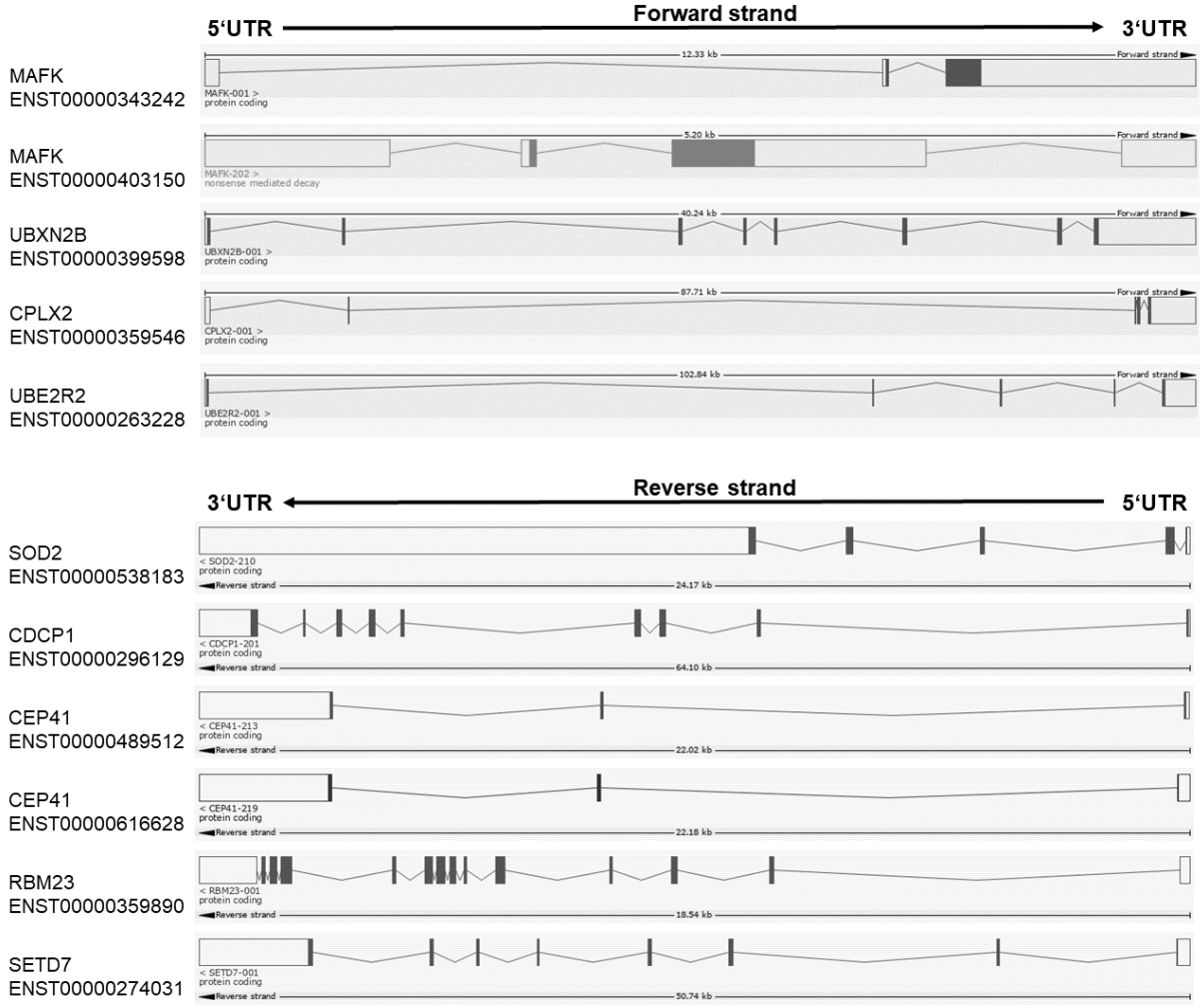

Figure 28: Transcripts from low stringency 3'UTR analysis.
Transcripts which harbor two (in case of CPLX2 three) CUGBP1 binding sites in the 3'UTR. For more details, see Table 17; appendix. All transcripts are protein coding except for MAFK ENST00000343242 which is predicted to be an NMD target. Downloaded from ensemble Human (GRCh38.p12).

Of these, only CEP41 and UBE2R2 depicted the "decoy regulation pattern" in the mass spectrometry data. However, they were not bound by CUGBP1 in the RIP assay of A549 cells (see Figure 25) and therefore excluded as novel decoy targets. This small number of proteins, together with the fact that the high stringency analysis did not provide any hits, strongly indicated that it is a very exceptional splice pattern and the decoy mechanism must be very specific.

4. Discussion

When it was revealed in 2010 that miRs can act as decoy to RBPs [193], this opened up a whole new field of miR research. Recently, the decoy mechanism was also described for CUGBP1 and miR-574-5p [196]. The resulting regulation of mPGES-1 expression and PGE_2 levels in non-small cell lung cancer gives hope for the development of novel therapeutic approaches and might even allow the use of miR-574-5p as a biomarker for lung cancer patient stratification.

4.1 Insights into the proteome of A549 lung cancer cells

A mass spectrometry-based proteomics study was conducted in order to elucidate existence and global distribution of novel targets of CUGBP1 and miR-574-5p. To this end, A549 lung cancer cells with manipulated levels of CUGBP1 or miR-574-5p were used. Of note, the proteomics study was used as shotgun procedure. It gives first indications which proteins might be regulated but does not always depict the exact expression changes. The regulation of mPGES-1 is a simple example for that. It was not regulated upon ΔCUGBP1 in the mass spectrometry data, although it is a described CUGBP1 target. Therefore, it was necessary that any information drawn from the data set was validated. Experimentally, the regulation of distinct proteins was successfully validated via Western blot analysis. Moreover, published data sets of CUGBP1 and miR-574-5p targets were compared with lists of potential targets from the proteomics study. For instance, a published Clip Seq (cross-linking immunoprecipitation-high-throughput sequencing) data set of Tonqueze et al. revealed a 25% overlap (102 proteins) with potential CUGBP1 targets [260]. For canonical miR-574-5p targets, a similar approach was conducted: 130 (20%) of them were also found in a list of predicted targets from the database targetscan.org [261]. Finally, one of the strongest downregulated proteins upon ΔCUGBP1 in the microsomal fraction was CUGBP1 itself (-3.1-fold), which validates the knockdown as well as the mass spectrometry data (see Table 16). With that the accuracy of the proteomics study was assured, both experimentally and by comparison to literature and databases.

In order to broaden the insights in compartment specific post-transcriptional regulation, proteins from soluble and microsomal fraction were separately analyzed in the proteomics study [250]. It is generally assumed that soluble proteins are translated from free ribosomes in the cytosol, whereas the microsomal fraction is associated with ribosomes of the rough endoplasmic reticulum [262]. Indeed, differential regulation between fractions was observed for many proteins. Concerning mass spectrometry data, 78 proteins were observed showing opposite regulation in soluble and microsomal fraction, thereof 48 in the two miR conditions

and 30 in the CUGBP1 condition. Using Western blot analysis during proteomics validation, the R-SMADs SMAD2 and SMAD3 were also observed to show opposite regulation in the two fractions. This underlines the theory that RBPs may allow different translational efficiencies concerning free and endoplasmic reticulum-bound ribosomes [263] [264].

The microsomal fraction appears to be of greater importance compared to the soluble fraction. On the one hand, there was a broader diversity of proteins detected (60% more different proteins than in the soluble fraction). Compared to other proteomics studies, this result is unusual. Since its establishment in 2008, the microsomal fractionation protocol has been used in a variety of proteomics studies [250]. For monocytic MM6 cells and A549 lung cancer cells, it was demonstrated in the last years that the soluble and microsomal fractions contained roughly the same amount of different proteins [265] [195] [266]. Thus, the discrepancy to this thesis could be potentially caused by technical variances such as differences in digestion protocol, labelling and buffer composition [265].

Another point to consider is that there was a higher percentage of microsomal proteins that actually revealed a regulation in response to the oe or knockdowns. An explanation could be that CUGBP1 exerts its functions more in the microsomal protein fraction. This hypothesis is supported by the fact that CUGBP1 protein itself can be found predominantly in the microsomal fraction as confirmed by Western blot analysis. Furthermore, it was previously shown that the decoy targets of miR-328 and hnRNP E2 are also predominantly found in the microsomal fraction of MM6 cells [195].

In conclusion, it can be assumed that effects of CUGBP1 and the decoy with miR-574-5p are more prominently found in the microsomal protein fraction. Hence, special emphasis was placed on this fraction in the course of this project.

4.2. Discovery and verification of new canonical CUGBP1 targets

In order to screen for potential new targets of CUGBP1, different approaches were combined. Concerning the mass spectrometry data, around 72% of the upregulated proteins were found to have a CUGBP1 binding site. Comparing this to total protein amounts, 4.5% of all detected proteins could potentially be CUGBP1 targets. This fits the general assumption that CUGBP1 is a multifunctional RBP, as a lot of transcripts contain its binding motif. Nevertheless, CUGBP1 is described to bind those potential targets strictly context specific [267]. Not only the binding alone but also the outcome is context specific, as CUGBP1 can influence a variety of mRNA processing steps, from AS [111] [112] in the nucleus to translation in the cytoplasm [133] [134] [135]. Furthermore, these assumptions are based on the repressive functions of CUGBP1. In specific cases CUGBP1 was also observed to have a positive impact on its targets [136] [137]. Therefore, the downregulated proteins in response to ΔCUGBP1 could potentially also be

positively regulated by CUGBP1. Moreover, CUGBP1 binding sites were only analyzed in 3'UTR sequences within this study. This was consequential, as most of the time CUGBP1 is described to bind to 3'UTRs of target mRNAs and additionally mPGES-1 was used as a model for a decoy target. Of note, in some rare cases CUGBP1 was also observed to bind to exon-intron boundaries within the CDS [268] or 5'UTR sequences [269] [270]. Therefore, the actual number of targets might be even higher.

The NADH-ubiquinone NDUFS2 was mentioned as potential CUGBP1 target in HeLa cells for the first time in a study by Rattenbacher et al. [84]. NDUFS2 is part of the core subunit of the mitochondrial membrane respiratory chain NADH dehydrogenase (mitochondrial complex I) [271] [272]. This complex is an assembly of at least 43 different subunits, while NDUFS2 belongs to a group of 7 iron-sulfur metalloproteins which stabilize the early intermediate complex [273]. In order to investigate the diverse binding motifs of CUGBP1, Rattenbacher et al. performed immunoprecipitation and subsequently microarray analysis. This resulted in a list of 613 potential CUGBP1 targets including their specific sequences. NDUFS2 was identified as one of 477 transcripts that were solely found in the CUGBP1-IP. With a short 3'UTR of only 202 nt, NDUFS2 contains a 31 nt long GU-repeat at position 77 that serves as binding site for CUGBP1. This motif was additionally present in 17% of the other detected transcripts in the study and has a 7% prevalence in the whole genome [84]. Furthermore, they could show that by binding of CUGBP1, the NDUFS2 mRNA as well as any other mRNA containing the specific motif was rapidly degraded, hinting towards a CUGBP1-mediated decay mechanism. This hypothesis does also match the results within this thesis. In A549 cells, CUGBP1 also seems to have a negative impact on NDUFS2 gene expression. However, NDUFS2 did not show the "decoy regulation pattern". Therefore, it cannot be considered as decoy target but only as canonical CUGBP1 target. It is described that mutations in the NDUFS2 gene go along with the autosomal recessive Mitochondrial Complex I Deficiency [274] [275] [276]. This heterogeneous disease can have a variety of phenotypes from lethal neonatal disease to adult-onset neurodegenerative disorders, cardiomyopathy or impaired liver function [277] [278] [279]. By influencing a protein of the respiratory chain, it can be assumed that CUGBP1 could have an impact on cellular energy supply as well as associated diseases.

Another protein family that was investigated are the SMADs. Functionally, they act as signal transducers for the Transforming growth factor (TGF)-β signaling pathway. They can be divided in the so-called receptor (R-) SMADs (SMAD1-3, SMAD5 and SMAD8-9), the Co-SMAD (SMAD4) and the inhibitory (I-) SMADs (SMAD6-7) [280] [281] [282]. Upon TGF-β receptor activation, two R-SMADs get phosphorylated by the receptor kinase and build a complex with a Co-SMAD [283] [284]. The trimer then translocates to the nucleus, where it

acts as transcription factor. As a result, upregulation of certain response genes like Snail Family Transcriptional Repressor 1 (Snail1), Zinc Finger E-Box Binding Homeobox 1 (ZEB1) and Twist Family BHLH Transcription Factor 1 (Twist1) [285] [286] [287] has been observed. As those are all associated with EMT, SMAD proteins are considered being essential for tumor metastasis throughout a variety of cancer types [288].

Thus, SMAD proteins were an interesting objective within this project, as metastasis was predicted by IPA and also some SMADs were detected in the proteomics study. It was verified that SMAD2 is a canonical target of CUGBP1. SMAD3 was another promising candidate, but the mRNA was not bound by CUGBP1, at least under the conditions investigated here. This does not necessarily exclude SMAD3 as CUGBP1 target. Potentially, binding of SMAD3 mRNA only occurs under certain conditions e.g. with a certain stimulus like TGF-β, some culture conditions like starvation or simply in another cell type [267]. Interestingly, another family member, SMAD7 was not detected in the proteomics study. Nevertheless, it is described as CUGBP1 target in C2C12, a murine myoblast cell line [110]. In a publication by Lee et al. RIP assays proved the interaction of CUGBP1 with SMAD7 mRNA. It was further elucidated that binding led to a destabilization of the SMAD7 transcript, while knockdown of CUGBP1 increased the stability of the mRNA [110]. This fits to the general assumption that CUGBP1 is a destabilizing factor. In A549 cells, SMAD7 is barely expressed, which might explain why it was not detected in the proteomics study. However, it is interesting that several members of the SMAD family seem to be affected by CUGBP1. In a similar way, this is already described for the signal recognition particles (SRP) [117] which underlines the existence of CUGBP1 regulons.

4.3 Decoy target search

One of the main aims of this project was it to investigate if the decoy mechanism affects other targets of CUGBP1 or if it is strictly specific for mPGES-1. In that regard, a first approach was it to screen for a “decoy regulation pattern” on protein level.

(I) CUGBP1 has generally negative effects on its targets, based on its role as a translational repressor or decay mediator. Therefore, it can be hypothesized that the majority of decoy and canonical CUGBP1 targets should react to the knockdown with an increased protein level.

(II) Taking a closer look at the miR-574-5p oe condition, it becomes clear that this also should have a positive effect on protein levels of the decoy targets. Similar to the ΔCUGBP1 condition, little to no CUGBP1 can bind to the binding sites as miR-574-5p acts as competitive inhibitor and sequesters CUGBP1 away from its target. Hence, an increased mPGES-1 protein level can be observed.

(III) In the ΔmiR-574-5p samples, CUGBP1 can easily bind its targets. Decoy target proteins were expected to be decreased compared to control, while canonical CUGBP1 targets should not be affected by the miR-574-5p levels. In the case of mPGES-1, binding of CUGBP1 leads to a lower amount of the 3'UTR splice variant and thus to a lower protein level.

When the proteomics data were analyzed concerning stringent criteria for this "decoy regulation pattern", it was revealed that only 7 microsomal proteins (0.1% of total proteins) did resemble this perfect pattern that matched all three criteria. In Western blot analyses, no proteins were found to reveal this "decoy regulation pattern" except for mPGES-1. The analyzed CUGBP1 targets NDUFS2, SMAD2 and SMAD3 did also not show the expected pattern. Unfortunately, the Odyssey Western blot system provided too little sensitivity for the detection of some weakly expressed proteins like HMGA2. Nevertheless, concerning the decoy target search on protein level it could be assumed that the decoy mechanism does not have a global impact on A549 proteome. This was especially intriguing, as it was initially assumed that the decoy mechanism would influence the expression of a variety of genes. In a recent study, it was shown that numerous proteins could be regulated by the decoy function of miR-328 and hnRNP E2 [195]. Therefore, it would have been reasonable that the miR-574-5p/CUGBP1 decoy would also have a global impact. However, the data within this thesis indicate the opposite.

Overall, it can be assumed that the CUGBP1 and miR-574-5p decoy mechanism would not promiscuously affect a lot of proteins.

4.4 Bioinformatical 3'UTR analysis revealed unique splice pattern

As it was demonstrated that both CUGBP1 and miR-574-5p were located predominantly in the nucleus, the CUGBP1 function as splicing factor came into focus. It was reasonable, as it was already described that mPGES-1 mRNA was alternatively spliced [196]. In fact, mPGES-1 mRNA is spliced in the 3'UTR creating a shorter isoform. Thereby, a 3'UTR ALU element is removed as well as a myriad of miR and RBP binding sites which allow for a higher translational efficiency [196]. It is generally known that shorter 3'UTRs are beneficial for a higher expression profile due to a diminishment of binding sites [289].

In a bioinformatical 3'UTR analysis it could be shown that the 3'UTR splicing pattern of mPGES-1 was not found in any other transcript and therefore was termed as being unique. This outcome was expected, as it was unlikely to find another 3'UTR with one 39 nt and one 46 nt CUGBP1 binding motive, with a 1000 nt intron in between. In a low stringency analysis, it was screened for a similar pattern with two shorter CUGBP1 binding sites and with only 100 nt in between. The resulting list of only 11 transcripts (0.5% of the analyzed transcripts) gave an additional hint that this was a quite specific pattern.

Of note, this approach only aimed to find potential other splice patterns in 3'UTRs, as the 3'UTR splicing of mPGES-1 was used as a model. Conventional splicing processes were not considered herein, although CUGBP1 does also influence (alternative) splicing in the CDS [111] [112]. Further, it has to be mentioned that CUGBP1 cannot only bind in 3'UTR sequences but also in CDS and 5'UTRs [268] [269]. Therefore, this bioinformatical study was just a first approach and needs to be followed by additional analyses like bioinformatical extension to CDS or experimental analysis of splice events.
Moreover, as two of the low stringency transcripts were not bound by CUGBP1 in RIP assays, further experiments need to be conducted. It is likely that with an additional stimulus or other cellular conditions the binding of CUGBP1 could be triggered. Unfortunately, as CUGBP1 binds strictly context specific and is described to function in various steps of mRNA processing this would have exceeded this project.

Overall, the screening for new decoy targets using several different approaches did not result in any conclusive hits. This highly complex proteomics study provided a broad insight into the proteome of A549 lung cancer cells, including compartment-specific regulation and new canonical targets of CUGBP1 but did not provide any new targets regulated by the interaction of CUGBP1 and miR-574-5p. Hence, it is assumable that in A549 cells mPGES-1 is the only protein regulated by the CUGBP1/miR-574-5p decoy mechanism.

4.5 Physiological impact

In order to investigate the overall physiological functions of CUGBP1, miR-574-5p and the decoy mechanism, a pathway analysis was performed that predicted biological functions, canonical pathways and upstream regulators based on the mass spectrometry data. As metastasis and migration were among the top ten predictions, it was an intriguing research topic.

4.5.1 Influence of miR-574-5p on metastasis

In wound healing and trans-well assays, surprisingly, no significant effects were measured with miR-574-5p oe cells compared to control cells. This clearly contradicts literature, where miR-574-5p was described as being pro-metastatic in small cell and non-small cell lung cancer cells, respectively [209] [210]. In these two publications from the same research lab, they investigated the influence of miR-574-5p on the migration of A549 cells with the same two methods described within this thesis but with a different outcome. However, there were differences in the procedures. For the wound healing assays within this project, cells were pre-starved, before the actual assay in order to minimize proliferation of the cells. This step was

skipped in the publications by Zhou et al.. Further, they performed trans-well assays for 24 h. This opens up the possibility of further proliferation of the migrated cells on the bottom of the membrane, as A549 cells are described to have a doubling time of around 18-22 h [290]. Indeed, transient miR-574-5p oe has a pro-proliferative effect on A549 cells [196] which could explain why they measured enhanced number of cells which potentially were falsely considered as migrated cells.

Another possible explanation could be that within this project a stable miR-574-5p oe cell line was used. Compared to a transient transfection, stable integration is dependent on position, copy number and site of integration. Potentially the viral particle transduction could have caused other variances in the cell, besides the miR-574-5p oe and therefore caused a different migratory behavior. An example that underlines this theory is that A549 cells transiently overexpressing miR-574-5p show an increased proliferation, while stable miR-574-5p oe cells do not [291]. In order to exclude those variances, it would be necessary to repeat the wound healing and trans-well assays with a transient overexpression or knockdown of the miR.

Another point to mention is that IPA predicted metastasis to be diminished with miR-574-5p oe, which does not fit the results of the migration assays and additionally stands in contrast to the two publications about the enhancing effects of miR-574-5p on migration [209] [210]. However, in this context, it has to be mentioned that the IPA is based on the mass spectrometry results which were performed with transient miR-574-5p oe (300-fold oe), while the migration assays were performed with a stable miR-574-5p oe (15-fold oe) [196].

What supports the IPA is the fact that it also predicted metastasis to be decreased upon ΔCUGBP1. Especially metastasis of breast cancer cells was predicted in that context. This underlines the recently published positive impact of CUGBP1 on EMT-proteins and tumor metastasis of breast cancer cells [136] [137].

Overall, the migration assays do not give any conclusive results and further experiments are needed to exclude any influence of miR-574-5p and CUGBP1 on tumor metastasis.

4.5.2 Influence of mPGES-1 on metastasis

In a further approach, the influence of mPGES-1 was investigated. A previous study showed that the pro-proliferative effect of miR-574-5p was solely caused by its influence on mPGES-1. Therefore, this was also an interesting point to investigate in the context of tumor migration.

The fact that mPGES-1 did not affect migration in the experiments within this thesis is controversial. Two publications describe mPGES-1 as promoter of cancer metastasis *in vivo* [292] [293]. Both injected tumor cells intravenously in wild type or mPGES-1 knockout mice and determined metastases of the lung by number and weight of the whole organ. Although

this is a common procedure, it does not fully cover the physiological background of tumor metastasis.

In general, to undergo metastasis the cancer cells do have to go through a process called EMT [294]. It includes an extensive phenotypical change from an epithelial to a more mesenchymal cell type. Thereby, the cells lose their cell-cell-adhesion and acquire migratory abilities, accompanied by a mayor change in the protein profile. This transition is crucial for invasion, meaning that the tumor cells gain the ability to enter the vascular system. Only then, the cells can migrate to distant sites within the body. Then, the migrated cells have to undergo the reverse process, called mesenchymal epithelial transition to regain their adhesive properties and form new metastases [295] [296].

By injecting tumor cells directly in the blood system, the metastasis process is tremendously facilitated. Further, *in vivo* models are only basally comparable with trans-well and wound healing assay in cell culture systems. Nevertheless, it is odd that mPGES-1 does not render migration of the lung cancer cells at all. Therefore, it could be interesting to perform further experiments in that regard. For example, invasion assays with 3D cell culture would provide a more physiological environment and potentially could reveal new insights.

4.6 Outlook

This thesis provided first evidence that the decoy mechanism of miR-574-5p and CUGBP1 could be specifically regulating mPGES-1. Using different screening approaches, no other target could be found that was regulated by the interaction of the miR and the RBP.

However, the decoy mechanism itself is still not fully understood. In the future it could be an intriguing research topic to investigate how the interaction of miR-574-5p and CUGBP1 is triggered. Until now it is described to happen in the presence of IL-1β. What exactly causes miR-574-5p to bind to CUGBP1 still remains unclear. The phosphorylation status of CUGBP1 could be the key, as it is a known regulator of CUGBP1 function [120] [121] [122] [123] [119]. Further, the existence of binding partners or chaperones could also be possible. Additionally, the exact impact of IL-1β is of great interest. Signaling downstream of the IL-1β receptor involves recruitment of myeloid differentiation primary response gene 88 (MyD88) and/or Toll-interleukin receptor domain containing adaptor-inducing interferon-β (TRIF) [297]. Interestingly, miR-574-5p is also described to act as TLR8 ligand and activate this exact signaling pathway, which provides a promising connection [184] [185] [186] [187].

Finally, specificity of the decoy mechanism is an interesting question. Until now, the mechanism is only described for two pairs: miR-328/hnRNP E2 and miR-574-5p/CUGBP1 [193] [196]. It would be interesting to investigate if there are more miR/RBP pairs or if the given ones can also interact with other partners. CUGBP1 could potentially bind other GU-rich miRs.

Vice versa, miR-574-5p is described to be bound by Transactive response DNA binding protein43 kDa (TDP-43) [298], an RBP which facilitates pri-miR processing and builds a complex with Drosha [299]. Further GU-binding RBPs are Nova-1 [300] and CUGBP2 [301] which could also potentially bind to miR-574-5p. Clearly, future experiments are needed to fully elucidate this topic.

The fact that the miR-574-5p/CUGBP1 decoy is specific for mPGES-1 was initially surprising. Eventually, the discovery of the unique 3'UTR splice pattern provided a possible explanation. Moreover, it has to be taken into account that the miR-574-5p effects on tumor progression were also based solely on mPGES-1 [196]. This was probably the first hint for this kind of specificity. Although one can never fully exclude each and every potential option, the results within this thesis clearly support the postulation that mPGES-1 is the only protein regulated by the miR-574-5p/CUGBP1 decoy in A549 cells. This would open up new options for NSCLC patients. It is well-known that not all patients benefit from a treatment with medication that aims to reduce PGE_2 levels [248] [249]. Presumably, because not all lung adenocarcinomas are dependent on PGE_2. Therefore, the miR-574-5p levels could serve as stratification marker to identify the subgroup with high mPGES-1 and PGE_2 levels. For those patients, treatment with NSAIDs could be a beneficial tool in the fight against NSCLC.

References

[1] P. W. B Alberts, A Johnson, J Lewis, M Raff, K Roberts, *Molecular Biology of the cell*, Fifth edit. Garland Science, 2008.

[2] F. Uchiumi, Ed., *Gene Expression and Regulation in Mammalian Cells - Transcription From General Aspects*. InTech, 2018.

[3] D. L. Bentley, “Coupling mRNA processing with transcription in time and space.,” *Nat. Rev. Genet.*, vol. 15, no. 3, pp. 163–75, 2014.

[4] T. Glisovic, J. L. Bachorik, J. Yong, and G. Dreyfuss, “RNA-binding proteins and post-transcriptional gene regulation.,” *FEBS Lett.*, vol. 582, no. 14, pp. 1977–86, Jun. 2008.

[5] A. H. Corbett, “Post-transcriptional regulation of gene expression and human disease.,” *Curr. Opin. Cell Biol.*, vol. 52, pp. 96–104, 2018.

[6] M. Stewart, “Polyadenylation and nuclear export of mRNAs.,” *J. Biol. Chem.*, vol. 294, no. 9, pp. 2977–2987, 2019.

[7] H. A. Meijer *et al.*, “A novel method for poly(A) fractionation reveals a large population of mRNAs with a short poly(A) tail in mammalian cells.,” *Nucleic Acids Res.*, vol. 35, no. 19, p. e132, 2007.

[8] K. Buiting, C. Körner, B. Ulrich, E. Wahle, and B. Horsthemke, “The human gene for the poly(A)-specific ribonuclease (PARN) maps to 16p13 and has a truncated copy in the Prader-Willi/Angelman syndrome region on 15q11-->q13.,” *Cytogenet. Cell Genet.*, vol. 87, no. 1–2, pp. 125–31, 1999.

[9] K. C. M. Moraes, C. J. Wilusz, and J. Wilusz, “CUG-BP binds to RNA substrates and recruits PARN deadenylase.,” *RNA*, vol. 12, no. 6, pp. 1084–91, Jun. 2006.

[10] W. S. Lai, E. Carballo, J. R. Strum, E. A. Kennington, R. S. Phillips, and P. J. Blackshear, “Evidence that tristetraprolin binds to AU-rich elements and promotes the deadenylation and destabilization of tumor necrosis factor alpha mRNA.,” *Mol. Cell. Biol.*, vol. 19, no. 6, pp. 4311–23, Jun. 1999.

[11] K. Leppek, J. Schott, S. Reitter, F. Poetz, M. C. Hammond, and G. Stoecklin, “Roquin promotes constitutive mRNA decay via a conserved class of stem-loop recognition motifs.,” *Cell*, vol. 153, no. 4, pp. 869–81, May 2013.

[12] W. Filipowicz, S. N. Bhattacharyya, and N. Sonenberg, “Mechanisms of post-transcriptional regulation by microRNAs: are the answers in sight?,” *Nat. Rev. Genet.*, vol. 9, no. 2, pp. 102–14, Feb. 2008.

[13] M. Brengues, D. Teixeira, and R. Parker, “Movement of eukaryotic mRNAs between polysomes and cytoplasmic processing bodies.,” *Science*, vol. 310, no. 5747, pp. 486–9, Oct. 2005.

[14] M. Kulkarni, S. Ozgur, and G. Stoecklin, “On track with P-bodies.,” *Biochem. Soc. Trans.*, vol. 38, no. Pt 1, pp. 242–51, Feb. 2010.

[15] S. N. Bhattacharyya, R. Habermacher, U. Martine, E. I. Closs, and W. Filipowicz, “Relief of microRNA-mediated translational repression in human cells subjected to stress.,” *Cell*, vol. 125, no. 6, pp. 1111–24, Jun. 2006.

[16] A. Nordheim and R. Knippers, Eds., *Molekulare Genetik*. Stuttgart: Georg Thieme Verlag, 2015.

[17] S. Gerstberger, M. Hafner, and T. Tuschl, “A census of human RNA-binding proteins,”

Nat. Rev. Genet., vol. 15, no. 12, pp. 829–845, 2014.

[18] P. J. Wittkopp and G. Kalay, “Cis-regulatory elements: molecular mechanisms and evolutionary processes underlying divergence.,” *Nat. Rev. Genet.*, vol. 13, no. 1, pp. 59–69, Dec. 2011.

[19] U. Dettmer, M. Folkerts, E. Kächler, and A. Sönnichsen, *Intensivkurs Biochemie*. 2005.

[20] F. E. Baralle and J. Giudice, “Alternative splicing as a regulator of development and tissue identity.,” *Nat. Rev. Mol. Cell Biol.*, vol. 18, no. 7, pp. 437–451, 2017.

[21] A. Kalsotra and T. A. Cooper, “Functional consequences of developmentally regulated alternative splicing.,” *Nat. Rev. Genet.*, vol. 12, no. 10, pp. 715–29, Sep. 2011.

[22] E. S. Lander *et al.*, “Initial sequencing and analysis of the human genome.,” *Nature*, vol. 409, no. 6822, pp. 860–921, Feb. 2001.

[23] Q. Pan, O. Shai, L. J. Lee, B. J. Frey, and B. J. Blencowe, “Deep surveying of alternative splicing complexity in the human transcriptome by high-throughput sequencing.,” *Nat. Genet.*, vol. 40, no. 12, pp. 1413–5, Dec. 2008.

[24] E. T. Wang *et al.*, “Alternative isoform regulation in human tissue transcriptomes.,” *Nature*, vol. 456, no. 7221, pp. 470–6, Nov. 2008.

[25] M. L. Tress, F. Abascal, and A. Valencia, “Alternative Splicing May Not Be the Key to Proteome Complexity.,” *Trends Biochem. Sci.*, vol. 42, no. 2, pp. 98–110, 2017.

[26] M. L. Tress, F. Abascal, and A. Valencia, “Most Alternative Isoforms Are Not Functionally Important.,” *Trends Biochem. Sci.*, vol. 42, no. 6, pp. 408–410, 2017.

[27] J. Tazi, N. Bakkour, and S. Stamm, “Alternative splicing and disease.,” *Biochim. Biophys. Acta*, vol. 1792, no. 1, pp. 14–26, Jan. 2009.

[28] Y. Lee and D. C. Rio, “Mechanisms and Regulation of Alternative Pre-mRNA Splicing.,” *Annu. Rev. Biochem.*, vol. 84, pp. 291–323, 2015.

[29] D. L. Black, “Mechanisms of alternative pre-messenger RNA splicing.,” *Annu. Rev. Biochem.*, vol. 72, pp. 291–336, 2003.

[30] L. P. Iñiguez and G. Hernández, “The Evolutionary Relationship between Alternative Splicing and Gene Duplication.,” *Front. Genet.*, vol. 8, p. 14, Feb. 2017.

[31] A. Hegele *et al.*, “Dynamic protein-protein interaction wiring of the human spliceosome.,” *Mol. Cell*, vol. 45, no. 4, pp. 567–80, Feb. 2012.

[32] M. S. Jurica and M. J. Moore, “Pre-mRNA Splicing,” *Mol. Cell*, vol. 12, no. 1, pp. 5–14, Jul. 2003.

[33] Y. Shi, “Mechanistic insights into precursor messenger RNA splicing by the spliceosome.,” *Nat. Rev. Mol. Cell Biol.*, vol. 18, no. 11, pp. 655–670, Nov. 2017.

[34] R. Martinez-Contreras, P. Cloutier, L. Shkreta, J.-F. Fisette, T. Revil, and B. Chabot, “hnRNP proteins and splicing control.,” *Adv. Exp. Med. Biol.*, vol. 623, pp. 123–47, 2007.

[35] J. C. Long and J. F. Caceres, “The SR protein family of splicing factors: master regulators of gene expression.,” *Biochem. J.*, vol. 417, no. 1, pp. 15–27, Jan. 2009.

[36] A. J. Matlin, F. Clark, and C. W. J. Smith, “Understanding alternative splicing: towards a cellular code.,” *Nat. Rev. Mol. Cell Biol.*, vol. 6, no. 5, pp. 386–98, May 2005.

[37] M. C. Wahl, C. L. Will, and R. Lührmann, “The spliceosome: design principles of a

dynamic RNP machine.," *Cell*, vol. 136, no. 4, pp. 701–18, Feb. 2009.

[38] A. N. Ladd and T. A. Cooper, "Finding signals that regulate alternative splicing in the post-genomic era.," *Genome Biol.*, vol. 3, no. 11, p. reviews0008, Oct. 2002.

[39] R. B. Voelker and J. A. Berglund, "A comprehensive computational characterization of conserved mammalian intronic sequences reveals conserved motifs associated with constitutive and alternative splicing.," *Genome Res.*, vol. 17, no. 7, pp. 1023–33, Jul. 2007.

[40] K. Kruger, P. J. Grabowski, A. J. Zaug, J. Sands, D. E. Gottschling, and T. R. Cech, "Self-splicing RNA: autoexcision and autocyclization of the ribosomal RNA intervening sequence of Tetrahymena.," *Cell*, vol. 31, no. 1, pp. 147–57, Nov. 1982.

[41] Dominic W. S. Wong, *The ABCs of Gene Cloning*. Boston, MA: Springer US, 2006.

[42] W. Janning and E. Knust, *Allgemeine Genetik Molekulare Genetik Entwicklungsgenetik*, no. Isbn 9783131287724. 2004.

[43] R. Sandberg, J. R. Neilson, A. Sarma, P. A. Sharp, and C. B. Burge, "Proliferating cells express mRNAs with shortened 3' untranslated regions and fewer microRNA target sites.," *Science*, vol. 320, no. 5883, pp. 1643–7, Jun. 2008.

[44] C. Mayr and D. P. Bartel, "Widespread shortening of 3'UTRs by alternative cleavage and polyadenylation activates oncogenes in cancer cells.," *Cell*, vol. 138, no. 4, pp. 673–84, Aug. 2009.

[45] O. Isken and L. E. Maquat, "Quality control of eukaryotic mRNA: safeguarding cells from abnormal mRNA function.," *Genes Dev.*, vol. 21, no. 15, pp. 1833–56, Aug. 2007.

[46] H. Le Hir, D. Gatfield, E. Izaurralde, and M. J. Moore, "The exon-exon junction complex provides a binding platform for factors involved in mRNA export and nonsense-mediated mRNA decay.," *EMBO J.*, vol. 20, no. 17, pp. 4987–97, Sep. 2001.

[47] C. Cenik, A. Derti, J. C. Mellor, G. F. Berriz, and F. P. Roth, "Genome-wide functional analysis of human 5' untranslated region introns.," *Genome Biol.*, vol. 11, no. 3, p. R29, 2010.

[48] L. G. Wilming, J. G. R. Gilbert, K. Howe, S. Trevanion, T. Hubbard, and J. L. Harrow, "The vertebrate genome annotation (Vega) database.," *Nucleic Acids Res.*, vol. 36, no. Database issue, pp. D753-60, Jan. 2008.

[49] J. L. Ashurst *et al.*, "The Vertebrate Genome Annotation (Vega) database.," *Nucleic Acids Res.*, vol. 33, no. Database issue, pp. D459-65, Jan. 2005.

[50] O. Anczuków and A. R. Krainer, "Splicing-factor alterations in cancers.," *RNA*, vol. 22, no. 9, pp. 1285–301, 2016.

[51] M. Ladomery, "Aberrant alternative splicing is another hallmark of cancer.," *Int. J. Cell Biol.*, vol. 2013, p. 463786, 2013.

[52] R. Holmila, C. Fouquet, J. Cadranel, G. Zalcman, and T. Soussi, "Splice mutations in the p53 gene: case report and review of the literature.," *Hum. Mutat.*, vol. 21, no. 1, pp. 101–2, Jan. 2003.

[53] Z. Kalnina, P. Zayakin, K. Silina, and A. Linē, "Alterations of pre-mRNA splicing in cancer.," *Genes. Chromosomes Cancer*, vol. 42, no. 4, pp. 342–57, Apr. 2005.

[54] M. Roy, Q. Xu, and C. Lee, "Evidence that public database records for many cancer-associated genes reflect a splice form found in tumors and lack normal splice forms.,"

Nucleic Acids Res., vol. 33, no. 16, pp. 5026–33, 2005.

[55] I. Shmulevich and W. Zhang, *Computational and Statistical Approaches to Genomics*. Boston, MA: Springer US, 2006.

[56] J. P. Venables, “Aberrant and alternative splicing in cancer.,” *Cancer Res.*, vol. 64, no. 21, pp. 7647–54, Nov. 2004.

[57] K. Musunuru, “Cell-specific RNA-binding proteins in human disease.,” *Trends Cardiovasc. Med.*, vol. 13, no. 5, pp. 188–95, Jul. 2003.

[58] I. Vlasova-St Louis and P. R. Bohjanen, “Post-transcriptional regulation of cytokine signaling by AU-rich and GU-rich elements.,” *J. Interferon Cytokine Res.*, vol. 34, no. 4, pp. 233–41, Apr. 2014.

[59] I. Vlasova-St Louis and P. R. Bohjanen, “Post-transcriptional regulation of cytokine and growth factor signaling in cancer.,” *Cytokine Growth Factor Rev.*, vol. 33, pp. 83–93, 2017.

[60] G. Dreyfuss, V. N. Kim, and N. Kataoka, “Messenger-RNA-binding proteins and the messages they carry.,” *Nat. Rev. Mol. Cell Biol.*, vol. 3, no. 3, pp. 195–205, Mar. 2002.

[61] M. Müller-McNicoll and K. M. Neugebauer, “How cells get the message: dynamic assembly and function of mRNA-protein complexes.,” *Nat. Rev. Genet.*, vol. 14, no. 4, pp. 275–87, Apr. 2013.

[62] R. J. Jackson, C. U. T. Hellen, and T. V Pestova, “The mechanism of eukaryotic translation initiation and principles of its regulation.,” *Nat. Rev. Mol. Cell Biol.*, vol. 11, no. 2, pp. 113–27, Feb. 2010.

[63] J. R. Buchan and R. Parker, “Eukaryotic stress granules: the ins and outs of translation.,” *Mol. Cell*, vol. 36, no. 6, pp. 932–41, Dec. 2009.

[64] R. Parker and U. Sheth, “P bodies and the control of mRNA translation and degradation.,” *Mol. Cell*, vol. 25, no. 5, pp. 635–46, Mar. 2007.

[65] M. W. Hentze, A. Castello, T. Schwarzl, and T. Preiss, “A brave new world of RNA-binding proteins.,” *Nat. Rev. Mol. Cell Biol.*, vol. 19, no. 5, pp. 327–341, 2018.

[66] V. Marchand, I. Gaspar, and A. Ephrussi, “An intracellular transmission control protocol: assembly and transport of ribonucleoprotein complexes.,” *Curr. Opin. Cell Biol.*, vol. 24, no. 2, pp. 202–10, Apr. 2012.

[67] C. E. Holt and S. L. Bullock, “Subcellular mRNA localization in animal cells and why it matters.,” *Science*, vol. 326, no. 5957, pp. 1212–6, Nov. 2009.

[68] C. Y. Chen and A. B. Shyu, “AU-rich elements: characterization and importance in mRNA degradation.,” *Trends Biochem. Sci.*, vol. 20, no. 11, pp. 465–70, Nov. 1995.

[69] G. Shaw and R. Kamen, “A conserved AU sequence from the 3’ untranslated region of GM-CSF mRNA mediates selective mRNA degradation.,” *Cell*, vol. 46, no. 5, pp. 659–67, Aug. 1986.

[70] S. S. Peng, C. Y. Chen, N. Xu, and A. B. Shyu, “RNA stabilization by the AU-rich element binding protein, HuR, an ELAV protein.,” *EMBO J.*, vol. 17, no. 12, pp. 3461–3470, Jun. 1998.

[71] I. A. Vlasova *et al.*, “Conserved GU-Rich Elements Mediate mRNA Decay by Binding to CUG-Binding Protein 1,” *Mol. Cell*, vol. 29, no. 2, pp. 263–270, 2008.

[72] A. S. Halees *et al.*, “Global assessment of GU-rich regulatory content and function in

the human transcriptome.," *RNA Biol.*, vol. 8, no. 4, pp. 681–691, 2011.

[73] L. Paillard, F. Omilli, V. Legagneux, T. Bassez, D. Maniey, and H. B. Osborne, "EDEN and EDEN-BP, a cis element and an associated factor that mediate sequence-specific mRNA deadenylation in Xenopus embryos.," *EMBO J.*, vol. 17, no. 1, pp. 278–87, Jan. 1998.

[74] J. Delaunay *et al.*, "The Drosophila Bruno paralogue Bru-3 specifically binds the EDEN translational repression element.," *Nucleic Acids Res.*, vol. 32, no. 10, pp. 3070–82, 2004.

[75] N. Charlet-B, R. S. Savkur, G. Singh, A. V Philips, E. A. Grice, and T. A. Cooper, "Loss of the muscle-specific chloride channel in type 1 myotonic dystrophy due to misregulated alternative splicing.," *Mol. Cell*, vol. 10, no. 1, pp. 45–53, Jul. 2002.

[76] A. Sureau, J. Sauliere, A. Expert-Bezancon, and J. Marie, "CELF and PTB proteins modulate the inclusion of the beta-tropomyosin exon 6B during myogenic differentiation.," *Exp. Cell Res.*, vol. 317, no. 1, pp. 94–106, Jan. 2011.

[77] V. A. Barron, H. Zhu, M. N. Hinman, A. N. Ladd, and H. Lou, "The neurofibromatosis type I pre-mRNA is a novel target of CELF protein-mediated splicing regulation.," *Nucleic Acids Res.*, vol. 38, no. 1, pp. 253–264, Jan. 2010.

[78] Z. Chen, T. L. Eggerman, and A. P. Patterson, "ApoB mRNA editing is mediated by a coordinated modulation of multiple apoB mRNA editing enzyme components.," *Am. J. Physiol. Gastrointest. Liver Physiol.*, vol. 292, no. 1, pp. G53-65, Jan. 2007.

[79] S. Anant *et al.*, "Novel role for RNA-binding protein CUGBP2 in mammalian RNA editing. CUGBP2 modulates C to U editing of apolipoprotein B mRNA by interacting with apobec-1 and ACF, the apobec-1 complementation factor.," *J. Biol. Chem.*, vol. 276, no. 50, pp. 47338–51, Dec. 2001.

[80] S. Millevoi *et al.*, "An interaction between U2AF 65 and CF I(m) links the splicing and 3' end processing machineries.," *EMBO J.*, vol. 25, no. 20, pp. 4854–64, Oct. 2006.

[81] F. Rigo and H. G. Martinson, "Functional coupling of last-intron splicing and 3'-end processing to transcription in vitro: the poly(A) signal couples to splicing before committing to cleavage.," *Mol. Cell. Biol.*, vol. 28, no. 2, pp. 849–62, Jan. 2008.

[82] P. Hilleren, T. McCarthy, M. Rosbash, R. Parker, and T. H. Jensen, "Quality control of mRNA 3'-end processing is linked to the nuclear exosome.," *Nature*, vol. 413, no. 6855, pp. 538–42, Oct. 2001.

[83] P. Iakova *et al.*, "Competition of CUGBP1 and calreticulin for the regulation of p21 translation determines cell fate.," *EMBO J.*, vol. 23, no. 2, pp. 406–417, Jan. 2004.

[84] B. Rattenbacher *et al.*, "Analysis of CUGBP1 targets identifies GU-repeat sequences that mediate rapid mRNA decay.," *Mol. Cell. Biol.*, vol. 30, no. 16, pp. 3970–80, 2010.

[85] I. Vlasova-St Louis and P. R. Bohjanen, "Coordinate regulation of mRNA decay networks by GU-rich elements and CELF1.," *Curr. Opin. Genet. Dev.*, vol. 21, no. 4, pp. 444–451, Aug. 2011.

[86] L. Paillard and H. B. Osborne, "East of EDEN was a poly(A) tail.," *Biol. cell*, vol. 95, no. 3–4, pp. 211–9.

[87] H. B. Osborne *et al.*, "Post-transcriptional regulation in Xenopus embryos: role and targets of EDEN-BP.," *Biochem. Soc. Trans.*, vol. 33, no. Pt 6, pp. 1541–3, Dec. 2005.

[88] A. N. Ladd, N. Charlet, and T. A. Cooper, "The CELF family of RNA binding proteins is

implicated in cell-specific and developmentally regulated alternative splicing.," *Mol. Cell. Biol.*, vol. 21, no. 4, pp. 1285–96, Feb. 2001.

[89] "UniProt: a worldwide hub of protein knowledge," *Nucleic Acids Res.*, vol. 47, no. D1, pp. D506–D515, Jan. 2019.

[90] D. K. Choi, T. Ito, F. Tsukahara, M. Hirai, and Y. Sakaki, "Developmentally-regulated expression of mNapor encoding an apoptosis-induced ELAV-type RNA binding protein.," *Gene*, vol. 237, no. 1, pp. 135–42, Sep. 1999.

[91] P. J. Good, Q. Chen, S. J. Warner, and D. C. Herring, "A family of human RNA-binding proteins related to the Drosophila Bruno translational regulator.," *J. Biol. Chem.*, vol. 275, no. 37, pp. 28583–92, Sep. 2000.

[92] D.-K. Choi, K.-W. Yoo, S.-K. Hong, M. Rhee, Y. Sakaki, and C.-H. Kim, "Isolation and expression of Napor/CUG-BP2 in embryo development.," *Biochem. Biophys. Res. Commun.*, vol. 305, no. 3, pp. 448–54, Jun. 2003.

[93] C. Kress, C. Gautier-Courteille, H. B. Osborne, C. Babinet, and L. Paillard, "Inactivation of CUG-BP1/CELF1 causes growth, viability, and spermatogenesis defects in mice.," *Mol. Cell. Biol.*, vol. 27, no. 3, pp. 1146–57, Feb. 2007.

[94] Y. Yang, C. L. Mahaffey, N. Bérubé, T. P. Maddatu, G. A. Cox, and W. N. Frankel, "Complex seizure disorder caused by Brunol4 deficiency in mice.," *PLoS Genet.*, vol. 3, no. 7, p. e124, Jul. 2007.

[95] J. Wu, C. Li, S. Zhao, and B. Mao, "Differential expression of the Brunol/CELF family genes during Xenopus laevis early development.," *Int. J. Dev. Biol.*, vol. 54, no. 1, pp. 209–14, 2010.

[96] G. Singh, N. Charlet-B, J. Han, and T. A. Cooper, "ETR-3 and CELF4 protein domains required for RNA binding and splicing activity in vivo.," *Nucleic Acids Res.*, vol. 32, no. 3, pp. 1232–41, 2004.

[97] C. Barreau, L. Paillard, A. Méreau, and H. B. Osborne, "Mammalian CELF/Bruno-like RNA-binding proteins: molecular characteristics and biological functions.," *Biochimie*, vol. 88, no. 5, pp. 515–25, May 2006.

[98] I. Lubin *et al.*, "Engraftment and development of human T and B cells in mice after bone marrow transplantation.," *Science*, vol. 252, no. 5004, pp. 427–31, Apr. 1991.

[99] A. Mankodi *et al.*, "Expanded CUG repeats trigger aberrant splicing of ClC-1 chloride channel pre-mRNA and hyperexcitability of skeletal muscle in myotonic dystrophy.," *Mol. Cell*, vol. 10, no. 1, pp. 35–44, Jul. 2002.

[100] A. N. Ladd and T. A. Cooper, "Multiple domains control the subcellular localization and activity of ETR-3, a regulator of nuclear and cytoplasmic RNA processing events.," *J. Cell Sci.*, vol. 117, no. Pt 16, pp. 3519–29, Jul. 2004.

[101] J. A. Dembowski and P. J. Grabowski, "The CUGBP2 splicing factor regulates an ensemble of branchpoints from perimeter binding sites with implications for autoregulation.," *PLoS Genet.*, vol. 5, no. 8, p. e1000595, Aug. 2009.

[102] T. Dasgupta and A. N. Ladd, "The importance of CELF control: molecular and biological roles of the CUG-BP, Elav-like family of RNA-binding proteins.," *Wiley Interdiscip. Rev. RNA*, vol. 3, no. 1, pp. 104–121, Jan. 2012.

[103] D. Mori, N. Sasagawa, Y. Kino, and S. Ishiura, "Quantitative analysis of CUG-BP1 binding to RNA repeats.," *J. Biochem.*, vol. 143, no. 3, pp. 377–83, Mar. 2008.

[104] J. Marquis *et al.*, “CUG-BP1/CELF1 requires UGU-rich sequences for high-affinity binding.,” *Biochem. J.*, vol. 400, no. 2, pp. 291–301, Dec. 2006.

[105] N. Takahashi, N. Sasagawa, K. Suzuki, and S. Ishiura, “The CUG-binding protein binds specifically to UG dinucleotide repeats in a yeast three-hybrid system.,” *Biochem. Biophys. Res. Commun.*, vol. 277, no. 2, pp. 518–23, Oct. 2000.

[106] J. R. Tollervey *et al.*, “Characterizing the RNA targets and position-dependent splicing regulation by TDP-43.,” *Nat. Neurosci.*, vol. 14, no. 4, pp. 452–8, Apr. 2011.

[107] J. Fallmann, V. Sedlyarov, A. Tanzer, P. Kovarik, and I. L. Hofacker, “AREsite2: an enhanced database for the comprehensive investigation of AU/GU/U-rich elements.,” *Nucleic Acids Res.*, vol. 44, no. D1, pp. D90-5, Jan. 2016.

[108] L. T. Timchenko *et al.*, “Identification of a (CUG)n triplet repeat RNA-binding protein and its expression in myotonic dystrophy.,” *Nucleic Acids Res.*, vol. 24, no. 22, pp. 4407–14, Nov. 1996.

[109] M. Giulietti *et al.*, “SpliceAid-F: A database of human splicing factors and their RNA-binding sites,” *Nucleic Acids Res.*, vol. 41, 2013.

[110] J. E. Lee, J. Y. Lee, J. Wilusz, B. Tian, and C. J. Wilusz, “Systematic analysis of Cis-elements in unstable mRNAS demonstrates that CUGBP1 is a key regulator of mRNA decay in muscle cells,” *PLoS One*, vol. 5, no. 6, 2010.

[111] J. E. Lee and T. A. Cooper, “Pathogenic mechanisms of myotonic dystrophy.,” *Biochem. Soc. Trans.*, vol. 37, no. Pt 6, pp. 1281–6, Dec. 2009.

[112] A. Masuda *et al.*, “CUGBP1 and MBNL1 preferentially bind to 3′ UTRs and facilitate mRNA decay,” *Sci. Rep.*, vol. 2, no. 1, p. 209, Dec. 2012.

[113] P. J. Webster, L. Liang, C. A. Berg, P. Lasko, and P. M. Macdonald, “Translational repressor bruno plays multiple roles in development and is widely conserved.,” *Genes Dev.*, vol. 11, no. 19, pp. 2510–21, Oct. 1997.

[114] N. Ezzeddine *et al.*, “EDEN-dependent translational repression of maternal mRNAs is conserved between Xenopus and Drosophila.,” *Proc. Natl. Acad. Sci. U. S. A.*, vol. 99, no. 1, pp. 257–62, Jan. 2002.

[115] D. Beisang, P. R., and I. A. Vlasova-St. Louis, “CELF1, a Multifunctional Regulator of Posttranscriptional Networks,” *Bind. Protein*, 2012.

[116] O. Le Tonquèze, B. Gschloessl, A. Namanda-Vanderbeken, V. Legagneux, L. Paillard, and Y. Audic, “Chromosome wide analysis of CUGBP1 binding sites identifies the tetraspanin CD9 mRNA as a target for CUGBP1-mediated down-regulation.,” *Biochem. Biophys. Res. Commun.*, vol. 394, no. 4, pp. 884–9, Apr. 2010.

[117] J. Russo *et al.*, “The CELF1 RNA-Binding Protein Regulates Decay of Signal Recognition Particle mRNAs and Limits Secretion in Mouse Myoblasts.,” *PLoS One*, vol. 12, no. 1, p. e0170680, 2017.

[118] R. Pullmann *et al.*, “Analysis of turnover and translation regulatory RNA-binding protein expression through binding to cognate mRNAs.,” *Mol. Cell. Biol.*, vol. 27, no. 18, pp. 6265–78, Sep. 2007.

[119] B. Schoser and L. Timchenko, “Myotonic dystrophies 1 and 2: complex diseases with complex mechanisms.,” *Curr. Genomics*, vol. 11, no. 2, pp. 77–90, Apr. 2010.

[120] I. Vlasova-St. Louis and P. Bohjanen, “Feedback Regulation of Kinase Signaling Pathways by AREs and GREs,” *Cells*, vol. 5, no. 1, p. 4, 2016.

[121] J. P. Orengo, P. Chambon, D. Metzger, D. R. Mosier, G. J. Snipes, and T. A. Cooper, “Expanded CTG repeats within the DMPK 3’ UTR causes severe skeletal muscle wasting in an inducible mouse model for myotonic dystrophy.,” *Proc. Natl. Acad. Sci. U. S. A.*, vol. 105, no. 7, pp. 2646–51, Feb. 2008.

[122] E. Salisbury *et al.*, “Ectopic expression of cyclin D3 corrects differentiation of DM1 myoblasts through activation of RNA CUG-binding protein, CUGBP1.,” *Exp. Cell Res.*, vol. 314, no. 11–12, pp. 2266–78, Jul. 2008.

[123] C. Huichalaf *et al.*, “Expansion of CUG RNA repeats causes stress and inhibition of translation in myotonic dystrophy 1 (DM1) cells.,” *FASEB J.*, vol. 24, no. 10, pp. 3706–19, Oct. 2010.

[124] M. Mahadevan *et al.*, “Myotonic dystrophy mutation: an unstable CTG repeat in the 3’ untranslated region of the gene.,” *Science (80-.).*, vol. 255, no. 5049, pp. 1253–5, Mar. 1992.

[125] C. Turner and D. Hilton-Jones, “The myotonic dystrophies: diagnosis and management.,” *J. Neurol. Neurosurg. Psychiatry*, vol. 81, no. 4, pp. 358–67, Apr. 2010.

[126] D. S. Berger, M. Moyer, G. M. Kliment, E. van Lunteren, and A. N. Ladd, “Expression of a dominant negative CELF protein in vivo leads to altered muscle organization, fiber size, and subtype.,” *PLoS One*, vol. 6, no. 4, p. e19274, Apr. 2011.

[127] A. N. Ladd, G. Taffet, C. Hartley, D. L. Kearney, and T. A. Cooper, “Cardiac tissue-specific repression of CELF activity disrupts alternative splicing and causes cardiomyopathy.,” *Mol. Cell. Biol.*, vol. 25, no. 14, pp. 6267–78, Jul. 2005.

[128] T. Katoh, H. Hojo, and T. Suzuki, “Destabilization of microRNAs in human cells by 3’ deadenylation mediated by PARN and CUGBP1.,” *Nucleic Acids Res.*, vol. 43, no. 15, pp. 7521–34, Sep. 2015.

[129] C. J. Wilusz, M. Wormington, and S. W. Peltz, “The cap-to-tail guide to mRNA turnover.,” *Nat. Rev. Mol. Cell Biol.*, vol. 2, no. 4, pp. 237–46, Apr. 2001.

[130] C.-Y. A. Chen and A.-B. Shyu, “Mechanisms of deadenylation-dependent decay.,” *Wiley Interdiscip. Rev. RNA*, vol. 2, no. 2, pp. 167–83.

[131] D. Beisang, C. Reilly, and P. R. Bohjanen, “Alternative polyadenylation regulates CELF1/CUGBP1 target transcripts following T cell activation.,” *Gene*, vol. 550, no. 1, pp. 93–100, Oct. 2014.

[132] D. Beisang, B. Rattenbacher, I. A. Vlasova-St Louis, and P. R. Bohjanen, “Regulation of CUG-binding protein 1 (CUGBP1) binding to target transcripts upon T cell activation.,” *J. Biol. Chem.*, vol. 287, no. 2, pp. 950–60, Jan. 2012.

[133] N. A. Timchenko, P. Iakova, Z. J. Cai, J. R. Smith, and L. T. Timchenko, “Molecular basis for impaired muscle differentiation in myotonic dystrophy.,” *Mol. Cell. Biol.*, vol. 21, no. 20, pp. 6927–38, Oct. 2001.

[134] L. D. Horb and M. E. Horb, “BrunoL1 regulates endoderm proliferation through translational enhancement of cyclin A2 mRNA.,” *Dev. Biol.*, vol. 345, no. 2, pp. 156–69, Sep. 2010.

[135] A. Nakamura, K. Sato, and K. Hanyu-Nakamura, “Drosophila cup is an eIF4E binding protein that associates with Bruno and regulates oskar mRNA translation in oogenesis.,” *Dev. Cell*, vol. 6, no. 1, pp. 69–78, Jan. 2004.

[136] A. Chaudhury *et al.*, “CELF1 is an EIF4E binding protein that promotes translation of epithelial-mesenchymal transition effector mRNAs,” *bioRxiv*, p. 640300, Jan. 2019.

[137] A. Chaudhury *et al.*, “CELF1 is a central node in post-transcriptional regulatory programmes underlying EMT,” *Nat. Commun.*, vol. 7, no. 1, p. 13362, Dec. 2016.

[138] R. C. Lee, R. L. Feinbaum, and V. Ambros, “The C. elegans heterochronic gene lin-4 encodes small RNAs with antisense complementarity to lin-14.,” *Cell*, vol. 75, no. 5, pp. 843–54, Dec. 1993.

[139] G. Ruvkun, “Molecular biology. Glimpses of a tiny RNA world.,” *Science (80-.).*, vol. 294, no. 5543, pp. 797–9, Oct. 2001.

[140] A. Rodriguez, S. Griffiths-Jones, J. L. Ashurst, and A. Bradley, “Identification of mammalian microRNA host genes and transcription units.,” *Genome Res.*, vol. 14, no. 10A, pp. 1902–10, Oct. 2004.

[141] Y.-K. Kim and V. N. Kim, “Processing of intronic microRNAs.,” *EMBO J.*, vol. 26, no. 3, pp. 775–83, Feb. 2007.

[142] S. Baskerville and D. P. Bartel, “Microarray profiling of microRNAs reveals frequent coexpression with neighboring miRNAs and host genes.,” *RNA*, vol. 11, no. 3, pp. 241–7, Mar. 2005.

[143] X. Zhou, J. Ruan, G. Wang, and W. Zhang, “Characterization and identification of microRNA core promoters in four model species.,” *PLoS Comput. Biol.*, vol. 3, no. 3, p. e37, Mar. 2007.

[144] Y. Lee *et al.*, “MicroRNA genes are transcribed by RNA polymerase II.,” *EMBO J.*, vol. 23, no. 20, pp. 4051–60, Oct. 2004.

[145] X. Cai, C. H. Hagedorn, and B. R. Cullen, “Human microRNAs are processed from capped, polyadenylated transcripts that can also function as mRNAs.,” *RNA*, vol. 10, no. 12, pp. 1957–66, Dec. 2004.

[146] Y. Lee *et al.*, “The nuclear RNase III Drosha initiates microRNA processing.,” *Nature*, vol. 425, no. 6956, pp. 415–9, Sep. 2003.

[147] R. I. Gregory *et al.*, “The Microprocessor complex mediates the genesis of microRNAs.,” *Nature*, vol. 432, no. 7014, pp. 235–40, Nov. 2004.

[148] R. I. Gregory, T. P. Chendrimada, and R. Shiekhattar, “MicroRNA biogenesis: isolation and characterization of the microprocessor complex.,” *Methods Mol. Biol.*, vol. 342, pp. 33–47, 2006.

[149] A. M. Denli, B. B. J. Tops, R. H. A. Plasterk, R. F. Ketting, and G. J. Hannon, “Processing of primary microRNAs by the Microprocessor complex.,” *Nature*, vol. 432, no. 7014, pp. 231–5, Nov. 2004.

[150] E. Berezikov, W.-J. Chung, J. Willis, E. Cuppen, and E. C. Lai, “Mammalian mirtron genes.,” *Mol. Cell*, vol. 28, no. 2, pp. 328–36, Oct. 2007.

[151] E. P. Murchison and G. J. Hannon, “miRNAs on the move: miRNA biogenesis and the RNAi machinery.,” *Curr. Opin. Cell Biol.*, vol. 16, no. 3, pp. 223–9, Jun. 2004.

[152] C. Okada *et al.*, “A high-resolution structure of the pre-microRNA nuclear export machinery.,” *Science (80-.).*, vol. 326, no. 5957, pp. 1275–9, Nov. 2009.

[153] H. Zhang, F. A. Kolb, L. Jaskiewicz, E. Westhof, and W. Filipowicz, “Single processing center models for human Dicer and bacterial RNase III.,” *Cell*, vol. 118, no. 1, pp. 57–68, Jul. 2004.

[154] T. P. Chendrimada *et al.*, “TRBP recruits the Dicer complex to Ago2 for microRNA

processing and gene silencing.," *Nature*, vol. 436, no. 7051, pp. 740–4, Aug. 2005.

[155] Z. Gao, Y. Dou, Y. Chen, and Y. Zheng, "MicroRNA roles in the NF- κB signaling pathway during viral infections.," *Biomed Res. Int.*, vol. 2014, p. 436097, 2014.

[156] L. P. Garo and G. Murugaiyan, "Contribution of MicroRNAs to autoimmune diseases.," *Cell. Mol. life Sci.*, vol. 73, no. 10, pp. 2041–51, May 2016.

[157] M. Tatsuguchi *et al.*, "Expression of microRNAs is dynamically regulated during cardiomyocyte hypertrophy.," *J. Mol. Cell. Cardiol.*, vol. 42, no. 6, pp. 1137–41, Jun. 2007.

[158] T. Thum *et al.*, "MicroRNAs in the human heart: a clue to fetal gene reprogramming in heart failure.," *Circulation*, vol. 116, no. 3, pp. 258–67, Jul. 2007.

[159] E. van Rooij *et al.*, "A signature pattern of stress-responsive microRNAs that can evoke cardiac hypertrophy and heart failure.," *Proc. Natl. Acad. Sci. U. S. A.*, vol. 103, no. 48, pp. 18255–60, Nov. 2006.

[160] Y. L. Phua, J. Y. S. Chu, A. K. Marrone, A. J. Bodnar, S. Sims-Lucas, and J. Ho, "Renal stromal miRNAs are required for normal nephrogenesis and glomerular mesangial survival.," *Physiol. Rep.*, vol. 3, no. 10, Oct. 2015.

[161] A. Mencía *et al.*, "Mutations in the seed region of human miR-96 are responsible for nonsyndromic progressive hearing loss.," *Nat. Genet.*, vol. 41, no. 5, pp. 609–13, May 2009.

[162] M. Acunzo, G. Romano, D. Wernicke, and C. M. Croce, "MicroRNA and cancer--a brief overview.," *Adv. Biol. Regul.*, vol. 57, pp. 1–9, Jan. 2015.

[163] S. M. Hammond, "RNAi, microRNAs, and human disease.," *Cancer Chemother. Pharmacol.*, vol. 58 Suppl 1, pp. s63-8, Nov. 2006.

[164] P. P. Medina, M. Nolde, and F. J. Slack, "OncomiR addiction in an in vivo model of microRNA-21-induced pre-B-cell lymphoma.," *Nature*, vol. 467, no. 7311, pp. 86–90, Sep. 2010.

[165] M.-L. Si, S. Zhu, H. Wu, Z. Lu, F. Wu, and Y.-Y. Mo, "miR-21-mediated tumor growth.," *Oncogene*, vol. 26, no. 19, pp. 2799–803, Apr. 2007.

[166] M. V Iorio *et al.*, "MicroRNA gene expression deregulation in human breast cancer.," *Cancer Res.*, vol. 65, no. 16, pp. 7065–70, Aug. 2005.

[167] A. J. Schetter *et al.*, "MicroRNA expression profiles associated with prognosis and therapeutic outcome in colon adenocarcinoma.," *JAMA*, vol. 299, no. 4, pp. 425–36, Jan. 2008.

[168] J. Lu *et al.*, "MicroRNA expression profiles classify human cancers.," *Nature*, vol. 435, no. 7043, pp. 834–8, Jun. 2005.

[169] J. M. Thomson, M. Newman, J. S. Parker, E. M. Morin-Kensicki, T. Wright, and S. M. Hammond, "Extensive post-transcriptional regulation of microRNAs and its implications for cancer.," *Genes Dev.*, vol. 20, no. 16, pp. 2202–7, Aug. 2006.

[170] A. Wilczynska and M. Bushell, "The complexity of miRNA-mediated repression," *Cell Death Differ.*, vol. 22, no. 1, pp. 22–33, 2015.

[171] A. Fire, S. Xu, M. K. Montgomery, S. A. Kostas, S. E. Driver, and C. C. Mello, "Potent and specific genetic interference by double-stranded RNA in Caenorhabditis elegans.," *Nature*, vol. 391, no. 6669, pp. 806–11, Feb. 1998.

[172] B. P. Lewis, I. Shih, M. W. Jones-Rhoades, D. P. Bartel, and C. B. Burge, “Prediction of mammalian microRNA targets.,” *Cell*, vol. 115, no. 7, pp. 787–98, Dec. 2003.

[173] I. Lee *et al.*, “New class of microRNA targets containing simultaneous 5’-UTR and 3’-UTR interaction sites.,” *Genome Res.*, vol. 19, no. 7, pp. 1175–83, Jul. 2009.

[174] J. J. Forman and H. A. Coller, “The code within the code: microRNAs target coding regions.,” *Cell cycle*, vol. 9, no. 8, pp. 1533–41, Apr. 2010.

[175] S. M. Hammond, E. Bernstein, D. Beach, and G. J. Hannon, “An RNA-directed nuclease mediates post-transcriptional gene silencing in Drosophila cells.,” *Nature*, vol. 404, no. 6775, pp. 293–6, Mar. 2000.

[176] G. Meister, M. Landthaler, A. Patkaniowska, Y. Dorsett, G. Teng, and T. Tuschl, “Human Argonaute2 mediates RNA cleavage targeted by miRNAs and siRNAs.,” *Mol. Cell*, vol. 15, no. 2, pp. 185–97, Jul. 2004.

[177] J. Liu *et al.*, “Argonaute2 is the catalytic engine of mammalian RNAi.,” *Science (80-.).*, vol. 305, no. 5689, pp. 1437–41, Sep. 2004.

[178] J. Martinez, A. Patkaniowska, H. Urlaub, R. Lührmann, and T. Tuschl, “Single-stranded antisense siRNAs guide target RNA cleavage in RNAi.,” *Cell*, vol. 110, no. 5, pp. 563–74, Sep. 2002.

[179] G. Hutvágner and P. D. Zamore, “A microRNA in a multiple-turnover RNAi enzyme complex.,” *Science (80-.).*, vol. 297, no. 5589, pp. 2056–60, Sep. 2002.

[180] R. I. Gregory, T. P. Chendrimada, N. Cooch, and R. Shiekhattar, “Human RISC couples microRNA biogenesis and posttranscriptional gene silencing.,” *Cell*, vol. 123, no. 4, pp. 631–40, Nov. 2005.

[181] J. B. Preall, Z. He, J. M. Gorra, and E. J. Sontheimer, “Short interfering RNA strand selection is independent of dsRNA processing polarity during RNAi in Drosophila.,” *Curr. Biol.*, vol. 16, no. 5, pp. 530–5, Mar. 2006.

[182] M. R. Fabian, N. Sonenberg, and W. Filipowicz, “Regulation of mRNA translation and stability by microRNAs.,” *Annu. Rev. Biochem.*, vol. 79, pp. 351–79, 2010.

[183] D. P. Bartel, “MicroRNAs: target recognition and regulatory functions.,” *Cell*, vol. 136, no. 2, pp. 215–33, Jan. 2009.

[184] M. Fabbri *et al.*, “MicroRNAs bind to Toll-like receptors to induce prometastatic inflammatory response,” *Proc. Natl. Acad. Sci.*, vol. 109, no. 31, pp. E2110–E2116, 2012.

[185] W. A. He, F. Calore, P. Londhe, A. Canella, D. C. Guttridge, and C. M. Croce, “Microvesicles containing miRNAs promote muscle cell death in cancer cachexia via TLR7.,” *Proc. Natl. Acad. Sci. U. S. A.*, vol. 111, no. 12, pp. 4525–9, Mar. 2014.

[186] Z.-J. Zhang *et al.*, “TLR8 and its endogenous ligand miR-21 contribute to neuropathic pain in murine DRG,” *J. Exp. Med.*, vol. 215, no. 12, pp. 3019–3037, Dec. 2018.

[187] K. B. Challagundla *et al.*, “Exosome-mediated transfer of microRNAs within the tumor microenvironment and neuroblastoma resistance to chemotherapy.,” *J. Natl. Cancer Inst.*, vol. 107, no. 7, Jul. 2015.

[188] S. M. Lehmann *et al.*, “An unconventional role for miRNA: let-7 activates Toll-like receptor 7 and causes neurodegeneration.,” *Nat. Neurosci.*, vol. 15, no. 6, pp. 827–35, Jun. 2012.

[189] R. F. Place, L.-C. Li, D. Pookot, E. J. Noonan, and R. Dahiya, “MicroRNA-373 induces expression of genes with complementary promoter sequences.,” *Proc. Natl. Acad. Sci. U. S. A.*, vol. 105, no. 5, pp. 1608–13, Feb. 2008.

[190] D. G. Zisoulis, Z. S. Kai, R. K. Chang, and A. E. Pasquinelli, “Autoregulation of microRNA biogenesis by let-7 and Argonaute.,” *Nature*, vol. 486, no. 7404, pp. 541–4, Jun. 2012.

[191] R. Tang *et al.*, “Mouse miRNA-709 directly regulates miRNA-15a/16-1 biogenesis at the posttranscriptional level in the nucleus: evidence for a microRNA hierarchy system.,” *Cell Res.*, vol. 22, no. 3, pp. 504–15, Mar. 2012.

[192] S. W. Chi, J. B. Zang, A. Mele, and R. B. Darnell, “Argonaute HITS-CLIP decodes microRNA-mRNA interaction maps.,” *Nature*, vol. 460, no. 7254, pp. 479–86, Jul. 2009.

[193] A. M. Eiring *et al.*, “miR-328 functions as an RNA decoy to modulate hnRNP E2 regulation of mRNA translation in leukemic blasts.,” *Cell*, vol. 140, no. 5, pp. 652–65, Mar. 2010.

[194] M. J. Saul, S. Stein, M. Grez, P.-J. Jakobsson, D. Steinhilber, and B. Suess, “UPF1 regulates myeloid cell functions and S100A9 expression by the hnRNP E2/miRNA-328 balance.,” *Sci. Rep.*, vol. 6, no. 1, p. 31995, 2016.

[195] M. J. Saul *et al.*, “Mass Spectrometry-Based Proteomics Approach Characterizes the Dual Functionality of miR-328 in Monocytes.,” *Front. Pharmacol.*, vol. 10, p. 640, 2019.

[196] M. J. Saul *et al.*, “miR-574-5p as RNA decoy for CUGBP1 stimulates human lung tumor growth by mPGES-1 induction.,” *FASEB J.*, vol. 33, no. 6, pp. 6933–6947, Jun. 2019.

[197] M. Boucquey *et al.*, “Noxp20 and Noxp70, two new markers of early neuronal differentiation, detected in teratocarcinoma-derived neuroectodermic precursor cells.,” *J. Neurochem.*, vol. 99, no. 2, pp. 657–69, Oct. 2006.

[198] R. Edgar, M. Domrachev, and A. E. Lash, “Gene Expression Omnibus: NCBI gene expression and hybridization array data repository.,” *Nucleic Acids Res.*, vol. 30, no. 1, pp. 207–10, Jan. 2002.

[199] T. Barrett *et al.*, “NCBI GEO: archive for functional genomics data sets--update.,” *Nucleic Acids Res.*, vol. 41, no. Database issue, pp. D991-5, Jan. 2013.

[200] T. Ku *et al.*, “NF-κB-regulated microRNA-574-5p underlies synaptic and cognitive impairment in response to atmospheric PM2.5 aspiration.,” *Part. Fibre Toxicol.*, vol. 14, no. 1, p. 34, 2017.

[201] W. Zhang *et al.*, “Amyloid precursor protein regulates neurogenesis by antagonizing miR-574-5p in the developing cerebral cortex.,” *Nat. Commun.*, vol. 5, p. 3330, Mar. 2014.

[202] C. Li *et al.*, “Non-coding RNA MFI2-AS1 promotes colorectal cancer cell proliferation, migration and invasion through miR-574-5p/MYCBP axis.,” *Cell Prolif.*, vol. 52, no. 4, p. e12632, Jul. 2019.

[203] P.-S. Wang *et al.*, “A novel long non-coding RNA linc-ZNF469-3 promotes lung metastasis through miR-574-5p-ZEB1 axis in triple negative breast cancer.,” *Oncogene*, vol. 37, no. 34, pp. 4662–4678, 2018.

[204] X. Wang, X. Lu, Z. Geng, G. Yang, and Y. Shi, “LncRNA PTCSC3/miR-574-5p Governs Cell Proliferation and Migration of Papillary Thyroid Carcinoma via Wnt/β-Catenin Signaling.,” *J. Cell. Biochem.*, vol. 118, no. 12, pp. 4745–4752, 2017.

[205] S. Ji *et al.*, “miR-574-5p negatively regulates Qki6/7 to impact β-catenin/Wnt signalling and the development of colorectal cancer.,” *Gut*, vol. 62, no. 5, pp. 716–26, 2013.

[206] Z. Zhang, X. Li, Q. Xiao, and Z. Wang, “MiR-574-5p mediates the cell cycle and apoptosis in thyroid cancer cells via Wnt/β-catenin signaling by repressing the expression of Quaking proteins.,” *Oncol. Lett.*, vol. 15, no. 4, pp. 5841–5848, Apr. 2018.

[207] X. Zhou *et al.*, “Quaking-5 suppresses aggressiveness of lung cancer cells through inhibiting β-catenin signaling pathway.,” *Oncotarget*, vol. 8, no. 47, pp. 82174–82184, Oct. 2017.

[208] Z. Cui, J. Tang, J. Chen, and Z. Wang, “Hsa-miR-574-5p negatively regulates MACC-1 expression to suppress colorectal cancer liver metastasis.,” *Cancer Cell Int.*, vol. 14, no. 1, p. 47, 2014.

[209] R. Zhou *et al.*, “MicroRNA-574-5p promotes metastasis of non-small cell lung cancer by targeting PTPRU.,” *Sci. Rep.*, vol. 6, p. 35714, 2016.

[210] R. Zhou *et al.*, “Tumor invasion and metastasis regulated by microRNA-184 and microRNA-574-5p in small-cell lung cancer.,” *Oncotarget*, vol. 6, no. 42, pp. 44609–22, Dec. 2015.

[211] Q. Li *et al.*, “MicroRNA-574-5p Was Pivotal for TLR9 Signaling Enhanced Tumor Progression via Down-Regulating Checkpoint Suppressor 1 in Human Lung Cancer,” *PLoS One*, vol. 7, no. 11, 2012.

[212] Z. Lai *et al.*, “MicroRNA-574-5p promotes cell growth of vascular smooth muscle cells in the progression of coronary artery disease.,” *Biomed. Pharmacother.*, vol. 97, pp. 162–167, Jan. 2018.

[213] M. Meyers-Needham *et al.*, “Concerted functions of HDAC1 and microRNA-574-5p repress alternatively spliced ceramide synthase 1 expression in human cancer cells.,” *EMBO Mol. Med.*, vol. 4, no. 2, pp. 78–92, Feb. 2012.

[214] Y. Belarbi, N. Mejhert, H. Gao, P. Arner, M. Rydén, and A. Kulyté, “MicroRNAs-361-5p and miR-574-5p associate with human adipose morphology and regulate EBF1 expression in white adipose tissue.,” *Mol. Cell. Endocrinol.*, vol. 472, pp. 50–56, 2018.

[215] D. Hanahan and R. a Weinberg, “Hallmarks of cancer: the next generation.,” *Cell*, vol. 144, no. 5, pp. 646–74, Mar. 2011.

[216] E. Ricciotti and G. A. FitzGerald, “Prostaglandins and inflammation.,” *Arterioscler. Thromb. Vasc. Biol.*, vol. 31, no. 5, pp. 986–1000, May 2011.

[217] P. Kalinski, “Regulation of Immune Responses by Prostaglandin E2,” *J. Immunol.*, vol. 188, no. 1, pp. 21–28, 2012.

[218] M. Nakanishi and D. W. Rosenberg, “Multifaceted roles of PGE2 in inflammation and cancer,” *Semin. Immunopathol.*, vol. 35, no. 2, pp. 123–137, 2013.

[219] D. Wang and R. N. Dubois, “Eicosanoids and cancer.,” *Nat. Rev. Cancer*, vol. 10, no. 3, pp. 181–93, Mar. 2010.

[220] W. L. Smith, Y. Urade, and P.-J. Jakobsson, “Enzymes of the cyclooxygenase pathways of prostanoid biosynthesis.,” *Chem. Rev.*, vol. 111, no. 10, pp. 5821–65, Oct. 2011.

[221] K. Yoshimatsu *et al.*, “Inducible microsomal prostaglandin E synthase is overexpressed in colorectal adenomas and cancer.,” *Clin. cancer Res.*, vol. 7, no. 12, pp. 3971–6, Dec. 2001.

[222] H. Hanaka *et al.*, “Microsomal prostaglandin E synthase 1 determines tumor growth in vivo of prostate and lung cancer cells.,” *Proc. Natl. Acad. Sci. U. S. A.*, vol. 106, no. 44, pp. 18757–18762, 2009.

[223] K. Yoshimatsu *et al.*, “Inducible prostaglandin E synthase is overexpressed in non-small cell lung cancer.,” *Clin. cancer Res.*, vol. 7, no. 9, pp. 2669–74, Sep. 2001.

[224] Y.-C. Wu *et al.*, “Co-overexpression of cyclooxygenase-2 and microsomal prostaglandin E synthase-1 adversely affects the postoperative survival in non-small cell lung cancer.,” *J. Thorac. Oncol.*, vol. 5, no. 8, pp. 1167–74, Aug. 2010.

[225] M. Heusinkveld *et al.*, “M2 macrophages induced by prostaglandin E2 and IL-6 from cervical carcinoma are switched to activated M1 macrophages by CD4+ Th1 cells.,” *J. Immunol.*, vol. 187, no. 3, pp. 1157–65, Aug. 2011.

[226] P. Nandi, G. V Girish, M. Majumder, X. Xin, E. Tutunea-Fatan, and P. K. Lala, “PGE2 promotes breast cancer-associated lymphangiogenesis by activation of EP4 receptor on lymphatic endothelial cells.,” *BMC Cancer*, vol. 17, no. 1, p. 11, 2017.

[227] M. Majumder, P. Nandi, A. Omar, K. Ugwuagbo, and P. Lala, “EP4 as a Therapeutic Target for Aggressive Human Breast Cancer,” *Int. J. Mol. Sci.*, vol. 19, no. 4, p. 1019, Mar. 2018.

[228] J. I. Kim, V. Lakshmikanthan, N. Frilot, and Y. Daaka, “Prostaglandin E2 Promotes Lung Cancer Cell Migration via EP4- Arrestin1-c-Src Signalsome,” *Mol. Cancer Res.*, vol. 8, no. 4, pp. 569–577, 2010.

[229] V. Karpisheh *et al.*, “Prostaglandin E2 as a potent therapeutic target for treatment of colon cancer.,” *Prostaglandins Other Lipid Mediat.*, vol. 144, p. 106338, Oct. 2019.

[230] E. Elwakeel, B. Brüne, and A. Weigert, “PGE2 in fibrosis and cancer: Insights into fibroblast activation.,” *Prostaglandins Other Lipid Mediat.*, vol. 143, p. 106339, Aug. 2019.

[231] W. H. S. Nasry, J. C. Rodriguez-Lecompte, and C. K. Martin, “Role of COX-2/PGE2 Mediated Inflammation in Oral Squamous Cell Carcinoma.,” *Cancers (Basel).*, vol. 10, no. 10, Sep. 2018.

[232] R. S. Bresalier *et al.*, “Cardiovascular events associated with rofecoxib in a colorectal adenoma chemoprevention trial.,” *N. Engl. J. Med.*, vol. 352, no. 11, pp. 1092–102, Mar. 2005.

[233] J. A. Baron *et al.*, “Cardiovascular events associated with rofecoxib: final analysis of the APPROVe trial.,” *Lancet (London, England)*, vol. 372, no. 9651, pp. 1756–64, Nov. 2008.

[234] T. Grosser, S. Fries, and G. A. FitzGerald, “Biological basis for the cardiovascular consequences of COX-2 inhibition: therapeutic challenges and opportunities.,” *J. Clin. Invest.*, vol. 116, no. 1, pp. 4–15, Jan. 2006.

[235] Y. Cheng, M. Wang, Y. Yu, J. Lawson, C. D. Funk, and G. A. Fitzgerald, “Cyclooxygenases, microsomal prostaglandin E synthase-1, and cardiovascular function.,” *J. Clin. Invest.*, vol. 116, no. 5, pp. 1391–9, May 2006.

[236] H. T. Sørensen *et al.*, “Risk of upper gastrointestinal bleeding associated with use of low-dose aspirin.,” *Am. J. Gastroenterol.*, vol. 95, no. 9, pp. 2218–24, Sep. 2000.

[237] K. Larsson and P.-J. Jakobsson, “Inhibition of microsomal prostaglandin E synthase-1 as targeted therapy in cancer treatment.,” *Prostaglandins Other Lipid Mediat.*, vol. 120, pp. 161–5, Jul. 2015.

[238] B. Samuelsson, R. Morgenstern, and P.-J. Jakobsson, “Membrane prostaglandin E synthase-1: a novel therapeutic target.,” *Pharmacol. Rev.*, vol. 59, no. 3, pp. 207–24, Sep. 2007.

[239] M. Wang, W.-L. Song, Y. Cheng, and G. A. FitzGerald, “Microsomal prostaglandin E synthase-1 inhibition in cardiovascular inflammatory disease,” *J. Intern. Med.*, vol. 263, no. 5, pp. 500–505, May 2008.

[240] M. Wang, A. M. Zukas, Y. Hui, E. Ricciotti, E. Pure, and G. A. FitzGerald, “Deletion of microsomal prostaglandin E synthase-1 augments prostacyclin and retards atherogenesis,” *Proc. Natl. Acad. Sci.*, vol. 103, no. 39, pp. 14507–14512, Sep. 2006.

[241] C. Cunningham and D. T. Skelly, “Non-steroidal anti-inflammatory drugs and cognitive function: are prostaglandins at the heart of cognitive impairment in dementia and delirium?,” *J. neuroimmune Pharmacol.*, vol. 7, no. 1, pp. 60–73, Mar. 2012.

[242] H.-H. Chang and E. J. Meuillet, “Identification and development of mPGES-1 inhibitors: where we are at?,” *Future Med. Chem.*, vol. 3, no. 15, pp. 1909–34, Nov. 2011.

[243] M. Korotkova and P.-J. Jakobsson, “Characterization of microsomal prostaglandin E synthase 1 inhibitors.,” *Basic Clin. Pharmacol. Toxicol.*, vol. 114, no. 1, pp. 64–9, Jan. 2014.

[244] P. Leclerc *et al.*, “Characterization of a human and murine mPGES-1 inhibitor and comparison to mPGES-1 genetic deletion in mouse models of inflammation,” *Prostaglandins Other Lipid Mediat.*, vol. 107, pp. 26–34, Dec. 2013.

[245] G. Ozen *et al.*, “Inhibition of microsomal PGE synthase-1 reduces human vascular tone by increasing PGI2 : a safer alternative to COX-2 inhibition.,” *Br. J. Pharmacol.*, vol. 174, no. 22, pp. 4087–4098, Nov. 2017.

[246] A. Kock *et al.*, “Inhibition of Microsomal Prostaglandin E Synthase-1 in Cancer-Associated Fibroblasts Suppresses Neuroblastoma Tumor Growth.,” *EBioMedicine*, vol. 32, pp. 84–92, Jun. 2018.

[247] N. Nishizawa *et al.*, “Inhibition of microsomal prostaglandin E synthase-1 facilitates liver repair after hepatic injury in mice.,” *J. Hepatol.*, vol. 69, no. 1, pp. 110–120, 2018.

[248] H. Yokouchi and K. Kanazawa, “Revisiting the role of COX-2 inhibitor for non-small cell lung cancer.,” *Transl. lung cancer Res.*, vol. 4, no. 5, pp. 660–4, Oct. 2015.

[249] M. J. Edelman *et al.*, “Randomized, double-blind, placebo-controlled, multicenter phase II study of the efficacy and safety of apricoxib in combination with either docetaxel or pemetrexed in patients with biomarker-selected non-small-cell lung cancer.,” *J. Clin. Oncol.*, vol. 33, no. 2, pp. 189–94, Jan. 2015.

[250] H. Eriksson *et al.*, “Quantitative membrane proteomics applying narrow range peptide isoelectric focusing for studies of small cell lung cancer resistance mechanisms,” *Proteomics*, vol. 8, no. 15, pp. 3008–3018, Aug. 2008.

[251] Z. Cao, H.-Y. Tang, H. Wang, Q. Liu, and D. W. Speicher, “Systematic comparison of fractionation methods for in-depth analysis of plasma proteomes.,” *J. Proteome Res.*, vol. 11, no. 6, pp. 3090–100, 2012.

[252] S. E. Hunt *et al.*, “Ensembl variation resources,” *Database (Oxford).*, vol. 2018, no. 8, pp. 1–12, 2018.

[253] S. S. Peng, C. Y. Chen, and A. B. Shyu, “Functional characterization of a non-AUUUA AU-rich element from the c-jun proto-oncogene mRNA: evidence for a novel class of AU-rich elements.,” *Mol. Cell. Biol.*, vol. 16, no. 4, pp. 1490–1499, Apr. 1996.

[254] A. Sandberg, R. M. M. Branca, J. Lehtiö, and J. Forshed, “Quantitative accuracy in mass spectrometry based proteomics of complex samples: The impact of labeling and precursor interference,” *J. Proteomics*, vol. 96, pp. 133–144, Jan. 2014.

[255] W. J. Kent *et al.*, “The human genome browser at UCSC.,” *Genome Res.*, vol. 12, no. 6, pp. 996–1006, Jun. 2002.

[256] F. Piva, M. Giulietti, L. Nocchi, and G. Principato, “SpliceAid: a database of experimental RNA target motifs bound by splicing proteins in humans.,” *Bioinformatics*, vol. 25, no. 9, pp. 1211–1213, May 2009.

[257] D. Betel, M. Wilson, A. Gabow, D. S. Marks, and C. Sander, “The microRNA.org resource: targets and expression.,” *Nucleic Acids Res.*, vol. 36, no. Database issue, pp. D149-53, Jan. 2008.

[258] K. Luo, “Signaling Cross Talk between TGF-β/Smad and Other Signaling Pathways.,” *Cold Spring Harb. Perspect. Biol.*, vol. 9, no. 1, Jan. 2017.

[259] A. Krämer, J. Green, J. J. Pollard, and S. Tugendreich, “Causal analysis approaches in Ingenuity Pathway Analysis.,” *Bioinformatics*, vol. 30, no. 4, pp. 523–530, Feb. 2014.

[260] O. Le Tonquèze, B. Gschloessl, V. Legagneux, L. Paillard, and Y. Audic, “Identification of CELF1 RNA targets by CLIP-seq in human HeLa cells,” *Genomics Data*, vol. 8, pp. 97–103, 2016.

[261] V. Agarwal, G. W. Bell, J.-W. Nam, and D. P. Bartel, “Predicting effective microRNA target sites in mammalian mRNAs,” *Elife*, vol. 4, Aug. 2015.

[262] G. Blobel and B. Dobberstein, “Transfer of proteins across membranes. I. Presence of proteolytically processed and unprocessed nascent immunoglobulin light chains on membrane-bound ribosomes of murine myeloma.,” *J. Cell Biol.*, vol. 67, no. 3, pp. 835–51, Dec. 1975.

[263] D. W. Reid and C. V Nicchitta, “Primary role for endoplasmic reticulum-bound ribosomes in cellular translation identified by ribosome profiling.,” *J. Biol. Chem.*, vol. 287, no. 8, pp. 5518–27, Feb. 2012.

[264] K. D. Mansfield and J. D. Keene, “The ribonome: a dominant force in co-ordinating gene expression.,” *Biol. cell*, vol. 101, no. 3, pp. 169–81, Mar. 2009.

[265] F. Bergqvist *et al.*, “Inhibition of mPGES-1 or COX-2 Results in Different Proteomic and Lipidomic Profiles in A549 Lung Cancer Cells.,” *Front. Pharmacol.*, vol. 10, p. 636, 2019.

[266] M. J. Ochs, E. Ossipova, G. Oliynyk, D. Steinhilber, B. Suess, and P. J. Jakobsson, “Mass spectrometry-based proteomics identifies UPF1 as a critical gene expression regulator in MonoMac 6 cells,” *J. Proteome Res.*, vol. 12, no. 6, pp. 2622–2629, 2013.

[267] I. A. Vlasova and P. R. Bohjanen, “Posttranscriptional regulation of gene networks by GU-rich elements and CELF proteins.,” *RNA Biol.*, vol. 5, no. 4, pp. 201–7.

[268] H. Xia *et al.*, “CELF1 preferentially binds to exon-intron boundary and regulates alternative splicing in HeLa cells,” *Biochim. Biophys. Acta - Gene Regul. Mech.*, vol. 1860, no. 9, pp. 911–921, 2017.

[269] A. D. Siddam *et al.*, “The RNA-binding protein Celf1 post-transcriptionally regulates p27Kip1 and Dnase2b to control fiber cell nuclear degradation in lens development.,” *PLoS Genet.*, vol. 14, no. 3, p. e1007278, 2018.

[270] N. A. Timchenko, A. L. Lu, X. Welm, and L. T. Timchenko, “CUG repeat binding protein (CUGBP1) interacts with the 5’ region of C/EBP mRNA and regulates translation of

C/EBP isoforms," *Nucleic Acids Res.*, vol. 27, no. 22, pp. 4517–4525, Nov. 1999.

[271] V. Procaccio *et al.*, "Mapping to 1q23 of the human gene (NDUFS2) encoding the 49-kDa subunit of the mitochondrial respiratory Complex I and immunodetection of the mature protein in mitochondria.," *Mamm. Genome*, vol. 9, no. 6, pp. 482–4, Jun. 1998.

[272] I. M. Fearnley, M. Finel, J. M. Skehel, and J. E. Walker, "NADH:ubiquinone oxidoreductase from bovine heart mitochondria. cDNA sequences of the import precursors of the nuclear-encoded 39 kDa and 42 kDa subunits.," *Biochem. J.*, vol. 278 (Pt 3, pp. 821–9, Sep. 1991.

[273] O. Zurita Rendón, L. Silva Neiva, F. Sasarman, and E. A. Shoubridge, "The arginine methyltransferase NDUFAF7 is essential for complex I assembly and early vertebrate embryogenesis.," *Hum. Mol. Genet.*, vol. 23, no. 19, pp. 5159–70, Oct. 2014.

[274] L. H. Ngu *et al.*, "A catalytic defect in mitochondrial respiratory chain complex I due to a mutation in NDUFS2 in a patient with Leigh syndrome.," *Biochim. Biophys. Acta*, vol. 1822, no. 2, pp. 168–75, Feb. 2012.

[275] S. E. Marin, R. Mesterman, B. Robinson, R. J. Rodenburg, J. Smeitink, and M. A. Tarnopolsky, "Leigh syndrome associated with mitochondrial complex I deficiency due to novel mutations In NDUFV1 and NDUFS2.," *Gene*, vol. 516, no. 1, pp. 162–7, Mar. 2013.

[276] H. A. L. Tuppen *et al.*, "The p.M292T NDUFS2 mutation causes complex I-deficient Leigh syndrome in multiple families.," *Brain*, vol. 133, no. 10, pp. 2952–63, Oct. 2010.

[277] R. H. Triepels, L. P. Van Den Heuvel, J. M. Trijbels, and J. A. Smeitink, "Respiratory chain complex I deficiency.," *Am. J. Med. Genet.*, vol. 106, no. 1, pp. 37–45, 2001.

[278] B. H. Robinson, "Human complex I deficiency: clinical spectrum and involvement of oxygen free radicals in the pathogenicity of the defect.," *Biochim. Biophys. Acta*, vol. 1364, no. 2, pp. 271–86, May 1998.

[279] J. Loeffen *et al.*, "Mutations in the complex I NDUFS2 gene of patients with cardiomyopathy and encephalomyopathy.," *Ann. Neurol.*, vol. 49, no. 2, pp. 195–201, Feb. 2001.

[280] J. W. Wu *et al.*, "Crystal structure of a phosphorylated Smad2. Recognition of phosphoserine by the MH2 domain and insights on Smad function in TGF-beta signaling.," *Mol. Cell*, vol. 8, no. 6, pp. 1277–89, Dec. 2001.

[281] Y. Shi, A. Hata, R. S. Lo, J. Massagué, and N. P. Pavletich, "A structural basis for mutational inactivation of the tumour suppressor Smad4.," *Nature*, vol. 388, no. 6637, pp. 87–93, Jul. 1997.

[282] F. Itoh, H. Asao, K. Sugamura, C. H. Heldin, P. ten Dijke, and S. Itoh, "Promoting bone morphogenetic protein signaling through negative regulation of inhibitory Smads.," *EMBO J.*, vol. 20, no. 15, pp. 4132–42, Aug. 2001.

[283] F. Liu, C. Pouponnot, and J. Massagué, "Dual role of the Smad4/DPC4 tumor suppressor in TGFbeta-inducible transcriptional complexes.," *Genes Dev.*, vol. 11, no. 23, pp. 3157–67, Dec. 1997.

[284] T. Gaarenstroom and C. S. Hill, "TGF-β signaling to chromatin: how Smads regulate transcription during self-renewal and differentiation.," *Semin. Cell Dev. Biol.*, vol. 32, pp. 107–18, Aug. 2014.

[285] A. Cano *et al.*, "The transcription factor snail controls epithelial-mesenchymal transitions by repressing E-cadherin expression.," *Nat. Cell Biol.*, vol. 2, no. 2, pp. 76–83, Feb.

2000.

[286] A. Eger *et al.*, “DeltaEF1 is a transcriptional repressor of E-cadherin and regulates epithelial plasticity in breast cancer cells.,” *Oncogene*, vol. 24, no. 14, pp. 2375–85, Mar. 2005.

[287] J. Yang *et al.*, “Twist, a master regulator of morphogenesis, plays an essential role in tumor metastasis.,” *Cell*, vol. 117, no. 7, pp. 927–39, Jun. 2004.

[288] Y. Katsuno, S. Lamouille, and R. Derynck, “TGF-β signaling and epithelial-mesenchymal transition in cancer progression.,” *Curr. Opin. Oncol.*, vol. 25, no. 1, pp. 76–84, Jan. 2013.

[289] A. Wilczynska and M. Bushell, “The complexity of miRNA-mediated repression,” *Cell Death Differ.*, vol. 22, no. 1, pp. 22–33, Jan. 2015.

[290] M. Brower, D. N. Carney, H. K. Oie, A. F. Gazdar, and J. D. Minna, “Growth of cell lines and clinical specimens of human non-small cell lung cancer in a serum-free defined medium.,” *Cancer Res.*, vol. 46, no. 2, pp. 798–806, Feb. 1986.

[291] I. Baumann, “Dissertation: Post-Transcriptional Regulation of mPGES-1 by the Balance between CUGBP1 and miR-574-5p,” 2017.

[292] D. Kamei *et al.*, “Microsomal prostaglandin E synthase-1 in both cancer cells and hosts contributes to tumour growth, invasion and metastasis.,” *Biochem. J.*, vol. 425, no. 2, pp. 361–71, Dec. 2009.

[293] R. Takahashi *et al.*, “Roles of microsomal prostaglandin E synthase-1 in lung metastasis formation in prostate cancer RM9 cells.,” *Biomed. Pharmacother.*, vol. 68, no. 1, pp. 71–7, Feb. 2014.

[294] D. Hanahan and R. A. Weinberg, “The hallmarks of cancer.,” *Cell*, vol. 100, no. 1, pp. 57–70, Jan. 2000.

[295] J. P. Thiery and J. P. Sleeman, “Complex networks orchestrate epithelial-mesenchymal transitions.,” *Nat. Rev. Mol. Cell Biol.*, vol. 7, no. 2, pp. 131–42, Feb. 2006.

[296] C. L. Chaffer and R. A. Weinberg, “A perspective on cancer cell metastasis.,” *Science (80-.).*, vol. 331, no. 6024, pp. 1559–64, Mar. 2011.

[297] P. Cohen, “The TLR and IL-1 signalling network at a glance.,” *J. Cell Sci.*, vol. 127, no. Pt 11, pp. 2383–90, Jun. 2014.

[298] A. Freischmidt, K. Müller, A. C. Ludolph, and J. H. Weishaupt, “Systemic dysregulation of TDP-43 binding microRNAs in amyotrophic lateral sclerosis.,” *Acta Neuropathol. Commun.*, vol. 1, p. 42, Jul. 2013.

[299] Y. Kawahara and A. Mieda-Sato, “TDP-43 promotes microRNA biogenesis as a component of the Drosha and Dicer complexes.,” *Proc. Natl. Acad. Sci. U. S. A.*, vol. 109, no. 9, pp. 3347–52, Feb. 2012.

[300] B. Beuth, M. F. García-Mayoral, I. A. Taylor, and A. Ramos, “Scaffold-independent analysis of RNA-protein interactions: the Nova-1 KH3-RNA complex.,” *J. Am. Chem. Soc.*, vol. 129, no. 33, pp. 10205–10, Aug. 2007.

[301] N. A. Faustino and T. A. Cooper, “Identification of putative new splicing targets for ETR-3 using sequences identified by systematic evolution of ligands by exponential enrichment.,” *Mol. Cell. Biol.*, vol. 25, no. 3, pp. 879–87, Feb. 2005.

Appendix

Abbreviations

µL	Microliter
5’ m^7G	5’ 7-methylguanylate cap
AGO	Argonaute protein
A_n 3’	3' Pol-A tails
ARE	AU-rich element
AS	Alternative splicing
ATCC	American Type Culture Collection
BACE1	β-site of APP cleaving enzyme
BCA	Bicinchoninic acid assay
BSA	Bovine serum albumine
C. elegans	Caenorhabditis elegans
CDCP1	CUB domain-containing protein 1
CDH1	Cadherin-1
CDS	Coding sequence
CEBPA	CCAAT/enhancer-binding protein alpha
CEP41	Centrosomal Protein 41
CerS1	Ceramid synthase 1
CHES1	Checkpoint suppressor 1
CID ITMS	Collision induced dissociation Ion Trap Mobility Spectroscopy
cJUN	Jun Proto-Oncogene, AP-1 Transcription Factor Subunit
Clip seq	Cross-linking immunoprecipitation-high-throughput sequencing
COX-2	Cyclooxygenase-2
CPLX2	Complexin-2
CRE	Cis-regulatory element
CSDC2	Cold Shock Domain Containing C2
CST5	Cystatin D
CUGBP1	CUG-RNA binding protein 1
Da	Dalton
DAPI	4´,6-Diamidine-2´-phenylindole dihydrchloride
DGCR8	DiGeorge Syndrome Critical Region 8
DIG	Digoxigenin
DM1	Myotonic dystrophy
DMEM	Dulbecco’s modified Eagle medium
DMSO	Dimethyl sulfoxide
DNA	Deoxyribonucleic acid
DTT	Dithiothreitol
EBF1	Early B Cell Factor 1
EDTA	Ethylenediaminetetraacetic acid
eIF	Eukaryotic Translation Initiation Factor
EMT	Epithelial-to-mesenchymal transition
et al.	And others
FCS	Fetal calf serum
FDR	False Discovery Rate
FISH	Fluorescence in situ hybridization
FTMS	Fourier transform mass analyzers
GLOD4	Glyoxalase domain-containing protein 4
GRE	GU-rich elements
GRIPAP1	GRIP1 Associated Protein 1
GTF2E2	General transcription factor IIE subunit 2

GTP	Guanosine-5'-triphosphate
h	Hour
HMGA2	High-mobility group AT-hook 2
HNF4A	Hepatocyte Nuclear Factor 4 Alpha
hnRNP E2	Heterogenous Nuclear Ribonucleoprotein E2
IL-1β	Interleukin 1 beta
IP	Immunoprecipitation
IPA	Ingenuity pathway analysis
Δ	Knockdown
LC-MS	Liquid chromatography–mass spectrometry
LEO1	LEO1 Homolog, Paf1/RNA Polymerase II Complex Component
lncRNA /lnc	Long non-coding RNA
MACC1	Metastasis-Associated In Colon Cancer Protein 1
MAFK	MAF BZIP Transcription Factor K
MAPT	Microtubule associated protein tau
MFI2	Melanotransferrin
min	Minute
miR	Micro RNA
mPGES-1	Microsomal prostaglandin E2 synthase 1
mRNA	Messenger RNA
MS	Mass spectrometry
mTOR	Mechanistic Target of Rapamycin
MYCBP	MYC Binding Protein
MYCN	MYCN Proto-Oncogene
MyD88	Myeloid differentiation primary response gene 88
NDUFS2	NADH- Ubiquinone Oxidoreductase Core Subunit S2
NMD	Nonsense-mediated mRNA decay
Nova-1	NOVA Alternative Splicing Regulator 1
NSCLC	Non-small cell lung cancer
nt	Nucleotides
oe	Overexpression
p38	Mitogen-Activated Protein Kinase 14
p70S6K	Ribosomal protein S6 kinase beta-1
PAGE	Polyacrylamide gel electrophoresis
PAIP2	Poly(A) Binding Protein Interacting Protein 2
PARN	Poly(A)-Specific Ribonuclease
p-body	Processing body
PBS	Phosphate buffered saline
PCR	Polymerase chain reaction
PG	Prostaglandin
PGE2	Prostaglandin E2
pre-miR	Precursor microRNA
pri-miR	Primary microRNA
PTCSC3	Papillary Thyroid Carcinoma Susceptibility Candidate 3
PTPRU.	Protein Tyrosine Phosphatase Receptor Type U
Qki	Quaking
qRT-PCR	Quantitative real time polymerase chain reaction
RAN	Ras-related nuclear protein
RBD	RNA-binding domain
RBM23	RNA Binding Motif Protein 23
RBP	RNA-binding protein
RICTOR	Rapamycin-Insensitive Companion Of MTOR
RIP	RNA immunoprecipitation
RISC	RNA-induced silencing complex

RNA	Ribonucleic acid
RNP	Ribonucleoprotein
rpm	Rounds per minute
RRM	RNA recognition motif
s	Second
SCAI	Suppressor Of Cancer Cell Invasion
SDS	Sodium dodecylsulfate
SELEX	Systematic Evolution of Ligands by EXponential Enrichment
SEM	Standard error of mean
SETD7	SET Domain Containing 7, Histone Lysine Methyltransferase
SLC39A6	Solute Carrier Family 39 Member 6
SMAD	Mothers against decapentaplegic homolog
Snail1	Snail Family Transcriptional Repressor 1
snRNP	Small ribonucleoproteins
SOD2	Superoxide dismutase 2,
SRP	Signal recognition particles
t	Time
TDP-43	Transactive response DNA binding protein43 kDa
TGF	Transforming growth factor
TMT	Tandem mass tag
TP53	Tumor protein 53
TRIF	Toll-interleukin receptor domain containing adaptor-inducing interferon-β
Tris	Tris(hydroxymethyl)-aminomethan
TSS	Transcription start site
TWIST1	Twist Family BHLH Transcription Factor 1
UBE2R2	Ubiquitin Conjugating Enzyme E2 R2
UBXN2B	UBX Domain Protein 2B
UTR	Untranslated region
V	Voltage
Wnt	Wingless-Type MMTV Integration Site Family, Member 1
ZDHHC14	Zinc Finger DHHC-Type Containing 14
ZEB1	Zinc Finger E-Box Binding Homeobox 1
ZNF469-3	Zinc Finger Protein 469

Supplementary data

Table 12. Top three upregulated proteins of the proteomics study.

	Accession number	Description	x-fold to control
ΔCUGBP1 soluble fraction	P04264	Keratin, type II cytoskeletal 1 OS=Homo sapiens GN=KRT1 PE=1 SV=6 - [K2C1_HUMAN]	20.43
	Q5XKE5	Keratin, type II cytoskeletal 79 OS=Homo sapiens GN=KRT79 PE=1 SV=2 - [K2C79_HUMAN]	6.50
	P13645	Keratin, type I cytoskeletal 10 OS=Homo sapiens GN=KRT10 PE=1 SV=6 - [K1C10_HUMAN]	3.80
ΔCUGBP1 microsomal fraction	F8WBR5	Isoform 3 of ADP-ribosylation factor-binding protein GGA1 OS=Homo sapiens GN=GGA1 - [GGA1_HUMAN]	3.47
	P10606	Ubiquitin carboxyl-terminal hydrolase OS=Homo sapiens GN=UCHL1 PE=1 SV=1 - [D6R974_HUMAN]	3.15
	E5RFX4	Isoform 2 of Glyoxalase domain-containing protein 4 OS=Homo sapiens GN=GLOD4 - [GLOD4_HUMAN]	2.65
ΔmiR-574-5p soluble fraction	P04264	Keratin, type II cytoskeletal 1 OS=Homo sapiens GN=KRT1 PE=1 SV=6 - [K2C1_HUMAN]	3.25
	A0A024QZ42	HCG1985580, isoform CRA_c OS=Homo sapiens GN=PDCD6 PE=1 SV=1 - [A0A024QZ42_HUMAN]	1.90
	H0YD99	Eukaryotic translation initiation factor 4 gamma 2 OS=Homo sapiens GN=EIF4G2 PE=1 SV=1 - [H0YD99_HUMAN]	1.76
ΔmiR-574-5p microsomal fraction	P19971	Pre-mRNA-splicing factor SYF1 OS=Homo sapiens GN=XAB2 PE=1 SV=2 - [SYF1_HUMAN]	3.56
	Q9NVX0-2	Thymidine phosphorylase OS=Homo sapiens GN=TYMP PE=1 SV=2 - [TYPH_HUMAN]	3.36
	P00403	Isoform 2 of HAUS augmin-like complex subunit 2 OS=Homo sapiens GN=HAUS2 - [HAUS2_HUMAN]	2.91
miR-574-5p oe soluble fraction	Q5XKE5	Keratin, type II cytoskeletal 79 OS=Homo sapiens GN=KRT79 PE=1 SV=2 - [K2C79_HUMAN]	5.46
	P04264	Keratin, type II cytoskeletal 1 OS=Homo sapiens GN=KRT1 PE=1 SV=6 - [K2C1_HUMAN]	5.12
	H0YL43	Reticulocalbin-2 (Fragment) OS=Homo sapiens GN=RCN2 PE=1 SV=1 - [H0YL43_HUMAN]	2.67
miR-574-5p oe microsomal fraction	Q32P28-4	Copine-1 OS=Homo sapiens GN=CPNE1 PE=1 SV=1 - [A6PVH9_HUMAN]	5.93
	Q92990-2	Protein S100 (Fragment) OS=Homo sapiens GN=S100A6 PE=1 SV=1 - [R4GN98_HUMAN]	5,70
	F8VZJ2	Tetratricopeptide repeat protein 6 OS=Homo sapiens GN=TTC6 PE=4 SV=1 - [G3V435_HUMAN]	4,54

X-fold regulation compared to each control upon ΔCUGBP1, ΔmiR-574-5p and miR-574-5p oe in in soluble and microsomal fraction of IL-1β-stimulated A549 cells.

Table 13. Top three downregulated proteins of the proteomics study.

	Accession number	Description	x-fold to control
ΔCUGBP1 soluble fraction	P55060-3	Isoform 3 of Exportin-2 OS=Homo sapiens GN=CSE1L - [XPO2_HUMAN]	-5.99
	Q9BQL6-3	Isoform 3 of Fermitin family homolog 1 OS=Homo sapiens GN=FERMT1 - [FERM1_HUMAN]	-4.15
	Q15427	Splicing factor 3B subunit 4 OS=Homo sapiens GN=SF3B4 PE=1 SV=1 - [SF3B4_HUMAN]	-3.80
ΔCUGBP1 microsomal fraction	O00566	Leucine-rich repeat-containing protein 41 (Fragment) OS=Homo sapiens GN=LRRC41 PE=1 SV=1 - [A0A087WTI9_HUMAN]	-5.22
	A0A0C4DFS8	Isoform 5 of CUGBP Elav-like family member 1 OS=Homo sapiens GN=CELF1 - [CELF1_HUMAN]	-3.09
	F8VSL3	Ankyrin repeat and IBR domain-containing protein 1 OS=Homo sapiens GN=ANKIB1 PE=1 SV=3 - [AKIB1_HUMAN]	-3.07
ΔmiR-574-5p soluble fraction	Q9Y5J9	Mitochondrial import inner membrane translocase subunit Tim8 B OS=Homo sapiens GN=TIMM8B PE=1 SV=1 - [TIM8B_HUMAN]	-3.51
	P62913-2	Isoform 2 of 60S ribosomal protein L11 OS=Homo sapiens GN=RPL11 - [RL11_HUMAN]	-3.18
	O00425	Insulin-like growth factor 2 mRNA-binding protein 3 OS=Homo sapiens GN=IGF2BP3 PE=1 SV=2 - [IF2B3_HUMAN]	-2.95

ΔmiR-574-5p microsomal fraction	J3KS17	Isoform 2 of Nucleolar protein 9 OS=Homo sapiens GN=NOP9 - [NOP9_HUMAN]	-4.10
	Q86U38-2	Calmodulin OS=Homo sapiens GN=CALM2 PE=1 SV=1 - [F8WBR5_HUMAN]	-3.00
	F8WBR5	Isoform 3 of ADP-ribosylation factor-binding protein GGA1 OS=Homo sapiens GN=GGA1 - [GGA1_HUMAN]	-2.87
miR-574-5p oe soluble fraction	P60903	Protein S100-A10 OS=Homo sapiens GN=S100A10 PE=1 SV=2 - [S10AA_HUMAN]	-4.48
	P09525	Annexin A4 OS=Homo sapiens GN=ANXA4 PE=1 SV=4 - [ANXA4_HUMAN]	-3.86
	Q8IVL5-2	Isoform 2 of Prolyl 3-hydroxylase 2 OS=Homo sapiens GN=LEPREL1 - [P3H2_HUMAN]	-2.43
miR-574-5p oe microsomal fraction	P17302	Ninjurin-1 OS=Homo sapiens GN=NINJ1 PE=1 SV=2 - [NINJ1_HUMAN]	-7.23
	Q9Y6A9	Transmembrane emp24 domain-containing protein 5 OS=Homo sapiens GN=TMED5 PE=1 SV=1 - [TMED5_HUMAN]	-5.16
	O75127	Signal peptidase complex catalytic subunit SEC11A OS=Homo sapiens GN=SEC11A PE=1 SV=1 - [H0YKT4_HUMAN]	-4.96

X-fold regulation compared to each control upon ΔCUGBP1, ΔmiR-574-5p and miR-574-5p oe in in soluble and microsomal fraction of IL-1β-stimulated A549 cells.

Table 14. IPA prediction of top five canonical pathways.

	Name	**p-value**	**Overlap**
ΔCUGBP1 soluble fraction	EIF2 Signaling	1.86E-45	55.7 % 103/185
	Regulation of eIF4 and p70S6K Signaling	6.46E-31	50.6 % 78/154
	Protein Ubiquitination Pathway	2.94E-27	39.0 % 99/254
	tRNA Charging	2.38E-19	76.3 % 29/38
	mTOR Signaling	2.92E-19	37.4 % 73/195
ΔCUGBP1 microsomal fraction	EIF2 Signaling	1.61E-48	69.7 % 129/185
	Protein Ubiquitination Pathway	3.78E-31	52.8 % 134/254
	Mitochondrial Dysfunction	5.21E-27	58.2 % 96/165
	Regulation of eIF4 and p70S6K Signaling	2.30E-26 5	59.1 % 91/154
	Oxidative Phosphorylation	8.96E-23	64.4 % 67/104
ΔmiR-574-5p soluble fraction	EIF2 Signaling	2.36E-45	55.7 % 103/185
	Regulation of eIF4 and p70S6K Signaling	1.02E-31	51.3 % 79/154
	Protein Ubiquitination Pathway	7.62E-28	39.4 % 100/254
	tRNA Charging	2.55E-19	76.3 % 29/38
	mTOR Signaling	3.37E-19	37.4 % 73/195
ΔmiR-574-5p microsomal fraction	EIF2 Signaling	1.47E-48	69.7 % 129/185
	Protein Ubiquitination Pathway	3.48E-31	52.8 % 134/254
	Mitochondrial Dysfunction	4.89E-27	58.2 % 96/165
	Regulation of eIF4 and p70S6K Signaling	2.17E-26	59.1 % 91/154
	Oxidative Phosphorylation	8.56E-23	64.4 % 67/104
miR-574-5p oe soluble fraction	EIF2 Signaling	2.45E-45	55.7 % 103/185
	Regulation of eIF4 and p70S6K Signaling	1.05E-31	51.3 % 79/154
	Protein Ubiquitination Pathway	7.88E-28	39.4 % 100/254
	tRNA Charging	2.58E-19	76.3 % 29/38
	mTOR Signaling	3.46E-19	37.4 % 73/195
miR-574-5p oe microsomal fraction	EIF2 Signaling	1.51E-48	69.7 % 129/185
	Protein Ubiquitination Pathway	3.58E-31	52.8 % 134/254
	Mitochondrial Dysfunction	5.00E-27	58.2 % 96/165
	Regulation of eIF4 and p70S6K Signaling	2.21E-26	59.1 % 91/154
	Oxidative Phosphorylation	8.69E-23	64.4 % 67/104

Table 15. IPA prediction of top five upstream regulators.

	Name	**p-value**
ΔCUGBP1 soluble fraction	MYC	8.25E-72
	HNF4A	2.34E-58
	TP53	1.54E-57
	MYCN	3.64E-50
	MAPT	3.90E-42

ΔCUGBP1 microsomal fraction	HNF4A	2.34E-82
	CST5	6.86E-70
	RICTOR	1.16E-53
	MYC	8.00E-49
	TP53	5.89E-43
ΔmiR-574-5p soluble fraction	MYC	1.54E-71
	TP53	9.48E-58
	HNF4A	1.39E-57
	MYCN	4.80E-50
	MAPT	7.02E-43
ΔmiR-574-5p microsomal fraction	HNF4A	4.44E-82
	CST5	6.03E-70
	RICTOR	1.04E-53
	MYC	6.60E-49
	TP53	4.75E-43
miR-574-5p oe soluble fraction	MYC	1.71E-71
	HNF4A	2.18E-58
	TP53	2.18E-58
	MYCN	5.02E-50
	MAPT	7.31E-43
miR-574-5p oe microsomal fraction	HNF4A	1.83E-82
	CST5	6.29E-70
	RICTOR	1.08E-53
	MYC	7.04E-49
	TP53	5.10E-43

Table 16. Summary of all analyzed proteins.

mPGES-1		**ΔCUGBP1**	**ΔmiR-574-5p**	**miR-574-5p oe**
Soluble fraction	TMT Proteomics	n.d.	n.d.	n.d.
	IPA (Z-score)	n.d.	n.d.	n.d.
	Western blot	n.d.	n.d.	n.d.
Microsomal fraction	TMT Proteomics	1.03	1.50	-1.07
	IPA (Z-score)	n.d.	n.d.	n.d.
	Western blot	1.42	0.5	2
Smad2		**ΔCUGBP1**	**ΔmiR-574-5p**	**miR-574-5p oe**
Soluble fraction	TMT Proteomics	1.1	-1.3	1.2
	IPA (Z-score)	n.d.	n.d.	n.d.
	Western blot	0.5	1.6	1.2
Microsomal fraction	TMT Proteomics	n.d.	n.d.	n.d.
	IPA (Z-score)	1.9	-2.1	n.d.
	Western blot	4.0	1.4	0.6
Smad3		**ΔCUGBP1**	**ΔmiR-574-5p**	**miR-574-5p oe**
Soluble fraction	TMT Proteomics	-2.1	1.0	-1.1
	IPA (Z-score)	n.d.	n.d.	n.d.
	Western blot	0.6	1.7	1.8
Microsomal fraction	TMT Proteomics	1.1	1.1	1.2
	IPA (Z-score)	2.3	n.d.	n.d.
	Western blot	2.2	1.4	0.6
NDUFS2		**ΔCUGBP1**	**ΔmiR-574-5p**	**miR-574-5p oe**
Soluble fraction	TMT Proteomics	1.3	-1.3	1.4
	IPA (Z-score)	n.d.	n.d.	n.d.
	Western blot	2.2	0.8	1.6
Microsomal fraction	TMT Proteomics	1.1	1.1	1.2
	IPA (Z-score)	n.d.	n.d.	n.d.
	Western blot	1.4	1.1	0.8

GLOD4		**ΔCUGBP1**	**ΔmiR-574-5p**	**miR-574-5p oe**
Soluble fraction	TMT Proteomics	-1.3	-1.0	-1.1
	IPA (Z-score)	n.d.	n.d.	n.d.
	Western blot	n.d.	n.d.	n.d.
Microsomal fraction	TMT Proteomics	2.6	-1.3	1.5
	IPA (Z-score)	2.7	n.d.	n.d.
	Western blot	n.d.	n.d.	n.d.
UBE2R2		**ΔCUGBP1**	**ΔmiR-574-5p**	**miR-574-5p oe**
Soluble fraction	TMT Proteomics	n.d.	n.d.	n.d.
	IPA (Z-score)	n.d.	n.d.	n.d.
	Western blot	no information	no information	no information
Microsomal fraction	TMT Proteomics	1.5	-1.5	1.8
	IPA (Z-score)	n.d.	n.d.	n.d.
	Western blot	no information	no information	no information
CPLX2		**ΔCUGBP1**	**ΔmiR-574-5p**	**miR-574-5p oe**
Soluble fraction	TMT Proteomics	1.2	-1.1	1.1
	IPA (Z-score)	n.d.	n.d.	n.d.
	Western blot	no information	no information	no information
Microsomal fraction	TMT Proteomics	2.0	-2.5	-1.7
	IPA (Z-score)	n.d.	n.d.	n.d.
	Western blot	no information	no information	no information
CEP41		**ΔCUGBP1**	**ΔmiR-574-5p**	**miR-574-5p oe**
Soluble fraction	TMT Proteomics	1.1	1.1	-1.2
	IPA(Z-score)	n.d.	n.d.	n.d.
	Western blot	no information	no information	no information
Microsomal fraction	TMT Proteomics	1.5	-1.9	1.8
	IPA (Z-score)	n.d.	n.d.	n.d.
	Western blot	no information	no information	no information
MAFK		**ΔCUGBP1**	**ΔmiR-574-5p**	**miR-574-5p oe**
Soluble fraction	TMT Proteomics	n.d.	n.d.	n.d.
	IPA (Z-score)	-1.3	-2.4	-0.7
	Western blot	no information	no information	no information
Microsomal fraction	TMT Proteomics	1.7	-1.5	1.0
	IPA (Z-score)	-0.7	0.4	2.2
	Western blot	no information	no information	no information
SETD7		**ΔCUGBP1**	**ΔmiR-574-5p**	**miR-574-5p oe**
Soluble fraction	TMT Proteomics	-1.40	1.02	1.01
	IPA (Z-score)	n.d.	n.d.	n.d.
	Western blot	no information	no information	no information
Microsomal fraction	TMT Proteomics	1.58	-1.46	3.25
	IPA (Z-score)	n.d.	n.d.	n.d.
	Western blot	no information	no information	no information
GRIPAP1		**ΔCUGBP1**	**ΔmiR-574-5p**	**miR-574-5p oe**
Soluble fraction	TMT Proteomics	1.31	1.00	1.05
	IPA (Z-score)	n.d.	n.d.	n.d.
	Western blot	no information	no information	no information
Microsomal fraction	TMT Proteomics	1.67	-1.52	2.53
	IPA (Z-score)	n.d.	n.d.	n.d.
	Western blot	no information	no information	no information

SLC39A6		ΔCUGBP1	ΔmiR-574-5p	miR-574-5p oe
Soluble fraction	TMT Proteomics	n.d.	n.d.	n.d.
	IPA (Z-score)	n.d.	n.d.	n.d.
	Western blot	no information	no information	no information
Microsomal fraction	TMT Proteomics	1.65	-1.68	1.74
	IPA (Z-score)	n.d.	n.d.	n.d.
	Western blot	no information	no information	no information
LEO1		**ΔCUGBP1**	**ΔmiR-574-5p**	**miR-574-5p oe**
Soluble fraction	TMT Proteomics	n.d.	n.d.	n.d.
	IPA (Z-score)	n.d.	n.d.	n.d.
	Western blot	n.d.	n.d.	n.d.
Microsomal fraction	TMT Proteomics	1.53	-1.65	1.58
	IPA (Z-score)	n.d.	n.d.	n.d.
	Western blot	no information	no information	no information
GTF2E2		**ΔCUGBP1**	**ΔmiR-574-5p**	**miR-574-5p oe**
Soluble fraction	TMT Proteomics	-1.42	1.14	-1.51
	IPA (Z-score)	n.d.	n.d.	n.d.
	Western blot	n.d.	n.d.	n.d.
Microsomal fraction	TMT Proteomics	1.51	-1.55	1.56
	IPA (Z-score)	n.d.	n.d.	n.d.
	Western blot	no information	no information	no information

Regulation in TMT proteomics study, IPA (Z-score) prediction and Western blot analysis in soluble and microsomal fraction upon ΔCUGBP1, ΔmiR-574-5p and miR-574-5p oe in IL-1β-stimulated A549 cells. TMT Proteomics: TMT ratio compared to control sample; no information: not analyzed via Western blot analysis; n.d.: not determined.

Table 17. Transcripts from bioinformatical 3'UTR analysis

Gene name	Ensemble transcript ID	CUGBP1 Binding motif	potential intron (nt)	Number of distinct binding sites	Fraction in TMT proteomics study
CEP41	ENST00000489512	TGTGTGTGT	199	2	microsomal
CEP41	ENST00000616628	TGTGTGTGT	199	2	microsomal
MAFK	ENST00000343242	TGTGTGTG	384	2	microsomal
MAFK	ENST00000403150	TGTGTGTG	384	2	microsomal
RBM23	ENST00000359890	TGTGTGTG	7513	2	microsomal
SETD7	ENST00000274031	TGTGTGTG	409	2	microsomal
UBE2R2	ENST00000263228	TGTGTGTG	592	2	microsomal
UBXN2B	ENST00000399598	TGTGTGTG	551	2	microsomal
CPLX2	ENST00000359546	TGTGTGTG	1548	3	microsomal
SOD2	ENST00000538183	TGTGTGTGTGT	7537	2	soluble
CDCP1	ENST00000296129	TGTGTGTG	2382	2	soluble

Curriculum vitae

Persönliche Daten

Name: Anne Caterina Emmerich, geboren am 20.11.1990 in Essen

Akademische Karriere

07/2016 – 01/2020 Promotion bei Dr. Meike Julia Saul, Prof. Dr. Beatrix Süß (Technische Universität Darmstadt), sowie Prof. Dr. Dieter Steinhilber (Goethe-Universität Frankfurt); Mitglied der Graduiertenschule FIRST und Stipendiatin des Else-Kröner-Fresenius Graduiertenkollegs

10/2013 – 10/2015 Masterstudiengang „Molekulare Medizin“ an der Goethe- Universität Frankfurt, Abschluss: Master of Science (1,4)

Masterarbeit am Institut für Allgemeine Pharmakologie und Toxikologie: „*The role of cAMP in expression of interleukin-22 by human T-cells*“

10/2010 – 09/2013 Bachelorstudiengang „Biologie“ an der Johannes Gutenberg-Universität Mainz, Abschluss: Bachelor of Science (1,6)

Bachelorarbeit am Institut für Zoologie, Abteilung Zell- und Matrixbiologie: „*Charakterisierung der humanen Metalloprotease Tolloid-like 2“*

08/2002 – 03/2010 Martin-von-Cochem-Gymnasium, Cochem (Mosel), Abitur (2,1)

Berufliche Erfahrung:

01/2016 – 07/2016 Industriepraktikum, Fresenius Medical Care, Bad Homburg von der Höhe, „Biomedizinisches Projektmanagement“, Technology and Innovation Management, Global R&D

Lehrtätigkeit:

2017 - 2019 Betreuung von Bachelor- und Masterstudenten
2017 - 2019 Tutorin des Bachelor Genetik Praktikums der TU-Darmstadt

Konferenzen/Symposien:

RMU RNA Salon: Pulldown your RNA, Mainz

RMU RNA Salon: Ribonomics for every taste, Frankfurt a. M.

RMU RNA Salon: Genomics approaches in RNA Biology, Mainz

ECCPS Symposium: New goals in Cardio-Pulmonary Research, Bad Nauheim

Resolution of inflammation: mechanisms, mediators & bio-markers, Pescara, Italien

Publikationen:

Saul MJ, Baumann I, Bruno A, Emmerich AC, Wellstein J, Ottinger SM, Contursi A, Dovizio M, Donnini S, Tacconelli S, Raouf J, Idborg H, Stein S, Korotkova M, Savai R, Terzuoli E, Sala G, Seeger W, Jakobsson PJ, Patrignani P, Suess B, Steinhilber D. miR-574-5p as RNA decoy for CUGBP1 stimulates human lung tumor growth by mPGES-1 induction. FASEB J. 2019

Saul MJ, Hegewald AB, Emmerich AC, Ossipova E, Vogel M, Baumann I, Kultima K, Lengqivst J, Steinhilber D, Jakobsson PJ. Mass spectrometry-based proteomics approach characterizes the dual functionality of miR-328 in monocytes. Front Pharmacol. 2019

Saul MJ, Emmerich AC, Steinhilber D, Süß B. Regulation of eicosanoid pathways by miRNAs. Front Pharmacol. 2019

Emmerich AC, Wellstein J, Ossipova E, Baumann I, Lengqivst J, Kultima K, Jakobsson PJ, Steinhilber D, Saul MJ. Proteomics-based characterization of miR-574-5p decoy to CUGBP1 suggests specificity for mPGES-1 regulation in human lung cancer cells. Front Pharmacol., 2020.

Ehrenwörtliche Erklärung

Ich erkläre hiermit ehrenwörtlich, dass ich die vorliegende Arbeit entsprechend den Regeln guter wissenschaftlicher Praxis selbstständig und ohne unzulässige Hilfe Dritter angefertigt habe.

Sämtliche aus fremden Quellen direkt oder indirekt übernommenen Gedanken sowie sämtliche von Anderen direkt oder indirekt übernommenen Daten, Techniken und Materialien sind als solche kenntlich gemacht. Die Arbeit wurde bisher bei keiner anderen Hochschule zu Prüfungszwecken eingereicht.

Darmstadt, den 08.01.2020

……..

Anne Caterina Emmerich

Teile dieser Arbeit wurden bereits publiziert in:
Saul MJ, Baumann I, Bruno A, Emmerich AC, Wellstein J, Ottinger SM, Contursi A, Dovizio M, Donnini S, Tacconelli S, Raouf J, Idborg H, Stein S, Korotkova M, Savai R, Terzuoli E, Sala G, Seeger W, Jakobsson PJ, Patrignani P, Suess B, Steinhilber D. miR-574-5p as RNA decoy for CUGBP1 stimulates human lung tumor growth by mPGES-1 induction. FASEB J. 2019

Emmerich AC, Wellstein J, Ossipova E, Baumann I, Lengqivst J, Kultima K, Jakobsson PJ, Steinhilber D, Saul MJ. Proteomics-based characterization of miR-574-5p decoy to CUGBP1 suggests specificity for mPGES-1 regulation in human lung cancer cells. Front Pharmacol., 2020.

Danksagungen

Als erstes möchte ich mich bei Dr. Meike Saul ganz herzlich bedanken für die Aufnahme in ihre Gruppe und die Möglichkeit meine Doktorarbeit durchzuführen. Nicht nur für die gute Betreuung und vielen fachlichen Diskussionen, sondern auch, dass du immer ein offenes Ohr hattest und mit Rat und Tat zur Seite standest.
Vielen Dank auch an Prof. Dr. Beatrix Süß und Prof. Dr. Dieter Steinhilber für ihre Unterstützung und die zahlreichen konstruktiven Diskussionen ob in Frankfurt, Darmstadt oder bei den Summer- und Winterschools.
Des Weiteren möchte ich mich bei der Else-Kröner-Fresenius Graduiertenschule für die Finanzierung bedanken und ganz besonders auch bei Dr. Brigitte Held.
Ein ganz großes Dankeschön geht auch an alle ehemaligen und derzeitigen Mitglieder der Arbeitsgruppen Süß und Weigand. Durch die tolle Arbeitsatmosphäre und Kollegialität habe ich mich immer gut aufgehoben gefühlt. Besonderen Dank an Sandra, Stephen, Theresa, Jamina und Britta. Es hat Spaß gemacht mit euch allen zusammenzuarbeiten.
Ebenfalls vielen Dank an unsere gar nicht mehr so kleine AG Saul. Besonders möchte ich mich bei Anett, Julia, Leon und Eva bedanken, für den tollen Zusammenhalt, die lustigen Mittagspausen und die allgemeine Labor-Madness. Ich werde noch lange an all die verrückten Pavarotti- und Dorie-Momente denken. Ich hoffe, dass es jetzt nicht all zu still wird. Jetzt muss einfach einer von euch durchs Labor tanzen und dabei sein Eis verschütten, ok?
Danke für die sehr schöne Zeit!
Mein besonderer Dank gilt auch meiner Eltern Norbert und Trudi, die mich immer unterstützt haben - vom Bachelor- über Masterstudium bis hin zum Doktor. Ohne euch wäre das nicht möglich gewesen!
Schließlich möchte ich mich bei Andi bedanken, der in der gesamten Zeit einfach immer für mich da war und mir Sicherheit und Rückhalt gegeben hat. Ohne dich hätte ich das niemals geschafft! Danke für Alles!